

P.171

NSG-58-60

N 64 23430
Code 1 Cat. 23
CR56226

PLASMA SHEATH AND SCREENING AROUND A STATIONARY CHARGED SPHERE
AND A RAPIDLY MOVING CHARGED BODY

by

Evan Harris Walker

OTS PRICE

XEROX \$ 1250 ph
MICROFILM \$ _____

Thesis submitted to the Faculty of the
Graduate School of the University of
Maryland in partial fulfillment of
the requirements for the degree of
Doctor of Philosophy
1964

UNPUBLISHED PRELIMINARY DATA

RC
#7

APPROVAL SHEET

Title of Thesis: Plasma Sheath and Screening Around a Stationary
Charged Sphere and a Rapidly Moving Charged Body

Name of Candidate: Evan Harris Walker
Doctor of Philosophy, 1964

Thesis and Abstract Approved:

S. F. Singer
Professor
Department of Physics and Astronomy

Date Approved:

VITA

Name: Evan Harris Walker

Date of Birth: February 15, 1935

Place of Birth: Birmingham, Alabama

Education:

B. S. University of Alabama, 1955

M. S. University of Alabama, 1956

Research Graduate Assistant, University of Maryland, 1958-present

Previous Experience:

Teaching Assistant, University of Alabama, 1955

Graduate Research Assistant, Iowa State College, 1956-57

Associate Professor of Physics, Memphis State University,
1957-58

Research Graduate Assistant, University of Maryland, Physics
Department, 1958-present

Memberships:

American Geophysical Union

Publications:

"Wake of a Charged Body in an Ionized Gas," Bull. Am. Phys. Soc.
5, 47 (1959). (with S. F. Singer)

"Wake of a Charged Body Moving in a Plasma," Bull. Am. Phys.
Soc. 5, 234 (1960). (with S. F. Singer)

"A Lunar Ionosphere," Trans. A. G. U. 42, 217 (1961). (with
S. F. Singer)

"Plasma Compression Effects Produced by Space Vehicles in a
Magneto-Ionic Medium," in Interaction of Space Vehicles with
an Ionized Atmosphere; ed. by S. F. Singer (Pergamon Press,
New York, 1964). (with S. F. Singer)

"Plasma Sheath and Screening Around a Rapidly Moving Body," in
Interaction of Space Vehicles with an Ionized Atmosphere; ed.
by S. F. Singer (Pergamon Press, New York, 1964).

"Photoelectric Screening of Bodies in Interplanetary Space,"
ICARUS 1, 7 (1962). (with S. F. Singer)

"Electrostatic Dust Transport on the Lunar Surface," ICARUS 1,
112 (1962). (with S. F. Singer)

"Comments on a Paper by P. D. Grannis, 'Electrostatic Erosion Mechanisms on the Moon'," J. Geophys. Research 67, 2586 (1962).

"Comments on a Paper by M. L. Coffman, 'Charging Grains of Dust'," J. Geophys. Research 69, 566 (1964).

"A Relationship for Plasma Sheaths About Langmuir Probes," University of Maryland, Physics Department, Technical Report 350 (1964). (with R. T. Bettinger)

ABSTRACT

Title of Thesis: Plasma Sheath and Screening Around a Stationary Charged Sphere and a Rapidly Moving Charged Body

Evan Harris Walker, Doctor of Philosophy, 1964

Thesis directed by: S. F. Singer, Professor of Physics

The potential and charge density distributions are derived quite generally for both a stationary charged sphere and a charged body moving rapidly through a plasma. Previous treatments were restricted to cases where either the body's potential was small, being at most only two or three times kT/e , or the body was small compared to the Debye length (i.e. $a \ll [kT/4\pi e^2 N_0]^{1/2}$).

We have calculated the potential and charge density as a function of position about a stationary charged sphere, using both monoenergetic and Maxwellian velocity distributions for the ions and electrons of the ambient plasma. The potential decreases with distance more slowly than in the case of local thermodynamic equilibrium; the density of the ions (if the body is negative, electrons if positive) is generally much smaller than given by the barometric formula and varies in a complicated way. We also calculate the ion and electron voltage-current probe characteristics and the equilibrium potential as a function of the radius of the body. We find the Mott-Smith and Langmuir equations for the ion current (if the body is negative, electrons if positive) are unsatisfactory unless the sheath thickness is expressed as a function of the potential and radius of the body. For a spherical body the appropriate expression for the sheath thickness σ is found to be $\sigma = 0.83 \psi_s^{1/2} \rho_s^{1/3}$, where ψ_s and ρ_s

are the nondimensional potential and radius for the body.

Eigenvalue solutions are obtained if the charged body neutralizes most of the ions and electrons that strike its surface, i.e., if the reflection coefficients for the surface of the body are small. Under these conditions the potential is found to vary more slowly than r^{-2} for small values of the potential.

For a rapidly moving body we have developed a self-consistent method for solving the screening problem which does not require iterative calculations. Equations for the solution of the screening of axially symmetric bodies are derived for plasmas in which the thermal motion of the ions can be neglected and for plasmas with a Maxwellian velocity distribution. We have calculated the potential and density variation in the wake, the probe characteristics, and the impact and electric drag characteristic curves for various bodies. These calculations show that there is a trough in the ion density surrounding a highly charged body. The drag calculations show that under certain conditions a negative drag is obtained if the potential on the body is large and if the ions are neutralized and elastically reflected at the surface of the body.

PLASMA SHEATH AND SCREENING AROUND A STATIONARY CHARGED SPHERE
AND A RAPIDLY MOVING CHARGED BODY

by

Evan Harris Walker

Thesis submitted to the Faculty of the
Graduate School of the University of
Maryland in partial fulfillment of
the requirements for the degree of
Doctor of Philosophy
1964

ACKNOWLEDGMENTS

I would like to acknowledge the assistance of all those who helped in this work. I wish to thank Dr. S. F. Singer who suggested the problem and supervised the work, Dr. E. J. ^{II}Opik who laid the foundations for an exact approach to these problems and offered helpful advice, Y. C. Laohavanich and L. N. Foster for their work on the numerical calculations and for the many useful discussions I had with them. I also wish to thank R. T. Bettinger for reducing the current-voltage probe characteristics, calculated here, to an analytic form, my wife, Helen Marie, for her work in the preparation of the graphs, and Ruth Beebe for typing and proofreading of the work.

This research was supported by the National Aeronautics and Space Administration Grant NsG - 58 - 60.

TABLE OF CONTENTS

<u>Chapter</u>		<u>Page</u>
I.	INTRODUCTION	1
II.	FORMULAE FOR THE CALCULATION OF THE SCREENING OF A STATIONARY CHARGED SPHERE	10
	A. Plasma of monoenergetic particles	10
	B. Results of calculations for a plasma of monoenergetic particles	17
	C. Plasma of particles with a Maxwellian velocity distribution	19
	D. Results of calculations for a plasma of particles with a Maxwellian velocity distribution	27
	E. Current-voltage characteristics for a sphere embedded in a plasma with a Maxwellian velocity distribution; comparison with Mott-Smith and Langmuir equations	30
	F. An expression for the Sheath "thickness" for calculating current-voltage characteristics	34
	G. The effects of secondary electrons on the screening of stationary charged bodies	36
III.	THE SCREENING OF A CHARGED BODY WHERE THE RETURN FACTOR Q_+ IS VARIABLE	37
	A. General arguments	37
	B. Solutions for a monoenergetic plasma	40
	C. Solution for a plasma with a Maxwellian velocity distribution	49
IV.	THE SELF-CONSISTENT FIELD CALCULATION FOR A RAPIDLY MOVING AXIALLY SYMMETRIC CHARGED BODY	50
	A. Discussion of the approach	50
	B. Validity of the approach	55

TABLE OF CONTENTS (continued)

<u>Chapter</u>	<u>Page</u>
V. THE DENSITY OF IONS AND ELECTRONS IN AN AXIALLY SYMMETRIC POTENTIAL FIELD FOR A RAPIDLY MOVING CHARGED BODY	58
A. The ion density n_+	58
B. The electron density n_-	64
VI. OTHER EQUATIONS FOR FOLLOWING TRAJECTORIES	69
A. Calculations of new orbit coordinates (ρ, θ)	69
B. Calculations of the particle's pitch angle α	70
C. Calculation of β from the coordinates of two test particles	71
D. The transformation of the Laplacian	72
VII. GROWTH OF ERRORS IN NUMERICAL CALCULATIONS	76
VIII. RESULTS OF THE NUMERICAL SOLUTION FOR THE SCREENING OF A RAPIDLY MOVING CHARGED BODY	85
A. The problems treated	85
B. Results of the numerical calculations and general observations	87
IX. PARTICLE ACCRETION BY A RAPIDLY MOVING CHARGED BODY	91
A. The ion and electron currents to the surface of a rapidly moving charged body ..	91
B. The drag on the body	92
LIST OF REFERENCES	101
FIGURES	103

FIGURE CAPTIONS

- Fig. 2.1 Diagram showing the parameters involved in the motion of a screening particle. The coordinates are fixed in the charged body. An ion with initial velocity u and impact parameter q is shown outside the electric field and at the point r , θ in the field with velocity v and pitch angle α .
- Fig. 2.2 ψ plotted against ρ , with pericritical surface indicated and showing one curve with secondary electrons. The curves a, b, c, d, e, f, and g are representative of the family of curves that give the potential as a function of the radius vector, the ambient plasma being monoenergetic. For example, assume a body with a radius of 23 Debye lengths has a potential of 15 kT/e volts (point A in the figure); thus the potential falls off according to curve e. The pericritical surface would occur at B at a distance of 35 h and at a potential (energy) of 0.105 kT. If we include the effects (see text for details) of secondary electrons and charge this sphere to a potential 20 kT, then this will put us at point C so that the curve e' represents the variation of ψ vs. ρ . A plot of the equilibrium potential as a function of the radius is also given for a monenergetic Hydrogen plasma.
- Fig. 2.3 A plot of h^*/h , the ratio of the effective Debye length to the actual value plotted against the nondimensional distance ρ . These curves correspond to those of Fig. (2.2) as indicated by the letter labels; they illustrate

the inadequacies of the linearized solution.

Fig. 2.4 A continuation of Fig. (2.3) for smaller values of ρ .

Fig. 2.5 Plot of N_+/N_0 and N_-/N_0 against ρ for the potential curves a, b, and c, corresponding to the curves in Fig. (2.2).

Fig. 2.6 Plot of N_+/N_0 and N_-/N_0 against ρ for the potential curves d, e, f, and g, corresponding to the curves in Fig. (2.2).

Fig. 2.7 An illustration of the dependence of the pericritical region on the value of the exponent n . Moving from outside in there are the four regions: Periastron with $n \leq 2$, pericritical with $n > 2$, pericritical with $n \leq 2$, and again periastron with $n \leq 2$. Along a typical trajectory A B C D E we have:

A: the initial situation in which $n \leq 2$ and all pitch angles $\alpha = 0$ to $\pi/2$ are allowed, the periastron case

B: there is a transition from $n \leq 2$ to $n > 2$. Here the allowed cone is still from 0 to $\pi/2$ but is now beginning to become smaller

C: we have the pericritical case with the allowed pitch angles from 0 to α_{\max} , $\alpha_{\max} < \pi/2$.

D: the transition from $n > 2$ to $n \leq 2$ occurs.

The allowed cone now begins to increase but

α_{\max} is still less than $\pi/2$.

E: the trajectory reaches its point of closest approach to the origin. Here its pitch angle is $\pi/2$ and the allowed cone of pitch angles will

be $\alpha = 0$ to $\pi/2$. Point E marks a boundary between the pericritical region on the outside and periastron region inside.

Fig. 2.8 The nondimensional potential ($-\psi$) plotted against ρ , for screening by a plasma with a Maxwellian velocity distribution at infinity. The curves are used in the same way as those of Fig. (2.2). The labels $\rho_0 = 1$, $\rho_0 = 2$, etc. give the value of ρ where $\psi = -0.001$, the initial point used in the numerical calculation of the curve. Since the ambient plasma is Maxwellian there are different pericritical surfaces for particles of different initial energy. Thus, typical pericritical surfaces have been drawn in. We also show the equilibrium potential curve for bodies in a hydrogen plasma and in a singly ionized oxygen plasma.

Fig. 2.9 This figure is a continuation of Fig. (2.8) to smaller values of ρ .

Fig. 2.10 ψ plotted against $\rho_0 - \rho$. Some of the data of Fig. (2.8) is presented in a different way here. The curves all begin at the same point: $\psi = -0.001$, $\rho_0 - \rho = 0$.

Fig. 2.11 n_+ plotted against $\rho_0 - \rho$. These curves show the variation in the ion density, starting outside the body at a distance ρ_0 from the center where the potential is $\psi = -0.001$ and moving toward the surface of the body. The curves shown here correspond to the ψ vs. ρ plots of Figs. (2.8) and (2.10) as indicated by the value of ρ_0 . To use these curves when ψ_s and ρ_s (the values of ψ and

ρ at the surface of the body) are given, find the appropriate curve in Fig. (2.8) or (2.10) and then find the corresponding curve (from the family of curves) here.

Fig. 2.12 $n_+ - n_-$ plotted against $\rho_0 - \rho$. These curves show the variation in the total space charge density starting outside the body at a distance ρ_0 from the center where the potential is $\psi = -0.001$, and moving toward the surface of the body. The use of the curves for specific examples is the same as for Fig. (2.11). These curves shown here correspond to the ψ vs. ρ plots of Figs. (2.8) and (2.10) as indicated by the value of ρ_0 .

Fig. 2.13 $\log(1 + T_+)$ plotted against $\rho_0 - \rho$. These curves show the variation in the non-dimensional ion current to a charged body, starting at a point ρ_0 and going toward the body. We have plotted $\log(1 + T_+)$ rather than $\log T_+$ so that the point $T_+ = 0$ would appear. The use of these curves for specific examples is the same as for Fig. (2.11). The curves shown here correspond to the ψ vs. ρ plots of Figs. (2.8) and (2.10) as indicated by the value of ρ_0 . An example of the use of this figure is given in the text.

Fig. 2.14 $\log(1 + T_+)$ plotted against $\rho_0 - \rho$. These curves are a continuation of the curves of Fig. (2.13) corresponding to the continuation of Fig. (2.8) shown in Fig. (2.9). The use of the curves for specific examples is the same as for Fig. (2.13) (except that information about the ψ vs. ρ curves is obtained from Fig. (2.9) instead of

Fig. (2.8)).

Fig. 2.15 $\log (1 + |T_+ - T_-|)$ plotted against $\rho_0 - \rho$ for a hydrogen plasma. These curves show the variation in the non-dimensional net current to a charged body starting at a point ρ_0 and going toward the body. We have plotted $\log (1 + |T_+ - T_-|)$ rather than $\log |T_+ - T_-|$ so that the point $T_+ - T_- = 0$ would be in the graph. This point corresponds to the equilibrium condition of Eq. (2.60) and can, therefore, be used with Fig. (2.8) or (2.10) to find the equilibrium potential. The use of these curves for specific examples is the same as for Fig. (2.11). The curves shown here correspond to the ψ vs. ρ plots of Figs. (2.8) and (2.10).

Fig. 2.16 $\log (1 + |T_+ - T_-|)$ plotted against $\rho_0 - \rho$ for a hydrogen plasma. These curves are a continuation of Fig. (2.15) corresponding to the continuation of Fig. (2.8) in Fig. (2.9). The use of the curves for specific examples is the same as for Fig. (2.15) (except that information about the ψ vs. ρ curves is obtained from Fig. (2.9) instead of Fig. (2.8)).

Fig. 2.17 A plot of the ion current-voltage characteristics obtained from the screening calculations. Here ρ_s , the nondimensional radius of the charged sphere, appears as the parameter in the plot of the nondimensional ion current T_+ against the nondimensional potential. In addition T_+^{MSL} (Mott-Smith, Langmuir ion current to a negative body, in nondimensional form, as given by Eq. (2.70)) is

plotted for three cases: $\rho_0 = 50$, $\alpha = 55$; $\rho_0 = 5$, $\alpha = 6$; $\rho_0 = 10$, $\alpha = 10$.

Fig. 4.1 The initial parameters involved in the self-consistent calculation of screening for a moving sphere. The figure shows an arbitrary boundary surface on which the potential, electric field and initial velocity of the test particles are given. A typical test particle trajectory is shown along with the surface of the negative body.

Fig. 4.2 A diagram showing a method for computing trajectories if the trajectory crosses the axis of symmetry. The first trajectory that does not intersect the surface of the charged body reaches the point A. By symmetry we can reflect the trajectory at the axis. A second trajectory is calculated to the point B. The density of ions at B given by the second trajectory calculation is added to that of the first. The first trajectory is then calculated to point B.

Fig. 4.3a, b A continuation of Fig. (4.2) showing two stages of the tracing out of the density and electric fields in regions where the test particles intersect. Extrapolations of the sum of the densities for the first two particles allow their trajectories to be calculated to B and to C, then to be extrapolated to D and to E. A third trajectory can then be calculated to F using the densities at D and E obtained from the first and second trajectories.

Fig. 4.4 The Gauss Flux Theorem can be used to determine the conditions under which the electric field can be traced

out along the trajectories of ions. Here we have broken a closed surface into four parts S_1 , S_2 , S_3 , and S_4 , with components of the electric field perpendicular to these surfaces E_1 , E_2 , E_3 , and E_4 . Here S_3 and S_4 are perpendicular to the equipotential surfaces; hence $E_3 = E_4 = 0$.

Fig. 5.1 Diagram showing the parameters for the initial position of the ion; u is the initial velocity, q the impact parameter and r_0 , θ_0 are the polar coordinates of the ion.

Fig. 5.2 A cross section of the element of area ΔS . The angle $\Delta\theta_{2p}$ is the angle between two of the particle trajectory intersections with the equipotential surface. The angle α is the angle between the velocity vector and the radius vector; β is the angle between the radius vector and the normal to the equipotential surface.

Fig. 5.3 Diagram illustrating the quantities used in deriving an expression for Δl (where Δl is finite).

Fig. 5.4 The addition of the thermal velocity \underline{w} to the drift velocity \underline{u} . The resulting velocity vector \underline{u}' lies in a new plane of "symmetry" with respect to the origin.

Fig. 6.1 Diagram showing the parameters involved in "updating" coordinate positions of test particles. The particle is shown at r_1 , θ_1 before and r_2 , θ_2 after displacement.

Fig. 6.2 Diagram showing the parameters used to "update" α from its value at the previous (or old) position at P to its value at the present (or new) position Q .

- Fig. 6.3 Diagram showing the relation between the coordinates of a pair of test particles on an equipotential surface to the angle β . The test particles are at r_1, θ_1 and r_2, θ_2 . The angle β can be calculated in terms of these coordinates.
- Fig. 6.4 Diagram showing the geometric relationship between the coordinates $\rho, \theta, \theta'; \lambda, \Theta, \theta'$, and $\lambda', \Theta', \theta'$ (in the plane $\theta = \text{constant}$).
- Fig. 6.5 The expression for $\frac{\partial^2 \psi}{\partial \theta^2}$ in the neighborhood of point 1 can be expressed in terms of $\partial \psi / \partial \lambda'$ by geometric quantities. The figure represents a neighborhood of point 1 in which a variation in $\partial \psi / \partial \theta$ is obtained from the expression for $\partial \psi / \partial \lambda'$.
- Fig. 6.6 Diagram illustrating the geometric relationship between $\lambda' \Delta \theta'$ and $\rho \Delta \theta$.
- Fig. 8.1 A plot of the trajectories and equipotential surfaces computed for a hemispheric boundary surface of radius $\rho_0 = 5$ with an initial potential of $\psi_0 = -0.001$. The ions are assumed completely cold so that $kT_i/U = 0$ (see Eq. (5.24)). The initial angle θ_0 of each trajectory is given in radians.
- Fig. 8.2 As Fig. (8.1) but with $\rho_0 = 10$.
- Fig. 8.3 As Fig. (8.1) but with $\rho_0 = 20$.
- Fig. 8.4 A plot of the equidensity surfaces computed for a hemispherical boundary surface of radius $\rho_0 = 5$ with an initial potential $\psi = -0.001$. The ions are completely cold so that $kT_i/U = 0$ (see Eq. (5.24)). An equipotential

surface from Fig. (8.1) is also shown.

Fig. 8.5 As Fig. (8.4) but with $\rho_0 = 10$.

Fig. 8.6 As Fig. (8.4) but with $\rho_0 = 20$.

Fig. 8.7 A plot of the trajectories and equipotential surfaces.

Here $\rho_0 = 5$ and $\psi_0 = -0.001$; the ions have a Maxwellian velocity distribution with $kT_i/U = 0.031812$. The initial angle θ_0 of each trajectory is given in radians.

Fig. 8.8 As Fig. (8.7) but with $\rho_0 = 10$.

Fig. 8.9 As Fig. (8.7) but with $\rho_0 = 20$.

Fig. 8.10 A plot of the equidensity surfaces. Here $\rho_0 = 5$ and $\psi_0 = -0.001$; the ions have a Maxwellian velocity distribution with $kT_i/U = 0.031812$. An equipotential surface from Fig. (8.7) is also shown.

Fig. 8.11 As Fig. (8.10) but with $\rho_0 = 10$.

Fig. 8.12 As Fig. (8.10) but with $\rho_0 = 20$.

Fig. 8.13 A plot of the potential variation as a function of ρ for several values of θ . The data comes from Fig. (8.1).
 $\rho_0 = 5, kT_i/U = 0$.

Fig. 8.14 As Fig. (8.13) but with $\rho_0 = 10$.

Fig. 8.15 As Fig. (8.13) but with $\rho_0 = 20$.

Fig. 8.16 A plot of the ion density variation as a function of ρ for several values of θ . This data comes from Fig. (8.4). $\rho_0 = 5, kT_i/U = 0$.

Fig. 8.17 As Fig. (8.16) but with $\rho_0 = 10$.

Fig. 8.18 As Fig. (8.16) but with $\rho_0 = 20$.

Fig. 8.19 A plot of ψ vs. ρ for several values of θ . The data comes from Fig. (8.7). $\rho_0 = 5, kT_i/U = 0.031812$.

- Fig. 8.20 As Fig. (8.19) but with $\rho_0 = 10$.
- Fig. 8.21 As Fig. (8.19) but with $\rho_0 = 20$.
- Fig. 8.22 A plot of n_+ vs. ρ for several values of θ . The data comes from Fig. (8.10). $\rho_0 = 5$, $kT_i/U = 0.031812$.
- Fig. 8.23 As Fig. (8.22) but with $\rho_0 = 10$.
- Fig. 8.24 As Fig. (8.22) but with $\rho_0 = 20$.
- Fig. 9.1 The parameters involved in the calculation of the currents to and the drag on a charged body moving rapidly through a plasma.
- Fig. 9.2 A plot of the current-voltage characteristics for bodies moving rapidly through a plasma. We have plotted here the nondimensional quantities $i_+ \rho_g^2$ vs. $-\psi$. The geometric radius ρ_g appears as a parameter. The data used is drawn from a limited number of calculations in which the shape of the charged body varied so that the curves in the lower part of the graph apply best to somewhat prolate spheroids. The first order correction for a Maxwellian velocity distribution of the ambient ions has been included here; we have taken $kT_e/U = kT_i/U = 0.031812$ (corresponding to a relative velocity $U = 7$ km/sec for a singly ionized oxygen plasma with $T = 1500^\circ\text{K}$). The curves should be only weakly dependent upon the value of T_e and T_i if kT_i or $kT_e \ll U$.
- Fig. 9.3 Plots of $D_T \rho_g^2$ and $D_T' \rho_g^2$ vs. $(-\psi)$ for bodies moving rapidly through a plasma. The geometric radius ρ_g appears as a parameter in both sets of curves. The

curves near the bottom of the graph apply best to somewhat prolate spheroids. These curves include the correction for a Maxwellian velocity distribution of the ambient ions (see Eq. (5.24)); here $kT_e/U = kT_i/U = 0.031812$. The occurrence of negative values of D_T (for $\rho_g = 2$, $\psi \gtrsim 4.6$ and $\rho_g = 3$, $\psi \gtrsim 22$) is discussed in the text.

CHAPTER I

INTRODUCTION

The problem of the screening of bodies at rest or moving in a collisionless plasma is necessary for several fields of investigation, including plasma physics, upper atmosphere and space research, and gaseous discharge research. The complete solution of this problem allows us to calculate the ion and electron currents to a probe embedded in a plasma; the equilibrium surface charge that a body will acquire in the plasma; the potential and density distribution of ions and electrons about the body, and the impact and electric field drag that the body will experience if moving relative to the plasma.

The problem of the screening of a charged body is in many respects similar to the problems of the neutral planetary exosphere¹ and the density of dust near the earth^{2, 3} except each of these problems benefits from the fact that the gravitational potential is everywhere given; the potential does not depend upon the density distribution of the particles as it does in the present case.

The literature on the subject of screening and related subjects is quite extensive, particularly for the case of a rapidly moving body. However, the solutions of the basic problems are either unsatisfactory or severely limited in their applicability. The limitations that beset the existing calculations are:

(a) The assumption of local thermodynamic equilibrium. In almost all practical screening problems, under laboratory or space conditions, the mean free path of particles is found to be large compared with the Debye screening length. Such treatments are,

therefore, unsatisfactory.

(b) The use of a barometric type of formula for the density of screening particles. Although this is equivalent to the previous assumption, it is sometimes used even though calculations are performed that take account of the motions of the particles. This result is generally obtained because of a failure to distinguish between periastron and pericritical orbits (see Chapter II). A barometric formula is applicable only if the body is small and the potential is small.

(c) The assumption that the ion density is constant since the deflection of the ions, which are massive compared to the electrons, is not significant. In the case of the screening of a stationary body, there is no distinction to be made between the screening of a positively charged body and a negatively charged body, if the ion and electron temperatures are equal. Secondly, it must be noted that as a particle with energy kT moves into a region where the potential is greater than kT , it must be subjected to considerable acceleration. It will be found that for satellite velocities, considerable deflections do occur.

(d) The limitation of the calculation to either small potentials or to small bodies. Since potentials on satellites may reach values of $50 kT$ and since the bodies are usually many times the Debye screening distance, these restrictions are of limited value.

(e) The assumption of a finite sheath. It will be shown that the space charge region falls off much slower than previously thought.

Let us now review a few of the more important papers on the

subject of the screening of bodies to see the applicability and the limitations of these works; let us first consider the work that has been done on the problems for stationary bodies imbedded in a plasma.

Mott-Smith and Langmuir⁴ considered the problem of the current to plane, cylindrical and spherical collectors in a plasma as a function of the potential on the bodies. The primary objection to this work is the assumption of a finite screening sheath of unknown thickness. If the body is very large compared to the thickness of the sheath, or if the body is small compared to a Debye length and the potential is small, the resulting error is small. However, the sheath thickness increases as we go to larger potentials or go to larger bodies, so that the body is large compared to the sheath thickness only for very large bodies. There is also no such thing as a finite sheath and, as we will see, the fall off of the potential is very slow. The results of Mott-Smith and Langmuir are, therefore, only satisfactory for very small bodies (compared to the Debye screening length) having moderate potentials.

In addition to the above difficulty with the Mott-Smith and Langmuir expressions, the equations lead to an erroneous asymptotic behavior for the current of attracted particles. In these equations the current of positive ions to a negatively charged collector (or electrons to a positive collector) is limited by the drift of these particles from the ambient plasma into the sheath; the maximum number of particles reaching the surface of the charged body can be no greater than the number drifting to the outer surface of the sheath no matter how negative the body becomes. This, of course, is not so.

There is no finite sheath. The field expands as the potential on the body becomes more negative (or more positive for electrons). The solution must be obtained by a much more detailed approach which we will give in Chapter II.

I. B. Bernstein and I. N. Rabinowitz⁵ have given a treatment of the problem of the screening of stationary charged spheres and infinite cylinders. Their work is severely limited by approximations employed which restrict the generality of their approach and by assumptions which are difficult to accept.

In their preliminary analysis of the types of orbits that will occur for various values of the angular momentum, they assume that the potential varies more slowly than r^{-2} , true only if the body is small and the potential is not large. They justify this by an a posteriori approach resulting in incorrect equations; these equations are then used to justify the original assumption. The authors next conclude that troughs of the effective radial potential energy exist so that ions may be injected by collisions into bound orbits which, they conclude, may result in large ion densities. Therefore, they exclude any consideration of bodies with small radius, thus excluding the only region where the previous assumption might hold (assuming the potential were not too large). Actually, even with a potential that allows for bound orbits, there is no satisfactory means by which particles can be injected into these orbits. Since the potential about the body provides a conservative field, injection can occur only by a process that changes the energy or angular momentum of the particle while in the field. Since the long range collisions between the trapped ion and the plasma particles that remove the ion is much more

important than the short range collision that can inject the ion into a bound orbit, such orbits will be very rarely occupied. The restriction on the size of the body, which these authors used, is therefore, unnecessary. Furthermore their analysis of the orbit types neglects pericritical orbits, i.e., spiral orbits which exist when the potential varies more rapidly than r^{-2} .

Bernstein and Rabinowitz further limit the applicability of their work by requiring that the potential energy $\phi(a) \gg kT_e$ where a is the radius of the body, k is Boltzmann's constant and T_e is the ambient electron temperature. This restriction means that there will be no electron current to the body, a considerable limitation. This condition on the potential of the body is introduced to enable the authors to ignore a formidable problem which arises if the reflection coefficient for the charged body is zero; one finds that the density of attracted particles $n_+ < n_-$, where n_- is the density of the repelled particles, over certain regions, unless a more detailed approach is employed (see Chapter III for further information).

Finally, Bernstein and Rabinowitz treat only a monoenergetic plasma and do not provide any information on the ion and electron density distributions that they obtain from their calculations.

Let us next consider a few of the papers that have dealt with electric screening, drag, and other problems of a rapidly moving body in a plasma.

Singer⁶ in treating the problem of the motion of interplanetary dust was the first to point out the importance of photoelectrons and the accretion of ions and electrons in the calculation of the charge on the dust. This author also provided the earliest calculation of

the electrostatic drag on bodies in interplanetary space, making use of the orbits of the ions in the coulomb field of the body. The calculation includes the effects of the relative velocity on the accretion and drag. Although the complex interdependence of the screening, drag and accretion was recognized in this paper, only approximate results were obtained.

This work was later extended and applied^{7, 8} to the calculation of the lifetime of the West Ford needles. The effects of photoelectrons was considered in greater detail by Singer and Walker⁹ who gave a self-consistent calculation of the screening and space charge distributions produced by photoelectrons.

Jastrow and Pearse¹⁰ considered the very simple case of a charge sheath spherically concentric about a moving charged body, having a uniform density. This treatment neglects the fore-aft asymmetry in ion density, the reduction in density due to the acceleration of ions near the charged body, the increase in density due to focusing effects, and the initial separation of the ion and electron constituents.

Beard and Johnson¹¹ have given an analysis of charging and drag effects on satellites that includes a consideration of the magnetic field. The effects of screening are treated differently from Jastrow and Pearse but the treatment is equivalent; thus the agreement between the papers is to be expected. The sheath is taken to be thin and the potential small. The magnetic field is not included in the calculation of the flux of either the ions or electrons (though for large bodies the Lorentz force on the electrons will be significant); the only magnetic field effect that is included is the

potential gradient along the satellite perpendicular to the magnetic field.

Beard and Johnson¹² in their paper on the "Ionospheric Limitations on Attainable Satellite Potentials" base much of their calculations on the expression for the flux of particles to the surface of a charged body that they derive using conservation of angular momentum, energy, and symmetry considerations. The calculations are equivalent to those by Mott-Smith and Langmuir, but Beard and Johnson do not recognize the limitations on their derivations (they obtain for the flux $(n_0/4) e^{-e\phi_0/kT} (8kT/\pi m)^{1/2}$). This expression is correct for the repelled constituent of the plasma but incorrect for the attracted constituent. For the attracted constituent, the existence of pericritical orbits means that in general

$$\int_0^{2\pi} \int_0^\alpha \cos \theta \sin \theta \, d\theta \, d\phi \neq \pi (1 - 2e\phi_0/mv^2) a^2/R^2 \quad (1.1)$$

(For the correct expression see the derivation of Eq. (2.19) in Chapter II or refer to E. J. Öpik's¹³ treatise on the motion of particles in a field of force.) This occurs because the maximum "pitch" angle (the maximum angle between the radius vector and the velocity vector of a test particle) α_m at any point in the pericritical region satisfies the relation $\alpha_m < \pi/2$. Thus, although angular momentum considerations allow Beard and Johnson's expression $P_m = a (1 - 2e\phi_0/mv^2)^{1/2}$, it is easily shown that when the potential field falls off more rapidly than r^{-2} no particles will satisfy this expression for P_m .

The work of Kraus and Watson¹⁴ is based on linearized equations and relates to bodies small compared to a Debye length in order to

avoid the complexities of hydrodynamic flow. Pitaevskii¹⁵ includes a recalculation of the results of Kraus and Watson. His paper deals primarily with the calculation of radar returns from the plasma perturbations induced by satellites. This work includes the same limitations that Kraus and Watson's work includes; the body is assumed small and linearized equations are used.

S. Rand¹⁶ treated the problem of the formation of the wake behind a cylinder with a radius much smaller than a Debye length and behind a disc, with its surface perpendicular to the direction of motion, having a large radius compared to the Debye length. The potential of the bodies were limited to quite small values so that linearized equations could be employed.

Lundgren and Chang¹⁷ give an approximate solution for the screening of rapidly moving bodies which is constructed from approximate solutions on the front of the body and in the wake at a distance of several body diameters. The solution is appropriate only for bodies very large compared to the Debye length and having a small potential (straight line trajectories are used for the calculation of ion densities).

The most direct approach to the problem of the interaction of a charged body with a plasma has been made by Davis and Harris¹⁸. They used an iterative procedure in which a trial potential field was used to calculate ion trajectories which in turn were used to calculate a new screened potential field. This procedure was repeated until a self-consistent solution was obtained.

The results obtained by Davis and Harris show a rather complex pattern for the ion density distribution in which there

exist several separate regions or pockets of reduced or enhanced density. On the leading surface of the satellite the calculations yield a density distribution that increases toward the axis as though a "singularity" existed along the axis on the front of the body. Such a "singularity" has not been explained by the authors and does not appear to arise from physical conditions. In view of these facts, it is not certain that successive iterations converge toward physically real solutions.

We wish to obtain solutions to the screening problems that will not be subject to the limitations of the above papers. We will obtain exact solutions to the problem of the screening of stationary spheres embedded in a plasma and also we will obtain solutions for the case of rapidly moving bodies which will be limited by less severe restrictions.

As already mentioned, the screening, accretion, density distribution, charging, and drag are complicated by the fact that the potential is not independent of these processes, but is strongly dependent on them. The treatment that we present here provides a self-consistent approach to all of these problems allowing a simultaneous calculation of all these interdependent quantities. Thus we do not make calculations based on an assumed potential or space charge distribution and we do not employ iteration calculations.

CHAPTER II
FORMULAE FOR THE CALCULATION OF THE SCREENING
OF A STATIONARY CHARGED SPHERE

A. Plasma of monenergetic particles. The subject of the screening of charged bodies in a collisionless plasma is best approached by giving consideration to the simplest of the problems, i.e., the screening of a charged sphere at rest relative to the plasma. The body's potential is assumed to be constant in time and not necessarily equal to the equilibrium potential (a wire to the body or high energy electrons in the plasma may be assumed to maintain the potential). The problem can be approached in several ways - principally, by the use of the Boltzmann-Vlasov equation, or by a consideration of the particle trajectory as limited by the conservation of energy and angular momentum. The latter treatment has the advantage that a more complete understanding of the mechanics of the screening process can be gained. We follow the formulation given by E. J. Öpik¹³.

In the neighborhood of any point in a spherically symmetric potential field (see Fig. (2.1)), we can express the potential energy ($\phi = \pm eV$, positive if attractive, negative if repulsive)

$$\phi = Kr^{-n} \quad (2.1)$$

where K and n must be evaluated in that neighborhood. It will be convenient for our calculations to use this expression.

The conservation of angular momentum and energy may be written in terms of the particle velocity v , at r , the impact parameter q , and the velocity of the particle at infinity u by

$$rv \sin \alpha = qu \quad (2.2)$$

and

$$\frac{1}{2} mv^2 = \emptyset + \frac{1}{2} mu^2 \quad , \quad (2.3)$$

where α is the angle between \underline{v} and \underline{r} that will be referred to as the "pitch" angle, and \emptyset is the potential energy of the particle relative to infinity and is positive for an attractive force and negative for a repulsive force. If we write U for the ambient anergy $mu^2/2$ we have on combining the angular momentum and energy equations

$$\sin^2 \alpha = \frac{q^2}{r^2 (1 + \emptyset/U)} \quad . \quad (2.4)$$

This expression can be used to distinguish between two types of particle motions. The first type is called periastron motion. For this type, as r decreases from infinity, there always exists a value of r for which

$$q^2 = r^2 (1 + \emptyset/U) \quad (2.5)$$

so that $\sin^2 \alpha$ becomes unity. Under this condition the space inside this value of r is not accessible to the particle. For a repulsive potential this condition can always be satisfied.

If we now substitute Eq. (2.1) into Eq. (2.4) we have

$$\sin^2 \alpha = \frac{q^2}{r^2 + Kr^{2-n}/U} \equiv q^2/F \quad . \quad (2.6)$$

When $n < 2$, the denominator F always approaches zero as r goes to zero.

However, if $n > 2$, there is a point r_c for which $\sin^2 \alpha$ reaches a maximum value. This value of r is obtained by setting the derivative of F equal to zero

$$\frac{\partial F}{\partial r} = 0 = 2 + 2\emptyset/U + r (d\emptyset/dr)/U, \quad (2.7)$$

or

$$2r_c + (2 - n) K r_c^{1-n}/U = 0 \quad (2.8)$$

which gives for the potential at r_c

$$\emptyset_c = \frac{2U}{(n_c - 2)} \quad (2.9)$$

The value of r_c is

$$r_c = \left[\frac{(n_c - 2) K_c}{2U} \right]^{\frac{1}{n_c}}, \quad (2.10)$$

where the subscripts refer to the values of the quantities at corresponding value of r_c . Thus, inside r_c the particle spirals toward the origin. Here the orbit is called pericritical. For a given value of q , the maximum value of α is obtained from Eq. (2.4)

$$(\sin^2 \alpha)_{\max} = q^2 \frac{(n_c - 2)^{(n_c-2)/n_c}}{n_c} \left(\frac{2U}{K_c} \right)^{2/n_c} \quad (2.11)$$

We note that n_c and K_c depend on U , but on nothing else. Hence $(\sin^2 \alpha)_{\max}$ varies directly as q^2 . Evidently, the limiting condition for entry into the pericritical region is

$$(\sin^2 \alpha)_{\max} \leq 1 \quad (2.12)$$

For entry into the periastron region the right side of (2.11) must become greater than 1 and $(\sin^2 \alpha)_{\max} = 1$. Thus Eq. (2.11) sets a lower limit on q_p for the target radius of periastron type orbits for the case $n > 2$,

$$q \geq q_p = n_c^{\frac{1}{2}} (K_c/2U)^{1/n_c} (n_c - 2)^{-(n_c-2)/2n_c} \quad (2.13)$$

or

$$q_p = r_c \sqrt{n_c / (n_c - 2)} \quad . \quad (2.14)$$

Particles satisfying Eq. (2.13) will enter along a periastron trajectory and emerge from the field in a way similar to a hyperbolic trajectory. Those with $q < q_p$, however, will always make an angle of less than 90° with the radius and spiral inwards until the particle hits the body or otherwise has its orbit changed. These orbits are of the pericritical type.

We are now in a position to calculate the accretion of particles through a spherical surface. The number of particles passing through a target ring q to $q + dq$ (see Fig. (2.1)) is

$$dA_q = 2\pi q dq u N_0 \quad , \quad (2.15)$$

where N_0 is the ambient density. Now from Eq. (2.4) we have

$$q dq = r^2 (1 + \emptyset/U) \sin \alpha \cos \alpha d\alpha \quad . \quad (2.16)$$

Thus

$$dA_\alpha = 2\pi r^2 u N_0 (1 + \emptyset/U) \sin \alpha \cos \alpha d\alpha \quad . \quad (2.17)$$

The integral of this for the periastron case for which all values of α are allowed is

$$\begin{aligned} A_{pa} &= 2\pi r^2 u N_0 (1 + \emptyset/U) \int_0^{\pi/2} \sin \alpha \cos \alpha d\alpha \\ &= \pi r^2 u N_0 (1 + \emptyset/U) \quad . \end{aligned} \quad (2.18)$$

Now for the pericritical interaction, where $\emptyset > 0$, $n > 2$ and $r < r_c$, the accretion is constant, involving all the particles that have reached the pericritical surface, r_c . Thus, the accretion has the

same value for all $r < r_c$:

$$A_{pc} = \pi r_c^2 u N_0 (1 + \emptyset_c/U) \quad (2.19)$$

This result is also obtained by using the limits 0 to α_{\max} in the integration of Eq. (2.18).

The particle density can now be obtained in terms of the potential energy from the above accretion formula. Thus, we have the density contributed by particles moving at an angle between α and $\alpha + d\alpha$

$$dN = dA/4\pi r^2 v \cos \alpha = \frac{1}{2} N_0 (1 + \emptyset/U)^{\frac{1}{2}} \sin \alpha d\alpha \quad (2.20)$$

For periastron orbits an integration of this yields

$$N_{pa} = \frac{1}{2} Q N_0 (1 + \emptyset/U)^{\frac{1}{2}} \int_0^{\pi/2} \sin \alpha d\alpha = \frac{1}{2} Q N_0 (1 + \emptyset/U)^{\frac{1}{2}} \quad (2.21)$$

The factor Q is the return factor. If a particle that passes through the spherical surface at r is elastically reflected by the body so as to return and again pass through the surface at r , the particle orbit must be counted twice and, thus, the return factor will have a value 2 for this particle. If the particle is absorbed and does not return, the value is 1 for this orbit. The return factor in Eq. (2.21) is an average value of the return factor taken over all particles. If the collision is inelastic, a more involved calculation may become necessary. It will be found, however, that inelastic collisions are not important since the reflection coefficient for both ions and electrons is small^{19, 20, 21, 22}. Furthermore, although secondary electrons are produced, they ordinarily can be neglected; a calculation that includes their effect will be made in Section G.

The density relation expressed in Eq. (2.21) is the same expression derived by Singer^{2, 3} for the problem of gravitational accretion of interplanetary dust. As shown here, Eq. (2.21) is applicable not only for the $1/r$ gravitational potential but for any potential field satisfying the periastron conditions.

The expression for the density in the case of pericritical interaction is obtained by an integration of Eq. (2.20) over the limits 0 to α_{\max} , where α_{\max} is given by Eq. (2.11):

$$N_{pc} = \frac{1}{2} Q N_0 (1 + \phi/U)^{\frac{1}{2}} \left\{ 1 - \left[1 - \frac{q_p^2}{r^2 (1 + \phi/U)} \right]^{\frac{1}{2}} \right\} \quad (2.22)$$

Equations (2.21) and (2.22) completely define the density of the ions and electrons anywhere in the screened electric field of the charged body. If N_- is the density of electrons and N_+ is the density of ions (here taken to be singly ionized), then the Poisson equation for spherical symmetry becomes

$$\frac{d^2 \phi}{dr^2} = 4\pi e^2 (N_- - N_+) - \frac{2}{r} \frac{d\phi}{dr} \quad (2.23)$$

Equation (2.23) can be rewritten in nondimensional form by expressing r in terms of the Debye length and ϕ in terms of the energy U of the plasma particles. However, since it is customary to express the potential in terms of the temperature T of the plasma, let us write $U = \frac{1}{2} m u^2 \approx \frac{3}{2} kT$ and define the nondimensional potential and radius to be

$$\begin{aligned} \psi &= \phi/kT & T &\approx 2U/3K \\ \rho &= r/h \end{aligned} \quad (2.24)$$

where k is the Boltzmann constant and h is the Debye screening distance as given by

$$h = \sqrt{\frac{kT}{4\pi e^2 N_0}} \quad (\text{cgs}),$$

$$h = \sqrt{\frac{\epsilon_0 kT}{e^2 N_0}} \quad (\text{MKS}) \quad (2.25)$$

where e is the electronic charge and N_0 is the ambient density.

If we consider the charged body to be negative (this choice is made for convenience only; the results hold equally well for a positive body), then the electron density will be given by Eq. (2.21), since the field is repulsive to the electrons. Thus we can write, using the definitions of Eq. (2.24),

$$n_- = N_-/N_0 = \frac{1}{2} Q (1 - \frac{2}{3} |\psi|)^{\frac{1}{2}} \quad (2.26)$$

Since the field is attractive to the ions, the ion density will be given by Eq. (2.21) in the periastron region and by Eq. (2.22) in the pericritical region. To be in the pericritical region the exponent n must be greater than 2 and r must be less than r_c as defined by Eq. (2.10). Thus, the ion density will be

$$n_+ = N_+/N_0 = \frac{1}{2} Q (1 + \frac{2}{3} |\psi|)^{\frac{1}{2}} W \quad (2.27)$$

where

$$W = \begin{cases} 1 & \text{when } n \leq 2 \text{ or when } (|n - 2| \psi/3)^{\frac{1}{n}} \leq 1 \\ 1 - [1 + \frac{n (|n - 2| \psi/3)^{\frac{1}{n}}}{|n - 2| (1 + 2\psi/3)}]^{-\frac{1}{2}} & \text{in all other cases.} \end{cases} \quad (2.28)$$

We can now write the Poisson equation, Eq. (2.23), as

$$\psi'' = n_- - n_+ - 2\psi'/\rho \quad (2.29)$$

where $\psi' = d\psi/d\rho$, $\psi'' = d^2\psi/d\rho^2$.

The value of n must be evaluated at each point in the integration of Eq. (2.29) since the potential does not follow a simple power law over a wide range of r .

B. Results of calculations for a plasma of monoenergetic particles. The integration of Eq. (2.26) using Eqs. (2.27), (2.28) and (2.29) for densities of the screening particles was obtained by numerical methods. The self-consistent field calculation proceeded from a position ρ_0 , for which a small value of the potential ψ_0 was specified, toward the origin (rather than starting from the surface of the charged body).

Approximating Eqs. (2.26) and (2.27) for small values of ψ and substituting in Eq. (2.29) gives a linear differential equation with a general solution of the form

$$\psi = \frac{A}{\rho} e^{-\sqrt{Q/3} \rho} \quad (2.30)$$

This expression can be used to obtain ψ_0' , the initial values of ψ'

$$\psi_0' = - (1 + \sqrt{Q/3} \rho_0) \psi_0 / \rho_0 \quad (2.31)$$

For a Maxwellian distribution 2 should replace $Q/3$; see Eq. (2.68).

(Small errors in the initial conditions will be automatically damped out with a proper choice for the integration integral $\Delta \rho$. See Chapter VII for a discussion of this point.) This procedure produces curves that are independent of the radius of the charged sphere provided either that few electrons reach the surface of the body or that the value of Q is 2. We have set the return factor for the electrons and for the ions to be equal in this calculation. It can be included as an additional parameter in ψ by setting $\psi = \frac{2\phi}{Q kT}$.

It is this function which is plotted in the curves.

In Fig. (2.2) we have plotted $\log \psi$ against $\log \rho$, to obtain a family of curves. As an example of the use of these curves, assume a body with a radius of 23 Debye lengths has a potential of 15 kT. This corresponds to point A and thus the potential falls off from A along curve e. A curve connecting the pericritical surfaces is shown along with the equilibrium potential curve for a hydrogen plasma. The curve for the pericritical surface is approximately a straight line satisfying $\psi_c \rho_c = 3.68$.

The potential curves fall off much more slowly than in the case of local thermodynamic equilibrium. This is shown in Figs. (2.3) and (2.4) using the linearized solution for the case of local thermodynamic equilibrium. Here we plot the ratio h^*/h against ρ , where h^* is the value of the Debye length necessary in the local thermodynamic equilibrium screening formula (see Eq. (2.68)) for ϕ_D to make $\phi_D(h^*, r) = \phi(h, r)$ and $\phi_D'(h^*, r) = \phi'(h, r)$ in our calculation for a given point. A set of curves are given which correspond to the set of curves in Fig. (2.2). Thus the Debye type formulation gives a much stronger screening than that presented here. The reason for this becoming obvious on consideration of the plots. The most interesting curves of N_+/N_0 and N_-/N_0 plotted against ρ , as shown in Figs. (2.5) and (2.6). In these curves the density of the ions first rises slightly, then falls rapidly to quite low values and finally rises rapidly as the screening particles converge toward the origin; the density of the electrons falls rapidly to zero. For the case of local thermodynamic equilibrium, the ion density does not drop off but rises exponentially.

C. Plasma of particles with a Maxwellian velocity distribution.

A derivation for the screening equations for the case of a charged sphere embedded in a plasma having a Maxwellian velocity distribution has been given by E. J. Öpik¹³. Since certain expressions must be expressed in a different form to be used in numerical calculations and since additional consideration must be given to the pericritical case, we will repeat briefly Öpik's derivation and include these modifications.

For a plasma with a velocity distribution Eqs. (2.21) and (2.22) can be used to relate the (differential) density, dN_0 , of ambient particles in the velocity range u to $u + du$ to their (differential) density dN_{pa} or dN_{pc} at a point in the potential field of the charged body. Replacing dN_{pa} and dN_0 for N_{pa} and N_0 in Eq. (2.21), we have

$$dN_{pa} = \frac{1}{2} Q (1 + \phi/U)^{\frac{1}{2}} dN_0 \quad (2.32)$$

For the density of ambient particles with velocity in the range u to $u + du$ in the case of a Maxwellian velocity distribution dN_0 is given by

$$dN_0 = N_0 P_x dx \quad (2.33)$$

where

$$P_x dx = \frac{4}{\sqrt{\pi}} x^2 e^{-x^2} dx \quad (2.34)$$

and

$$x = (m/2kT)^{\frac{1}{2}} u ; \quad \text{or } U = \frac{1}{2} mu^2 = kT x^2 \quad (2.35)$$

By integrating Eq. (2.32) over the proper limits for the case of repulsion we obtain

$$N_r = \frac{1}{2} Q N_0 e^{\theta/kT} ; \quad (\theta < 0) \quad (2.36)$$

For pericritical attraction we integrate over $dN_a = dN_r$, the limits differing from the case of repulsion, to obtain

$$N_a = \frac{1}{2} Q N_0 \left[\frac{2}{\sqrt{\pi}} \sqrt{\theta/kT} + \theta \left(\sqrt{\theta/kT} \right) e^{\theta/kT} \right] ; \quad (\theta > 0, n < 2) \quad (2.37)$$

where the function $\theta(x)$ is given by

$$\theta(x) = \frac{2}{\sqrt{\pi}} \int_x^\infty e^{-y^2} dy \quad (2.38)$$

For the general case in which some particles are pericritical and the rest are periastron we integrate dN_a over all those particles that are periastron and for the pericritical particles we use dN_{pc} corresponding to Eq. (2.22)

$$\begin{aligned} dN_{pc} &= \frac{1}{2} Q N_0 (1 + \theta/U)^{\frac{1}{2}} \left\{ 1 - \left[1 - \frac{q_p^2}{r^2 (1 + \theta/U)} \right]^{\frac{1}{2}} \right\} P_x dx \\ &= dN_a + \frac{1}{2} Q N_0 [(1 + \theta/U) - q_p^2/r^2]^{\frac{1}{2}} P_x dx \quad (2.39) \end{aligned}$$

At a given position r and with $n > 2$, the ambient kinetic energy U will determine whether a particle is pericritical or periastron. According to Eq. (2.9) a particle is pericritical if $U < U_c$ and periastron is $U > U_c$ where

$$U_c = \frac{n-2}{2} \theta \quad (2.40)$$

The total density, N_p , will be obtained by an integration of dN_{pc} from 0 to U_c and dN_a from U_c to ∞ . Thus we obtain

$$N_p = \int_0^\infty dN_a + \frac{1}{2} Q N_0 \int_0^{U_c} [(1 + \theta/U) - q_p^2/r^2]^{\frac{1}{2}} P_x dx \quad (2.41)$$

where

$$x_c^2 = U_c/kT \quad (2.42)$$

The integral over dN_a is given by Eq. (2.37). If we write

$$Z = x^2, \quad Z_c = x_c^2,$$

$$\psi = \phi/kT, \quad \rho = r/h \quad (2.43)$$

we obtain for N_p :

$$N_p = \frac{1}{2} Q N_0 \left\{ \frac{2}{\sqrt{\pi}} \psi^{\frac{1}{2}} + \theta(\psi^{\frac{1}{2}}) e^{\psi} - \frac{2}{\sqrt{\pi}} \int_0^{Z_c} \left[Z + \psi - \frac{\rho_c^2}{\rho^2} (Z + \psi_c) \right]^{\frac{1}{2}} e^{-Z} dZ \right\} \quad (2.44)$$

where q_p has been replaced by $r_c \sqrt{1 + \phi_c/U}$, ϕ_c being a function of r_c . In a numerical integration of Poisson's equation the integral in Eq. (2.44) must be evaluated at each point in a step-by-step integration. The integration must begin at a boundary condition at a large distance from the charged body and proceed to the surface of the body. We find as we proceed to smaller values of ρ and higher values of ψ that particles with increasingly higher values of U will attain pericritical trajectories. Thus it is necessary to compile a table of ψ_c and ρ_c for successive values of U_c as they are reached in the integration.

A complication arises if Z_c , the limit on the integral in Eq. (2.44), rises to a maximum value Z_m (as the integration proceeds from the boundary condition toward the surface of the charged body) and then drops in value. The integral in Eq. (2.44) extends over all pericritical trajectories. Pericritical means that all particles

with ambient energy U will have velocity vectors confined to a cone of angle 0 to α_{\max} , $\alpha_{\max} < \pi/2$ (see Fig. (2.7)).

In order for particles with ambient energy U to become pericritical they must enter a region where $n > 2$. It does not follow, however, that they will become periastron where n again becomes less than 2. The upper limit on the integral in Eq. (2.44) must be selected accordingly. Thus Z_c must be chosen to correspond to the value of Z for which $\alpha_{\max} = \pi/2$. This condition yields

$$\rho_c^2 (Z_c + \psi_c) / \rho^2 (Z_c + \psi) = 1 \quad (2.45)$$

The complete set of equations for the solution of the screening problem where the plasma has a Maxwellian velocity distribution includes Eq. (2.26) where for a negatively charged body N_- is given by N_r , Eq. (2.36), and N_+ is given by N_p , Eq. (2.44). Since the mass of the ions and electrons does not appear in the basic equations, the results will be identical for a positively charged body except for the sign. The variable Z_c is given by Eqs. (2.42) and (2.43); if Z_c drops from its maximum value, it is given by Eq. (2.45).

Using Eq. (2.18) and making the changes made in the transition from Eq. (2.21) to Eq. (2.32), the differential expression for the accretion of attracted particles with a Maxwellian velocity distribution is

$$dA_r = \pi r^2 N_0 u (1 + \phi/U) P_u du \quad (2.46)$$

where r is the radius of the spherical surface and

$$P_u du = \sqrt{\frac{2}{\pi}} \left(\frac{m}{kT}\right)^{3/2} u^2 e^{-mu^2/2kT} du \quad (2.47)$$

Here it is assumed that ϕ is positive for an attractive field. Substituting

$$Z = U/kT = mu^2/2kT; \psi = \phi/kT \quad (2.48)$$

we obtain

$$dA_r = \sqrt{\frac{8\pi kT}{m}} N_o r^2 (Z + \psi) e^{-Z} dZ. \quad (2.49)$$

The total accretion is obtained by integrating (2.49) over all Z . It must be remembered, however, that r and ψ will become $r_c(Z)$ and $\psi_c(Z)$ for all particles that are pericritical at r, ψ . Thus

$$A_r = \sqrt{\frac{8\pi kT}{m}} N_o \left\{ r^2 \int_{Z_c}^{\infty} (Z + \psi) e^{-Z} dZ + \int_0^{Z_c} r_c^2(Z) [Z + \psi_c(Z)] e^{-Z} dZ \right\} \quad (2.50)$$

where Z denotes pericritical energies within the range $0 < Z < Z_c$.

The first integral in Eq. (2.50) yields

$$e^{-Z_c} (1 + Z_c + \psi); \quad (2.51)$$

therefore,

$$A_r = \sqrt{\frac{8\pi kT}{m}} N_o \left\{ r^2 (1 + Z_c + \psi) e^{-Z_c} + \int_0^{Z_c} r_c^2(Z) [Z + \psi_c(Z)] e^{-Z} dZ \right\} \quad (2.52)$$

where, from Eq. (2.40),

$$Z_c = \begin{cases} \frac{n-2}{2} \psi & \text{for } n > 2 \\ 0 & n \leq 2 \end{cases} \quad (2.53)$$

Expressing the accretion for the attracted particles in a nondimensional form T_+ ,

$$T_+ = \frac{A_r}{N_0 h^2} \sqrt{\frac{m}{8\pi kT}} \\ = \rho^2 (1 + Z_c + \psi) e^{-Z_c} + \int_0^{Z_c} \rho_c^2(Z) [Z + \psi_c(Z)] e^{-Z} dZ \quad (2.54)$$

Again, let us mention that ψ is positive for an attractive field.

A comparison of Eq. (2.54) with the corresponding equation derived by Mott-Smith and Langmuir⁴ shows that the two expressions are completely different. Their results, based on the assumption that the screened field may be treated as a finite sheath, do not appear to be consistent with our results.

Opik¹³ has shown that the accretion A_r' of the repelled particles, having a Maxwellian velocity distribution at infinity is

$$A_r' = \pi r^2 N_0 u_s \sqrt{8/3\pi} e^{3\phi/m' u_s^2} \quad (\phi < 0) \quad (2.55)$$

where m' is the mass of the repelled particles as opposed to m for the attracted particles and u_s is given by

$$u_s = \sqrt{3kT/m'} \quad (2.56)$$

Therefore, we can write A_r' in terms of $\rho = r/h$ and $\psi = \phi/kT$.

$$A_r' = \sqrt{\frac{8\pi kT}{m'}} N_0 h^2 \rho^2 e^{\psi} \quad (2.57)$$

Multiplying A_r' by $\sqrt{m/8\pi kT} / N_0 h^2$ as in Eq. (2.54) we obtain

$$T_- = \frac{A_r'}{N_0 h^2} \sqrt{\frac{m}{8\pi kT}} = \sqrt{\frac{m}{m'}} \rho^2 e^{\psi} \quad (2.58)$$

This result is identical to that of Mott-Smith and Langmuir⁴ for a repulsive field.

The total current I_s to the body is

$$I_s = e N_0 h^2 \sqrt{\frac{8\pi kT}{m}} [T_+ - T_-] \Big|_{\rho = \rho_s} \quad (2.59)$$

where e is the electronic charge and ρ_s is the radius of the body in Debye lengths. In order for the charge on the body to be in equilibrium with the current from the plasma, the current to the body must zero,

$$I_s = 0 \quad (2.60)$$

Substituting Eq. (2.59) for the current into Eq. (2.60) and changing the former definition of ψ so that it is positive when ions are repelled and electrons are attracted we obtain

$$\begin{aligned} \frac{1}{\sqrt{\tau}} \rho_s^2 (1 + \tau Z_c - \tau \psi_s) e^{-\tau Z_c} + \tau^{\frac{3}{2}} \int_0^{Z_c} \rho_c^2(Z) [Z - \psi_c(Z)] e^{-\tau Z} dZ \\ = \sqrt{\frac{m_i}{m_e}} \rho_s^2 e^{\psi_s} \end{aligned} \quad (2.61)$$

Here we have included the ion and electron temperatures T_i, T_e in $\tau = T_e/T_i$. The value of Z_c must be that appropriate for the surface of the charged body; m_i and m_e are the ion and electron mass, respectively. We have defined ψ_s and ρ_s in terms of the electron temperature.

For a sufficiently small value of ρ_s (about 5 or less) Z_c will be approximately zero. For this approximation the integral in Eq. (2.61) is zero. We obtain for ψ_s therefore

$$\psi_s = -\ln [\sqrt{\tau m_i/m_e} / (1 - \tau \psi_s)] \quad (2.62)$$

For moderately large to large values of ρ_s we can approximate $\rho_c \approx \rho_s$ since the pericritical surface will lie close to the surface of the

body. The integral in Eq.(2.61) becomes

$$\frac{1}{\tau} \int_0^{Z_c} \rho_c^2(Z) [Z - \psi_c(Z)] e^{-\tau Z} dZ$$

$$\approx \sqrt{\tau} \rho_s^2 \left[\frac{1}{\tau} (1 - e^{-\tau Z_c} - \tau Z_c e^{-\tau Z_c}) - \bar{\psi}_c (1 - e^{-\tau Z_c}) \right] \quad (2.63)$$

where $\bar{\psi}_c$ is the averaged value of ψ_c . For moderately large values of ρ_s (about 20) Z_c is small and thus $\exp(-Z_c)$ will be nearly 1. We have in that case from Eq. (2.61)

$$\psi_s = -\ln \left[\sqrt{\tau m_i / m_e} / (1 - \tau \psi_s) \right] \quad (2.64)$$

If ρ_s is large, then Z_c will be large and $\bar{\psi}_s$ will be close to ψ_s in value. Assuming $\bar{\psi}_c = k\psi_s$ where $1 > k \gtrsim 0.5$, we obtain from Eq. (2.61)

$$\frac{1}{\sqrt{\tau}} \left[1 - \tau \bar{\psi}_c + \tau e^{-\tau Z_c} (\bar{\psi}_c - \psi_s) \right] - \sqrt{m_i / m_e} e^{\psi_s} = (1 - \tau k \psi_s) / \sqrt{\tau} - \sqrt{m_i / m_e} e^{\psi_s} = 0. \quad (2.65)$$

Therefore, rewriting Eq. (2.65) we have

$$\psi_s = -\ln \left[\sqrt{\tau m_i / m_e} / (1 - \tau k \psi_s) \right] \quad (2.66)$$

Thus we obtain the same or approximately the same expression for ψ_s in each case.

Evaluating Eq. (2.62) or (2.64) for a plasma of ionized hydrogen, $m_i / m_e = 1836.5$ and $T_e = T_i$, yields $\psi_s = -2.504$. Using Eq. (2.66) to obtain ψ_s for large ρ_s yields $\psi_s = -2.87$ where $k = 0.5$. We see, therefore, that the value of ψ_s is fairly insensitive to the value of k . For a plasma of ionized oxygen, $m_i / m_e = 29167$ and $T_e = T_i$ we find using Eq. (2.62) $\psi_s' = -3.61$.

The results of the numerical calculation (section D) may be compared to the above values for ψ_s . For a hydrogen plasma in which $T_e = T_i$ the numerical calculations give $\psi_s = 2.508$ for $\rho_s = 0.0013$, $\psi_s = 2.811$ for $\rho_s = 3.83$

and $\psi_s = 3.495$ for $\rho_s = 83.67$. In the case of an oxygen plasma the values are $\psi_s = 3.669$ for $\rho_s = 0.0064$, $\psi_s = 4.418$ for $\rho_s = 11.45$ and $\psi_s = 4.856$ for $\rho_s = 82.77$. The above approximate equations for ψ_s (Eqs. (2.62), (2.64), (2.66)) appear to be valid and applicable for smaller values of ρ_s than anticipated.

D. Results of Calculations for a Plasma of Particles with a Maxwellian Velocity Distribution.

The numerical solution of Eq. (2.26) using Eqs. (2.36), (2.44), (2.42) and (2.45) is obtained for a plasma with a Maxwellian velocity distribution in the same way it was obtained for a plasma of monoenergetic particles. A self-consistent field calculation begins at the point ρ_0 where we specify an arbitrary but small value for $\psi = \psi_0$, the nondimensional potential. The calculations proceed from ρ_0 toward the origin. To start from the surface of the body and calculate toward the edge of the sheath would require an iterative procedure.

As in Section B of this chapter, the formula derived for the screening under local thermodynamic equilibrium provides an approximate value for ψ_0 (See Eq. (2.31)) and any error in the initial conditions will be damped out if $\Delta\rho$ is sufficiently small. Again, we have used $Q = 2$ in our calculation but Eq. (2.31) may be used to obtain results for $Q = \frac{1}{2}$.

To obtain the ion and electron currents to a spherical surface of radius ρ , which may be the surface of a body, or a surface concentric to the body, we evaluated Eq. (2.54) and (2.58) at every point with $m' = m_e$ (electron mass), $m = m_p$ (proton mass), and m_o (oxygen mass). The evaluation of Eq. (2.54) for the ion (in the case of a negative body) current and Eq. (2.44) for the ion density involves an integration at each point.

Figure (2.8) shows a logarithmic plot of ψ versus ρ . This plot corresponds to Fig. (2.2) in which the results for the monoenergetic equations were presented. The labels for these curves $\rho_0 = 5, 10, 20$ etc. refer to the initial value of ρ at which $\psi = \psi_0$ ($\psi_0 = 0.001$ or less for every curve). Starting at any point on one of the family of curves, we have a pair of values ρ', ψ' which can be set equal to ψ_s, ρ_s , the radius of a spherical body and its potential. The remainder of the curve (for $\rho > \rho_s$) gives the relation $\psi(\rho)$ for this particular situation (i.e., for ψ_s, ρ_s). The portion of the curve where $\rho < \rho_s$ is inside the body and has no application for the particular example. For a demonstration of the use of Fig. (2.8) refer to Fig. (2.2).

For a plasma of particles having a Maxwellian velocity distribution the ambient energy U of particles takes on all values. Thus there is no one pericritical surface for all particles. In Fig. (2.8) we therefore illustrate the ψ_p, ρ_p curve where ρ_p is the radius of the pericritical surface for particles of energy U/kT and ψ_p is the potential for that surface.

When the ion current to a body equals the electron current to that body, the potential on the body will be in equilibrium (Eq. (2.60)). Since we can calculate the ion current using Eq. (2.54) and the electron current using Eq. (2.58) step-by-step as we calculate $\psi(\rho)$ we can obtain the ψ, ρ curve for which the total current to the body is zero. The resulting curve for the equilibrium potential ψ_e vs. ρ is shown in Fig. (2.8). Results for both a hydrogen plasma and an oxygen plasma are illustrated. It will be noted that the results are similar to those already obtained (see Eq. (2.64)).

In Fig. (2.9) we show a continuation of the logarithmic plot of ψ and ρ extended to small values of ρ . There are no pericritical surfaces here. The curves are almost straight, yielding an approximate equation

$$\psi = k\rho^{-1} \quad \rho \ll 1 \quad (2.67)$$

which is also to be expected from the solution of the linearized form of

$$\nabla^2 \psi = e^{+\psi} - e^{-\psi} \quad (\text{using our sign convention})$$

$$\psi = \psi_s e^{-\sqrt{2}(\rho - \rho_s)} \quad \rho_s / \rho \quad (2.68)$$

which becomes

$$\psi = \psi_s \quad \rho_s / \rho \quad (2.69)$$

for $\rho \ll 1$.

The equilibrium potentials for an ionized hydrogen and a singly ionized oxygen plasma are shown. They are nearly constant throughout the range of ρ .

In Fig. (2.10) we have plotted $\psi(\rho)$ using a linear scale for ρ . The coordinate $\rho_0 - \rho$ used gives the distance from the initial point ρ_0 of the numerical calculations. The origin for a particular curve in Fig. (2.10), therefore, will be at $\rho_0 - \rho = \rho_0$ (rather than $\rho_0 - \rho = 0$). It will be seen that for $\rho_0 = 100$, ψ increases from 0.001 to 1.0 in about 13.5 Debye lengths. This should be compared with about 5 Debye lengths using the solution to the linearized equation (see Eq. (2.68)).

This difference arises from differences in the screening equations derived here and the solution to the linearized screening equation using $n_{\pm} = e^{\pm\psi}$ for the densities. The basic difference lies in the existence of pericritical orbits, ignored in the simple $e^{\pm\psi}$ expression for densities. As may be seen in Fig. (2.8), all particles with energy less than 8 kT are pericritical on the $\rho_0 = 100$ curve before $\psi = 1$. In addition, a distance of seventy-five Debye lengths is required for a six order increase ($\psi = 10^{-3}$ to 10^3) in the potential, compared with 15 Debye lengths using Eq. (2.68).

An example of the use of ψ, ρ curves is shown in Fig. (2.10). The position corresponding to a body of radius 10 Debye lengths and potential

energy 10 kT is shown. The dashed curve shows the subsequent drop in the potential.

The variation in the density of the ions (or attracted particles) for a plasma with a Maxwellian velocity distribution, Fig. (2.11), shows the same general features as the monoenergetic case Figs. (2.5) and (2.6). The density drops as the screening ions are accelerated by the electric field and then increases as the ions converge toward the origin. There still exists for some values of ρ_0 a slight increase in density, initially followed by a decrease and then a large rise in density (observe $\rho_0 = 10$ in Fig. (2.8)), but this is much less pronounced than for a monoenergetic plasma.

Figure (2.12) gives the difference between the ion density and the electron density, $n_+ - n_-$, again plotted against $\rho_0 - \rho$. The initial rise in the curve indicates the drop in the electron density and the rise in the ion density. For the larger distances, however, the ion density also drops as a result of the acceleration of the ions. For smaller initial values of ρ_0 , this dip does not occur since the convergence of the particles toward the origin (thereby occupying a smaller volume) is more important than their acceleration.

E. Current-voltage characteristics for a sphere embedded in a plasma with a Maxwellian velocity distribution; comparison with Mott-Smith and Langmuir equations. As we have seen, the ion current (if the body is negative, electron current if positive) to any surface concentric to the surface of the body, as well as to the body itself can be obtained using Eq. (2.54), and the electron current from Eq. (2.58). Figure (2.13) shows a plot of the quantity $\log_{10} (1 + T_+)$ versus $\rho_0 - \rho$. (This function of T_+ is used so we can

include both large values of T_+ and $T_+ = 0$.) Let us consider how this graph is to be used. The example in Fig. (2.10) for a body of radius 10 Debye lengths and potential energy 10 kT shows that the surface of the body lies at $\rho_0 - \rho = 10.15$. In Fig. (2.13) the point corresponding to the surface of this body lies slightly off the $\rho_0 = 20$ curve as indicated. The value of T_+ , the nondimensional current, at the surface of the body is $T_+ = 214$ for this example.

In Fig. (2.14) the same quantity, $\log_{10}(1 + T_+)$, is plotted against $\rho_0 - \rho$ for small values of ρ_0 . The curves in this graph correspond to the ψ, ρ curves in Fig. (2.9).

In Fig. (2.15) the total nondimensional current for both ions and electrons is given. The graph is similar to Fig. (2.13). Since $(T_+ - T_-)$ is initially a negative quantity, it is necessary to take the absolute value. When the total current to the body is zero, $\log_{10}(1 + |T_+ - T_-|)$ equals zero. The value of $\rho_0 - \rho$ for which the total current is zero can be used with Fig. (2.8) or (2.10) to obtain the equilibrium potential.

Figure (2.16) shows $\log_{10}(1 + |T_+ - T_-|)$ plotted against $\rho_0 - \rho$ for small values of ρ_0 . The curves in this graph correspond to the ψ, ρ curves in Fig. (2.9).

As seen above in the examples, the use of Figs. (2.13) and (2.14) is rather cumbersome. It is more useful to plot T_+ vs. ψ_s for bodies of various radius ρ_s , the subscript referring to the value of the quantity at the surface of the body. This gives the current-potential probe characteristics for probes of various sizes. Mott-Smith and Langmuir⁴ (we will use MSL as an abbreviation) derived equations for the probe characteristics of flat planes, for infinitely long cylinders, and for spheres for both a monoenergetic and a Maxwellian velocity distribution.

For the probe characteristics of spherical bodies their expression for the repelled constituent of the plasma (electrons, if the body is negative) is identical with our result, Eq. (2.58). The MSL equation for the attracted constituent (ions, for a negative body) is quite different from our results; expressed in terms of the nondimensional current (see Eq. (2.54)) they obtain,

$$T_+^{MSL} = \alpha^2 \left\{ 1 - (1 - \rho_s^2/\alpha^2) \exp [-\rho_s^2 |\psi_s|/(\alpha^2 - \rho_s^2)] \right\} \quad (2.70)$$

where ρ_s is the radius of the body in terms of the Debye length, h , and α is the nondimensional distance from the center of the body to the outer edge of the ion sheath around the body. These authors assume the sheath has a sharp edge and therefore, is essentially finite in thickness. No equation is given for the thickness of this sheath, nor is there a satisfactory criterion for estimating the sheath thickness. The sheath is, however, assumed by Mott-Smith and Langmuir to be of the order of a Debye length. If so, the exact value would not be necessary in order to obtain accurate calculations for very small or very large bodies. Our work does not support these assumptions in general. However, if $\rho_s \ll \alpha$ and $\rho_s \psi_s \ll 1$, Eq. (2.54) reduces to the same expression as T_+^{MSL} , Eq. (2.70); namely, $T_+ = \rho_s^2 (1 + \psi_s)$.

Figure (2.17) illustrates the current-voltage characteristics for a spherical probe obtained in the numerical solutions of the screening using Eq. (2.54) for T_+ . The radius appears as a parameter of the family of curves. For small values of the potential, the current depends primarily on the geometric cross-section. As the potential increases on the body, the current increases without any apparent limit.

Figure (2.17) also shows three typical Mott-Smith and Langmuir

characteristics using Eq. (2.70) for T_+^{MSL} . For ρ_s , the nondimensional radius of the charged body, equal to 5 we show T_+^{MSL} using for the sheath thickness the values 1 and 5, making $\alpha = 6$ and 10. Sheaths of such thickness are commonly used and have been considered satisfactory by many workers. This arises, however, from a misunderstanding of the complexity of the screening problem. The space charge about a probe is not properly represented by a finite sheath. We find, therefore, in Fig. (2.17) that T_+^{MSL} does not resemble T_+ . The Mott-Smith, Langmuir function underestimates for potentials below 1 kT, gives too large an increase near 1 kT (rising exponentially), and finally for larger values of ψ , T_+^{MSL} approaches the value α^2 as an upper limit. It is the asymptotic behavior of T_+^{MSL} for large ψ that is particularly objectionable about the Mott-Smith, Langmuir equations. The theory is misleading, for it implies that the current approaches a maximum value which depends upon the rate at which ions can drift across the sheath boundary, rather than upon the potential. An effort to adjust the MSL equation to fit the data of Fig. (2.17) would have to allow for a considerable variation in the sheath thickness. For example, the differences exhibited between our result using Eq. (2.54) for T_+ and Eq. (2.70) for the Mott-Smith, Langmuir function T_+^{MSL} are quite large; consider the case where $\rho_s = 5$ and $\psi_s = 1000$. We obtain $T_+ = 3620$; for T_+^{MSL} to equal 3620 the sheath thickness must be 55 Debye lengths ($\alpha = 60$). Such a large value is not difficult to understand. Near a body charged to 1000 kT, the high velocity of the ions would depress the density by a factor of 32. If the sheath were only 5 Debye lengths thick, the maximum value of the ion density would be only 0.12 of the ambient density

and would produce little screening. The field must, therefore, be much more extensive than just a few Debye lengths. In Fig. (2.17) an additional T_+^{MSL} curve is shown for $\rho_s = 50$. This comparison is included to show that the value of the sheath thickness does not become less important even for relatively large bodies. It would appear, then, that the Mott-Smith, Langmuir equations for the probe characteristics are not valid in general for an attractive potential.

F. An expression for the sheath "thickness" for calculating current-voltage characteristics. Let us consider the possibility of finding a simple expression for the "sheath thickness" s which can be used with the MSL equation to obtain results in agreement with ours. Such an expression would be quite useful although not entirely satisfactory theoretically since the idea of a finite screening sheath is an approximation.

The charge q_b on a spherical body surrounded by a concentric charge layer of radius $\alpha = \rho_s + \sigma$ Debye lengths given by

$$\begin{aligned} q_b &= C_s \psi_s \quad kT/e \\ &= \frac{hkT}{e} \rho_s \frac{\rho_s + \sigma}{2\rho_s + \sigma} \psi_s \quad (\text{cgs units}) \end{aligned} \quad (2.71)$$

where C_s is the capacitance of the concentric charge layer and $\sigma = s/h$. An equal and opposite charge must lie in the sheath. The density of the ions is given by Eq. (2.28) and (2.29). If the variation in the potential is very rapid (i.e. if in Eq. (2.29) the exponent $n \gg 1$) and if $\psi \gg 1$, then Eq. (2.28) becomes, approximately,

$$n_+ = \frac{Q}{4 \sqrt{1 + \frac{2}{3} \psi}} \quad (2.72)$$

where Q is the return factor. The charge in the sheath q_s can be written

$$q_s = \frac{\pi}{3} h^3 [(\rho_s + \sigma)^3 - \rho_s^3] N_0 e Q / (C_1 \sqrt{1 + \frac{2}{3} \psi_s}) \quad (2.73)$$

where $C_1 \sqrt{1 + \frac{2}{3} \psi_s}$ is taken to be the averaged value of n_+ for the sheath. Equating (2.71) and (2.73), and setting $\sigma \gg \rho$ we obtain for σ

$$\sigma = (2 \sqrt{6} C_1)^{\frac{1}{3}} \rho_s^{\frac{1}{3}} \psi_s^{\frac{1}{2}} \quad (2.74)$$

where $\psi \gg 1$ and $Q = 2$.

Bettinger and Walker²³ have found that the data given in Fig. (2.17) can be represented using the MSL equation (Eq. (2.70)) and

$$\sigma = 0.83 \rho_s^{\frac{1}{3}} \psi_s^{\frac{1}{2}} \quad (2.75)$$

Values of T_+^{MSL} calculated using Eq. (2.75) are surprisingly accurate over the entire range of Fig. (2.17).

If we use Eq. (2.75) in Eq. (2.70) and substitute into Eq. (2.59), we can obtain an expression for the equilibrium potential on the spherical body. If we assume $\sigma \gg \rho_s$, we obtain

$$\psi_s = - \ln \left[\frac{\sqrt{m_i/m_e} \rho_s^{\frac{4}{3}}}{0.69 \psi_s (1 - e^{-1.45 \rho_s^{\frac{4}{3}}})} \right] \quad (2.76)$$

$$(\text{where } \sigma \gg \rho_s \text{ or } 0.83 \psi_s^{\frac{1}{2}} \rho_s^{-\frac{2}{3}} \gg 1)$$

If, on the other hand, we assume $\rho_s \gg \sigma$, we obtain,

$$\psi_s = - \ln \left[\sqrt{m_i/m_e} / (1 + 1.66 \psi_s^{1/2} / \rho_s^{2/3}) \right]$$

$$(\text{where } \rho_s \gg \sigma \text{ or } 0.725 \rho_s^{4/3} \gg 1) \quad (2.77)$$

Equations (2.76) and (2.77) are in good agreement with the results of the numerical calculations. Equations (2.76) and (2.77) show that the equilibrium potential varies slowly with ρ_s . In a hydrogen plasma the maximum (absolute) value of ψ_s is about -3.76 and for an oxygen plasma it is -5.14. For a body with $\rho_s = 1000$ in an oxygen plasma where $T_e = T_i = 1000, 1500, \text{ or } 2200^\circ\text{K}$, ϕ_s will be -0.707, -1.06, or -1.56 e.v.

G. The effects of secondary electrons on the screening of stationary charged bodies. Experiments performed by Hagstrum^{19, 20, 21}, and H. A. Fowler and H. E. Farnsworth²² have shown that as the result of the neutralization of ions striking a metal surface, secondary electrons will be produced with an efficiency of about 25 per cent. These electrons have not been included in our previous calculations. Their effect may be easily included into the calculations by introducing into the Poisson equation the term N_s/N_0 where

$$N_s/N_0 = \frac{\delta \rho_c^2 (1 + \frac{2}{3} \psi_c)}{4 \rho^2 \sqrt{\frac{2}{3} (\psi_s - \psi)}} \quad (2.78)$$

where δ is the efficiency of secondary electron production, and ψ_s is the potential at the surface of the charged body (or alternatively at the surface for which the secondary electron energy is zero).

In Fig. (2.2) we have plotted a curve to show the effect of this term on the screening. The effect on our previously calculated results will be small if the surface of the body has a high potential.

CHAPTER III

THE SCREENING OF A CHARGED BODY WHERE THE RETURN FACTOR Q_+ IS VARIABLE

A. General Arguments. In experiments performed by Fowler and Farnsworth²², it has been found that the reflection coefficient for low energy electrons striking a metallic surface is, for our purposes, small; its value is of the order of 5%. Hagstrum^{19, 20, 21} has found that ions striking a metal surface will be neutralized by Auger charge exchange with an efficiency of nearly 100%. It would therefore seem that it is not satisfactory to set Q equal to 2 for particles which strike the surface of the body. We will derive an expression for the return factor for the ions, Q_+ , and we will assume a sufficiently large negative potential on the body to allow us to use a value of 2 for the electron return factor, Q_- .

If Q is variable, then we can obtain the particle density by inserting Q under the integral in Eq. (2.21). From Eq. (2.4) we obtain for the limiting pitch angle α_L separating those particles that will be accreted from those that will not

$$\alpha_L = \arcsin \left[\frac{r_c}{r} \left(\frac{1 + \Phi_c}{1 + \Phi} \right)^{\frac{1}{2}} \right] \quad (3.1)$$

where $\Phi = |\phi|/U$, and r_c and Φ_c are the values of r and Φ on the pericritical surface or on the surface of the charged body, whichever is reached first by the particles. Corresponding to Eq. (2.21), therefore, we will have for the density

$$\begin{aligned} N_{pa} &= \frac{1}{2} N_0 (1 + \Phi)^{\frac{1}{2}} \int_0^{\pi/2} Q(\alpha) \sin \alpha \, d\alpha \\ &= \frac{1}{2} N_0 (1 + \Phi)^{\frac{1}{2}} \left[\int_0^{\alpha_L} \sin \alpha \, d\alpha + 2 \int_{\alpha_L}^{\pi/2} \sin \alpha \, d\alpha \right] \\ &= \frac{1}{2} N_0 (1 + \Phi)^{\frac{1}{2}} (1 + \cos \alpha_L) \end{aligned} \quad (3.2)$$

Substituting for α_L from Eq. (3.1) into Eq. (3.2) we obtain

$$N_{pa} = \frac{1}{2} N_0 (1 + \Phi)^{\frac{1}{2}} \left\{ 1 + \left[1 - \frac{r_c^2 (1 + \Phi_c)^{\frac{1}{2}}}{r^2 (1 + \Phi)} \right]^{\frac{1}{2}} \right\} \quad (3.3)$$

We can define for the effective return factor for all particles,

$$Q_{pa} = \left\{ 1 + \left[1 - \frac{r_c^2 (1 + \Phi_c)^{\frac{1}{2}}}{r^2 (1 + \Phi)} \right]^{\frac{1}{2}} \right\} \quad (3.4)$$

The use of two different expressions for the ionic and electronic return factor modifies the screening most strongly for small values of Φ . If we assume Φ to be small, the Poisson equation can be written as

$$\begin{aligned} \frac{\partial^2}{\partial \rho^2} (-\Phi) + \frac{2}{\rho} \frac{\partial}{\partial \rho} (-\Phi) &= \frac{1}{2} Q_- (1 - \Phi)^{\frac{1}{2}} - \frac{1}{2} Q_+ (1 + \Phi)^{\frac{1}{2}} \\ &= \frac{1}{2} (Q_- - Q_+) - \frac{1}{4} (Q_- + Q_+) \Phi \end{aligned} \quad (3.5)$$

where $\rho = r/h$. If we take ρ to be large, then on the pericritical surface Φ_c , as obtained from our previous calculations, will be less than 1. Thus the first derivative term in Eq. (3.5) will be small (these conditions are met if ρ is about 10 or more) and we can neglect it. Substituting for Q_+ from Eq. (3.4) in Eq. (3.5), we have the condition

$$\frac{Q_-}{2} - \frac{1}{2} \left\{ 1 + \left[1 - \frac{r_c^2 (1 + \Phi_c)^{\frac{1}{2}}}{r^2 (1 + \Phi)} \right]^{\frac{1}{2}} \right\} < \frac{1}{4} (Q_- + Q_+) \Phi \quad (3.6)$$

which must be satisfied if a steady state screening equation is valid.

Substituting $Q_- = 2$, $Q_- + Q_+ \approx 4$, subtracting 1 from both sides and squaring Eq. (3.6), we obtain,

$$\left[1 - \frac{r_c^2 (1 + \Phi_c)^{\frac{1}{2}}}{r^2 (1 + \Phi)} \right] > (1 - 2\Phi)^2 \quad (3.7)$$

Since

$$\Phi^2 \ll 1 \quad , \quad (3.8)$$

Eq. (3.7) becomes

$$\Phi > \frac{r_c^2(1 + \Phi_c)}{4r^2(1 + \Phi)} \quad (3.9)$$

and therefore the potential must fall off more slowly than r^{-2} . We also have the condition that if no screening at all occurs, then

$$\Phi = \Phi_c \rho_c / \rho \quad (3.10)$$

This shows that Φ must vary as

$$\Phi = Kr^{-n} \quad ; \quad 1 < n < 2 \quad (3.11)$$

for small values of Φ . Furthermore, this result will hold in a modified form even for the case of local thermodynamic equilibrium.

If $Q_+ = 2$, then Eq. (3.6) is always satisfied, and for the region of small Φ an integral of the equation can be obtained of the form

$$\Phi = \frac{k}{\rho} e^{-\rho} \quad (3.12)$$

It might appear that if one chooses r/r_c to be large enough, the difference between Q_+ and Q_- could be neglected. By the substitution of Eq. (3.4) into the Poisson equation, we can show what prevents this. We have approximately,

$$\frac{\partial^2}{\partial \rho^2} (-\Phi) + \frac{2}{\rho} \frac{\partial}{\partial \rho} (-\Phi) = \frac{r_c^2(1 + \Phi_c)}{4r^2(1 + \Phi)} - \Phi \quad (3.13)$$

for small Φ . Thus, if we choose

$$\frac{r_c^2(1 + \Phi_c)}{4r^2(1 + \Phi)} \ll \Phi \quad , \quad (3.14)$$

we would obtain a potential of the form given in Eq. (3.12). However,

r_c , r , and Φ cannot be chosen independently. Furthermore, if Eq. (3.14) does not hold, then the condition in Eq. (3.14) cannot be satisfied for any Φ since Φ varies as ρ^{-2} . It appears that the potential does not vary according to Eq. (3.12) over any portion of the curve for which Φ is small and Q_+ is given by Eq. (3.4).

B. Solution for a monoenergetic plasma. A solution to the screening equation approximated for small values of $1/r$ and Φ can be obtained which will show explicitly how the potential falls off at large distances from the charged body. This equation also leads to eigenvalue conditions on the total accretion for a monoenergetic plasma and to eigenvalue conditions on r_c for a plasma with a Maxwellian velocity distribution.

The equation for the periastron density in terms of $\rho = r/h$, $\Phi = \phi/U$ (the absolute signs are removed here) is, by Eq. (3.3),

$$N_{pa} = \frac{1}{2} N_0 (1 + \Phi)^{\frac{1}{2}} \left\{ 1 + \left[1 - \frac{\rho_c^2 (1 + \Phi_c)^{\frac{1}{2}}}{\rho^2 (1 + \Phi)} \right]^{\frac{1}{2}} \right\} \quad (3.15)$$

Let us again consider the charge on the body to be negative (for convenience only). Substituting,

$$A_+ = \rho_c^2 (1 - \Phi_c) \quad (3.16)$$

into Eq. (3.15) gives for the ion density,

$$n_+ = \frac{1}{2} (1 - \Phi)^{\frac{1}{2}} \left\{ 1 + \left[1 - \frac{A_+}{\rho^2 (1 - \Phi)} \right]^{\frac{1}{2}} \right\} \quad (3.17)$$

Using a similar definition for A_- , with $\rho_c \rightarrow \rho_s$ and $\Phi_L \rightarrow \Phi_s$, S referring to the surface values of the quantities, we have:

$$n_- = \frac{1}{2} (1 + \Phi)^{\frac{1}{2}} \left\{ 1 + \left[1 - \frac{A_-}{\rho^2 (1 + \Phi)} \right]^{\frac{1}{2}} \right\} \quad (3.18)$$

Substituting Eqs. (3.17) and (3.18) into Poisson's equation we obtain:

$$\Phi'' + \frac{2}{\rho}\Phi' = \frac{1}{2}(1 + \Phi)^{\frac{1}{2}} \left\{ 1 + \left[1 - \frac{A_-}{\rho^2(1+\Phi)} \right]^{\frac{1}{2}} \right\} - \frac{1}{2}(1 - \Phi)^{\frac{1}{2}} \left\{ 1 + \left[1 - \frac{A_+}{\rho^2(1-\Phi)} \right]^{\frac{1}{2}} \right\}. \quad (3.19)$$

For large values of ρ and $\Phi \ll 1$ we can write for Eq. (3.19)

$$\Phi'' + \frac{2}{\rho}\Phi' - \Phi \left(1 + \frac{A_+ + A_-}{8\rho^2} \right) - \frac{A_+ - A_-}{4\rho^2} = 0. \quad (3.20)$$

The solution to Eq. (3.20) can be obtained in series form by substituting

$$\Phi = \sum_{n=1}^{\infty} \alpha_n \rho^{-2n} \quad (3.21)$$

into Eq. (3.20). This yields

$$\sum_{n=1}^{\infty} \alpha_n \left(4n^2 - 2n - \frac{A_+ + A_-}{8} \right) \rho^{-2(n+1)} - \sum_{n=1}^{\infty} \alpha_n \rho^{-2n} - \frac{A_+ - A_-}{4\rho^2} = 0. \quad (3.22)$$

Now, since n is simply a dummy index, we can write

$$\sum_{n=1}^{\infty} \alpha_n \rho^{-2n} = \alpha_1 \rho^{-2} + \sum_{n=1}^{\infty} \alpha_{n+1} \rho^{-2(n+1)} \quad (3.23)$$

If Eq. (3.23) is substituted into Eq. (3.22), we obtain

$$\begin{aligned} & \sum_{n=1}^{\infty} \left\{ \rho^{-2(n+1)} \left[\alpha_n \left(4n^2 - 2n - \frac{A_+ + A_-}{8} \right) - \alpha_{n+1} \right] \right\} - \left(\alpha_1 + \frac{A_+ - A_-}{4} \right) \rho^{-2} \\ & = 0 \end{aligned} \quad (3.24)$$

Therefore, we see that in order for Eq. (3.21) to be a solution of Eq. (3.20), the value of α_1 must be

$$\alpha_1 = -\frac{1}{4}(A_+ - A_-) \quad (3.25)$$

with a recursion equation for all other α 's

$$\alpha_{n+1} = \left(4n^2 - 2n - \frac{A_+ + A_-}{8} \right) \alpha_n \quad (3.26)$$

Thus the solutions are of the form

$$\Phi = -\frac{1}{4}(A_+ - A_-)\rho^{-2} - \frac{1}{2}(A_+ - A_-)\left(1 - \frac{A_+ + A_-}{16}\right)\rho^{-4} \dots \quad (3.27)$$

The solution will not be convergent unless it is terminated. (This is apparent from the fact that for large values of n the n th term in the series will be $-(A_+ - A_-)4^{n-3}[(n-1)!]^2\rho^{-2n}$ in which as $n \rightarrow \infty$ the factorial term in the numerator becomes greater than the ρ^{2n} in the denominator for any given value of ρ ; thus the terms of the series and the series itself diverge as n approaches infinity.) If the series is to terminate at some value of $n = \ell$ then we obtain for the condition for the termination of the series

$$\ell = \frac{1}{4} \left\{ 1 \pm \sqrt{1 + \frac{1}{2}(A_+ + A_-)} \right\} \quad , \quad (3.28)$$

or in terms of ℓ , we have

$$A_+ + A_- = 16\ell(2\ell - 1) \quad (3.29)$$

which gives values $A_+ + A_- = 16, 96, 240$ etc. for $\ell = 1, 2, 3$, etc.

Thus the first two values of Φ will be

$$\begin{aligned} \Phi_1 &= -\frac{1}{4}(A_+ - A_-)\rho^{-2} \\ \Phi_2 &= -\frac{1}{4}(A_+ - A_-)\rho^{-2} + \frac{5}{2}(A_+ - A_-)\rho^{-4} \end{aligned} \quad (3.30)$$

Since $A_+ - A_-$ must be positive, Eq. (3.30) verifies the earlier contention that the potential must fall off at least as slowly as ρ^{-2} . We have also shown the rather remarkable fact that for this completely classical problem, we have eigenvalue conditions on the value of $A_+ + A_-$.

If we write for the current to the surface of the charged body I_S , then

$$I_S = e\pi N_0 h^2 (u_i A_+ - u_e A_-) \quad (3.31)$$

where e is the electronic charge, N_0 is the ambient density, u_i and u_e are the ion and electron velocity at infinity, h is the Debye length. We have from the eigenvalue condition Eq. (3.29)

$$I_S = e\pi N_0 h^2 u_i [16l(2l-1) - (1 + \frac{u_e}{u_i})A_-] \quad (3.32)$$

In order to have an equilibrium charge on the body, the net current to the body must be zero. Thus, for a body receiving current only from the plasma, Eq. (3.32) must be zero for equilibrium. Therefore A_- must be

$$A_- = 16l(2l-1)/(1 + u_e/u_i) \quad (3.33)$$

Since A_- is given by

$$A_- = \rho_S^2 (1 + \Phi_S) \quad (3.34)$$

where Φ_S is the value of Φ on the surface of the body, the equilibrium value of Φ_S is given by

$$\Phi_S = \frac{16l(2l-1)}{\rho_S^2 (1 + u_e/u_i)} - 1 \quad (3.35)$$

Eq. (3.35) arises from the requirement that the charge on the body be in equilibrium.

Returning to Eq. (3.29), which must be satisfied if a solution is to exist, and substituting for A_+ and A_- from Eqs. (3.16) and (3.34), we have

$$\rho_C^2 (1 - \Phi_C) + \rho_S^2 (1 + \Phi_S) = 16l(2l-1) \quad (3.36)$$

For any given values of ρ_S and Φ_S , ρ_C and Φ_C will be determined by the detailed solution as functions of l . Thus Eqs. (3.35) and (3.36) constitute a system of two equations in two unknowns giving a satisfactory ρ_S , Φ_S pair for various values of l . Thus, for a given size body,

and

$$n_- = \frac{1}{2} \int_{\sqrt{-2\phi/m}}^{\infty} (1 + \phi/U)^{\frac{1}{2}} \left\{ 1 + \left[1 - \frac{A_-}{\rho^2 (1 + \phi/U)} \right]^{\frac{1}{2}} \right\} \frac{dn}{du} du \quad (3.45)$$

where A_+ and A_- are

$$A_+(U) = \rho_c^2 (1 - \phi_c/U) \quad (3.46)$$

$$A_-(U) = \rho_s^2 (1 - \phi_s/U) \quad (3.47)$$

where the subscript c refers to the pericritical surface (or the body surface if there is no pericritical surface), and s refers to the surface of the body. We can write Eq. (3.44) and (3.45) as

$$n_+ = \frac{2\alpha^{\frac{3}{2}}}{\sqrt{\pi}} \left\{ J_1 + J_2 \right\} \quad (3.48)$$

$$n_- = \frac{2\alpha^{\frac{3}{2}}}{\sqrt{\pi}} \left\{ I_1 + I_2 \right\} \quad (3.49)$$

where

$$J_1 = \int_0^{\infty} (1 - \phi/U)^{\frac{1}{2}} u^2 e^{-\alpha u^2} du \quad (3.50)$$

$$J_2 = \int_0^{\infty} (1 - \phi/U)^{\frac{1}{2}} \left[1 - \frac{A_+(U)}{\rho^2 (1 - \phi/U)} \right]^{\frac{1}{2}} u^2 e^{-\alpha u^2} du \quad (3.51)$$

$$I_1 = \int_{\sqrt{-2\phi/m}}^{\infty} (1 + \phi/U)^{\frac{1}{2}} u^2 e^{-\alpha u^2} du \quad (3.52)$$

$$I_2 = \int_{\sqrt{-2\phi/m}}^{\infty} (1 + \phi/U)^{\frac{1}{2}} \left[1 - \frac{A_-(U)}{\rho^2 (1 + \phi/U)} \right]^{\frac{1}{2}} u^2 e^{-\alpha u^2} du \quad ; \quad (3.53)$$

Eqs. (3.50) to (3.53) become, on rearranging the quantities and integrating,

$$I_1 = \frac{\sqrt{\pi}}{4\alpha^{\frac{3}{2}}} e^{\psi}, \quad \psi = \phi/kT \quad (3.54)$$

$$J_1 = \frac{\sqrt{\pi}}{4\alpha^{\frac{3}{2}}} e^{-\psi} \left\{ 1 - \frac{4}{3\sqrt{\pi}} [(-\psi)^{\frac{3}{2}} - \frac{3}{5}(-\psi)^{\frac{5}{2}} \dots] \right\} \quad (3.55)$$

$$I_2 = \frac{\sqrt{\pi}}{4\alpha^2} (1 - \rho_S^2/\rho^2)^{\frac{1}{2}} \exp\left(\frac{\psi\rho^2 - \psi_S\rho_S^2}{\rho^2 - \rho_S^2}\right) \left\{ 1 - \frac{4}{3\sqrt{\pi}} \left[\left(\frac{\psi\rho^2 - \psi_S\rho_S^2}{\rho^2 - \rho_S^2} - \psi \right)^{\frac{3}{2}} + \dots \right] \right\} \quad (3.56)$$

$$J_2 = \frac{\sqrt{\pi}}{4\alpha^2} (1 - \rho_C^2/\rho^2)^{\frac{1}{2}} \exp\left[-\frac{\psi\rho^2 - \psi_C\rho_C^2}{\rho^2 - \rho_C^2}\right] \cdot \left\{ 1 - \frac{4}{3\sqrt{\pi}} \left[\left(-\frac{\psi\rho^2 - \psi_C\rho_C^2}{\rho^2 - \rho_C^2} \right)^{\frac{3}{2}} + \dots \right] \right\} \quad (3.57)$$

where ψ and ψ_C are small and ρ_C is assumed constant. Substituting Eqs. (3.54), (3.55), (3.56), and (3.57) into Eq. (3.48) and (3.49) gives, dropping higher terms:

$$n_+ = \frac{1}{2} \left\{ e^{-\psi} \left[1 - \frac{4}{3\sqrt{\pi}} (-\psi)^{\frac{3}{2}} \right] + (1 - \rho_C^2/\rho^2)^{\frac{1}{2}} \exp\left[-\frac{\psi\rho^2 - \psi_C\rho_C^2}{\rho^2 - \rho_C^2}\right] \cdot \left[1 - \frac{4}{3\sqrt{\pi}} \left(-\frac{\psi\rho^2 - \psi_C\rho_C^2}{\rho^2 - \rho_C^2} \right)^{\frac{3}{2}} \right] \right\} \approx \frac{1}{2} \left\{ e^{-\psi} \left[1 - \frac{4}{3\sqrt{\pi}} (-\psi)^{\frac{3}{2}} \right] + (1 - \frac{\rho_C^2}{\rho^2})^{\frac{1}{2}} \exp\left[-\frac{\psi\rho^2 - \psi_C\rho_C^2}{\rho^2 - \rho_C^2}\right] \right\} \quad (3.58)$$

$$n_- = \frac{1}{2} \left\{ e^{\psi} + (1 - \rho_S^2/\rho^2)^{\frac{1}{2}} \exp\left[\frac{\psi\rho^2 - \psi_S\rho_S^2}{\rho^2 - \rho_S^2}\right] \cdot \left[1 - \frac{4}{3\sqrt{\pi}} \left(\frac{\psi\rho^2 - \psi_S\rho_S^2}{\rho^2 - \rho_S^2} - \psi \right)^{\frac{3}{2}} \right] \right\} \approx \frac{1}{2} \left\{ e^{\psi} + (1 - \rho_S^2/\rho^2)^{\frac{1}{2}} \exp\left[\frac{\psi\rho^2 - \psi_S\rho_S^2}{\rho^2 - \rho_S^2}\right] \left[1 - \frac{4}{3\sqrt{\pi}} (-\psi)^{\frac{3}{2}} \right] \right\} \quad (3.59)$$

Thus we obtain, on expanding the exponential terms

$$n_- - n_+ = (2 + \frac{\rho_C^2 + \rho_S^2}{4\rho^2})\psi + \frac{1}{4\rho^2} [\rho_C^2 (1 - 2\psi_C) - \rho_S^2 (1 + 2\psi_S)] \quad (3.60)$$

Thus substituting Eq. (3.60) into Poisson's equation, we have

$$\begin{aligned} \psi'' + \frac{2}{\rho} \psi' - \left(\frac{\rho_c^2 + \rho_s^2}{4} \right) \psi / \rho^2 - 2\psi - \frac{1}{4\rho^2} [\rho_c^2 (1 - 2\psi_c) \\ - \rho_s^2 (1 + 2\psi_s)] = 0 \end{aligned} \quad (3.61)$$

We can obtain a series solution of Eq. (3.61) by substituting

$$\psi = \sum_{n=1}^{\infty} \alpha_n \rho^{-2n} \quad (3.62)$$

The substitution yields

$$\begin{aligned} \sum_{n=1}^{\infty} \alpha_n (4n^2 - 2n) \rho^{-2(n+1)} - 2 \sum_{n=1}^{\infty} \alpha_n \rho^{-2n} - 2\alpha_0 - \frac{\rho_c^2 + \rho_s^2}{4\rho^2} \\ \cdot (\alpha_0 + \sum_{n=1}^{\infty} \alpha_n \rho^{-2n}) - \frac{1}{4} [\rho_c^2 (1 - 2\psi_c) - \rho_s^2 (1 + 2\psi_s)] \frac{1}{\rho^2} = 0 \end{aligned} \quad (3.63)$$

Since

$$\sum_{n=1}^{\infty} \alpha_n \rho^{-2n} = \alpha_1 \rho^{-2} + \sum_{n=1}^{\infty} \alpha_{n+1} \rho^{-2(n+1)} \quad (3.64)$$

we can write Eq. (3.63) as

$$\begin{aligned} \sum_{n=1}^{\infty} \left[\alpha_n \left(4n^2 - 2n - \frac{\rho_c^2 + \rho_s^2}{4} \right) - 2\alpha_{n+1} \right] \rho^{-2(n+1)} - 2\alpha_1 \rho^{-2} \\ - \frac{1}{4} [\rho_c^2 (1 - 2\psi_c) - \rho_s^2 (1 + 2\psi_s)] \frac{1}{\rho^2} - 2\alpha_0 - \frac{\rho_c^2 + \rho_s^2}{4\rho^2} \alpha_0 = 0 \end{aligned} \quad (3.65)$$

Solving for α_0 and α_1 by setting the coefficient of each power of ρ equal to 0, we obtain

$$\alpha_0 = 0 \quad (3.66)$$

$$\alpha_1 = -\frac{1}{8} [\rho_c^2 (1 - 2\psi_c) - \rho_s^2 (1 + 2\psi_s)] \quad (3.67)$$

and the recursion relation

$$\alpha_{n+1} = \alpha_n \left(2n^2 - n - \frac{\rho_c^2 + \rho_s^2}{8} \right) \quad (3.68)$$

If Eq. (3.62) is to be a solution, then the series must terminate (since (3.68) leads to infinite coefficients as $n \rightarrow \infty$). Thus for some value of $n = l$

$$\rho_c^2 + \rho_S^2 = 8l(2l - 1) \quad (3.69)$$

Let us find the effect of Eq. (3.69) on the equilibrium potential. From Eqs. (2.54), (2.58), and (2.60) we obtain the equation for the equilibrium potential,

$$\begin{aligned} \rho_S^2 (1 + Z_c - \psi_S) e^{-Z_c} + \int_0^{Z_c} \rho_c^2(Z) [Z - \psi_c(Z)] e^{-Z} dZ \\ - \sqrt{m_i/m_e} \rho_S^2 e^{\psi_S} = 0 \end{aligned} \quad (3.70)$$

Assuming ρ_c and ψ_c constant, and Z_c large, we have,

$$\rho_c^2 (1 - \psi_c) - \sqrt{m_i/m_e} \rho_S^2 e^{\psi_S} = 0 \quad (3.71)$$

Therefore, substituting Eq. (3.71) into Eq. (3.69) gives,

$$\psi_S = - \ln \left\{ \frac{\rho_S^2 \sqrt{m_i/m_e}}{(1 + \psi_c) [8l(2l - 1) - \rho_S^2]} \right\} \quad (3.72)$$

Equation (3.72) shows that $8l(2l - 1) > \rho_S^2$, if ψ_S is to be negative.

It is possible that Eq. (3.72) leads to unusually large potentials in some cases. If Z_c is assumed small with ρ_c and ψ_c constant in Eq. (3.70) we obtain

$$\psi_S = - \ln \left\{ \frac{\sqrt{m_i/m_e}}{1 - \psi_S + Z_c [\psi_S - \psi_c 8l(2l - 1)/\rho_S^2]} \right\} \quad (3.73)$$

for the potential. Since $Z_c [\psi_S - \psi_c 8l(2l - 1)/\rho_S^2]$ is small, Eq. (3.73) is essentially the same as Eq. (2.62).

there may exist no steady state equilibrium potential at all.

Let us find the approximate value of Φ_S . If the pericritical surface lies within ρ_S , then $\rho_c \rightarrow \rho_S$, $\Phi_c \rightarrow \Phi_S$ and Eq. (3.36) becomes

$$\rho_S^2 = 8l(2l - 1) \quad . \quad (3.37)$$

Substitution of Eq. (3.37) into (3.35) yields, approximately,

$$\Phi_S = - \left(1 - \frac{2}{1 + u_e/u_i} \right) \quad . \quad (3.38)$$

Since $u_e \gg u_i$, $\Phi_S \approx -1$. Because of the requirement that the pericritical surface lie within ρ_S , Eq. (3.38) is probably invalid for ρ_S much greater than 10. (Since the value of $\rho_c = 10$ is not known, it cannot be definitely stated that Eq. (3.38) serves as more than a demonstration of the use of Eqs. (3.35) and (3.36) in obtaining a solution for Φ_S .)

If we rewrite ρ_c as

$$\rho_c^2 = \rho_S^2(1 + x) \quad (3.39)$$

and substitute into Eq. (3.36), we obtain

$$\rho_S^2 = 8l(2l - 1) / \left[1 + \frac{x}{2} + \Phi_S/2 - (1 + x)\Phi_c/2 \right] \quad . \quad (3.40)$$

Substituting (3.40) into (3.35) gives

$$\Phi_S = -1 + (1 - \Phi_c)(1 + x)/2u \quad . \quad (3.41)$$

Since x is small for large ρ and $u_e \gg u_i$, Eq. (3.41) yields $\Phi_S = -1$. It should be noted that Eqs. (3.35), (3.38) and (3.41) apply to a monoenergetic plasma and give quite different results for Φ_S from those one should expect for a plasma with a Maxwellian velocity distribution.

These results apply to a monoenergetic plasma. We will see presently that for the case of a plasma with a Maxwellian velocity

distribution. The screening equations will lead to eigenvalue solutions and eigen value conditions on the parameters. It should be noted, however, that a monoenergetic plasma is not physically unrealistic. It is possible to imagine experimental arrangements for producing a monoenergetic plasma. In any case, the eigenvalue conditions definitely do not arise from physically unrealizable assumptions concerning the velocity distribution of the constituents.

C. Solution for a plasma with a Maxwellian velocity distribution.

We can extend the above treatment to the case of a plasma with a Maxwellian velocity distribution. Equation (3.15) gives the expression for the equilibrium ion density for a monoenergetic plasma. The comparable expression for the case of a Maxwellian velocity distribution can be obtained by integrating the product of Eq. (3.15) and the appropriate expression for the velocity distribution dn/du over all velocities allowable.

$$N_{pa} = \frac{1}{2} \int_0^{\infty} (1 + \theta/U)^{\frac{1}{2}} \left\{ 1 + \left[1 - \frac{\rho_c^2 (1 + \theta_c/U)}{\rho^2 (1 + \theta/U)} \right]^{\frac{1}{2}} \right\} \frac{dn}{du} du \quad (3.42)$$

The appropriate distribution function dn/du is

$$\frac{dn}{du} = \frac{4\alpha^{\frac{3}{2}}}{\sqrt{\pi}} u^2 e^{-\alpha u^2} \quad (3.43)$$

where $\alpha = m/2kT$, which gives the fraction of the ions that will have initial speeds in the range u to $u + du$.

For a negatively charged body, the expressions for the ion and electron densities will be:

$$n_+ = \frac{1}{2} \int_0^{\infty} (1 - \theta/U)^{\frac{1}{2}} \left\{ 1 + \left[1 - \frac{A_+}{\rho^2 (1 - \theta/U)} \right]^{\frac{1}{2}} \right\} \frac{dn}{du} du \quad (3.44)$$

CHAPTER IV
THE SELF-CONSISTENT FIELD CALCULATION FOR A
RAPIDLY MOVING AXIALLY SYMMETRIC CHARGED BODY

A. Discussion of the Approach. In many cases in which we wish to know the nature of the screening of a charged body that is embedded in a plasma, the situation is complicated by a motion of the body relative to the plasma. If the motion is slow, i.e., if the drift velocity relative to the plasma is small compared to the thermal velocity of the ions, then the problem can be treated as a perturbation on the spherically symmetric case in which the charged body is at rest. If, however, the velocity of the body, relative to the plasma, is large, then the problem becomes far more complicated and a quite different approach is required. We will consider this more complicated problem in which we take the velocity of the charged body, relative to the plasma, to be much greater than the thermal velocity of the ions.

We assume that we have an axially symmetric negatively charged body moving relative to the plasma with a velocity that is great compared to the thermal velocity of the ions, but is small compared to the thermal velocity of the electrons. We will consider only the case of a negatively charged body. The approach that we use is capable of providing the equipotential surfaces, the electric field, the density of the ions and electrons at every point, the current to the charged body, the trajectories of the ions, the structure of the plasma wake, and the electric drag on the body.

The accretion and density formulae obtained in Chapter II depend heavily upon the spherical symmetry of the problem. This symmetry makes it possible to integrate over α and q to obtain the

particle density without having to incorporate a functional dependence of α and q on the angles θ and ϕ (in the spherical coordinates r , θ , ϕ).

For the calculation of the screening of a moving body, it will be necessary to follow individual particle orbits in order to calculate the space charge density. The density of this space charge will then be used to calculate the potential in the neighborhood of the particle's position, and then the potential is used to continue the orbit calculations.

If the mean velocity of the ions is much smaller than the velocity of the charged body, then in the coordinate system at rest with the charged body, we may consider the incident ions to be moving along the axis of symmetry. The fact that the ions do have random thermal motions may be introduced as a later refinement.

We are, therefore, able to begin our calculations with a test particle (or as we will find to be necessary, a group of test particles) moving with its velocity vector initially parallel to the axis of symmetry. The calculations proceed from an assumed boundary surface on the front side on the body (for example, a hemispherical equipotential surface, $\psi = -0.001$) as shown in Fig. (4.1). The electric field is determined approximately by using Eq. (2.30) as in Chapter II. We first calculate an incremental step in the particle's trajectory, then the resulting density at the new position on the trajectory, and the new values of the potential and the electric fields.

This procedure is repeated at each step along the trajectory. The result is that we are able to use this technique to "trace out" the electric field and the equipotential surfaces. The method is straightforward enough as long as the successive ion trajectories do not intersect. When the trajectories of the test particles do intersect, a more complicated procedure must be used as we will see later.

With this objective in mind, we will derive the expressions necessary for following the particle trajectories and for solving the Poisson equation.

It will be found necessary to employ several particles lying in a neighborhood, following their trajectories in order to obtain all the information needed in the trajectory calculations. That is to say, if we were to try to solve for the trajectory of a single particle, using only the information derivable from following one trajectory, then we would discover that we could not calculate the density of ions in the neighborhood of this particle nor would we have the necessary information regarding the direction and variation of the electric field in the neighborhood of the test particle. In order to obtain this information, we will follow four test particles simultaneously. A comparison of the positions of test particles 1 and 2 or of test particles 3 and 4 can be used to obtain the ion density; the comparison also yields the direction of the electric field. The comparison of the electric field vector obtained for particles 1 and 2 with that for particles 3 and 4 will yield the rate of change of the electric field vector in the neighborhood of the particles (later we will refer to the angle β , which is the angle between the normal to the equipotential surface and the radius vector, and the

derivative of β with respect to θ along an equipotential surface). This information could be obtained using only three test particles in the group; however, since the separation between these particles cannot be reduced below certain practical limits, the accuracy that can be achieved using only three particles might not be sufficient.

In the approach to the problem that is made here, the boundary conditions are placed on a surface outside the body, rather than being specified for the surface of the charged body. The shape of the charged body is obtained as a result of the calculations. If the surface of the body is a conductor, then the surface of the body will be an equipotential surface. The charged body will merely be designated as one of the equipotential surfaces. If there exists a pericritical surface, so that the ions are accreted toward the origin and do not reemerge, then any equipotential surface lying completely inside the pericritical surface can be considered as the surface of a charged body. At the surface of a body the ions are assumed to be neutralized and those equipotential surfaces shown inside the body are superfluous.

If, on the other hand, the equipotential surface lies outside this pericritical surface, then a different procedure is required to take care of those trajectories that emerge from the equipotential surface corresponding to the body. First of all, the trajectories are terminated where they first encounter the equipotential surface corresponding to the body. Secondly, since these particles will not reemerge from the body, there will be a space devoid of space charge and of trace trajectories. The equipotentials in this space must be recalculated using $\nabla^2 \psi = 0$. The boundary conditions must be taken from the trajectories that bound the empty space.

One can also use trajectories to trace out the field if the ion and electron densities are set to zero.

If we desire a solution for a body of a particular shape, the shape and position of the boundary surface must be selected through a process of trial and error or, if sufficient data has been compiled, by the extrapolation of previous results to obtain a satisfactory boundary surface.

Of course there exists the possibility that a particular boundary cannot lead to a real solution in certain areas of the space. For example, if we assume the boundary surface to be at a potential of ψ_0 , and hemispheric with a radius of curvature ρ_0 , it may be found impossible to obtain self-consistent traces inside a certain region, say, with a radius ρ_1 . This does not mean that the technique fails, but rather that no charged body of any given shape lying entirely within a radius ρ_1 can give rise to a hemispherical equipotential surface of radius ρ_0 and potential ψ_0 with all the other conditions of streaming velocity, etc. also applying.

If the trajectory of a test particle crosses the axis of symmetry, a new difficulty arises. We then have the problem of test particle trajectories crossing each others path requiring us to sum the density contribution from both groups of particles in order to find the total charge density at that point and the resulting electric fields. The problem is actually only one of computational complications, so that we need merely indicate the computational procedure to use whenever we wish to solve the screening problem in a region in which the test particle trajectories intersect.

In Fig. (4.2), we have drawn the trajectory of the first

particle to cross the axis of symmetry at point A. The particle is assumed reflected here and its trajectory is extended to point B. A second trajectory is computed starting from the initial boundary surface and is extended to point B also. Here the sum of the densities of the first and second trajectories can be obtained. Furthermore, the sum can be extrapolated for the neighborhood of the point B. The trajectory from A to B can now be accurately computed. In Fig. (4.3a), we see that the second trajectory has been extended to point C using the extrapolated value of the total charge density obtained at point B. In Fig. (4.3b), a third trajectory is being computed beginning at the initial boundary surface and intersecting at the approximate positions E and D. At D, a new extrapolation expression is obtained and used to correctly compute the segment of the first particles trajectory from B to D. At E an extrapolation can be made to yield the segments D E and C E. The third trajectory can then be extended to F and reflected. This procedure can be continued until the entire space is traced out.

Since the technique would require considerable computation, it is at present beyond our scope. For this reason, it will not be employed in this paper. This should not be taken to mean that the author does not consider the results in such regions to be important. Such results, when they are obtained, will be quite valuable to the understanding of the structure of the wake of a charged body moving in a plasma.

B. Validity of the approach. We must consider the validity of the solution to a screening problem that is obtained by the above approach in which test particles are used to "trace out" the electric

and potential fields. It might appear that a solution could not be obtained by a procedure in which a particle (or as will actually be the case, a group of particles) is followed along its path tracing out the field without any consideration of what is going on anywhere else in the field except in the immediate neighborhood of the particle.

To answer the question, let us consider the uniqueness theorem for electrostatics. This theorem states essentially that the boundary conditions in an electrostatics problem will uniquely determine the solution within the boundary, if the charge distribution within the boundary is known. Let us consider two closed equipotential surfaces, one inside the other, separated by a very small distance. If the boundary conditions are specified on the outer surface, then the distance to the inner equipotential surface at any point can be determined simply from a knowledge of the charge density between the two surfaces. To do this, we need know nothing of the distribution of the charge within the inner surface. This fact is obvious either from the uniqueness theorem or, more simply, from the Faraday "Ice Pail" experiments.

These considerations show that it is quite satisfactory to begin on a boundary surface and calculate with the knowledge of the particle trajectories from one surface to the next until the entire region has been calculated down to the surface of the charged body. However, are we justified or is it possible to do this piecemeal, by tracing out a small region at a time along particle trajectories?

To answer this question, consider the Gauss Flux Theorem for the closed surface shown in Fig. (4.4). We can write

$$\int_S \mathbf{E} d\mathbf{S} = \int_{S_1} \mathbf{E}_1 d\mathbf{S} + \int_{S_2} \mathbf{E}_2 d\mathbf{S} + \int_{S_3} \mathbf{E}_3 d\mathbf{S} + \int_{S_4} \mathbf{E}_4 d\mathbf{S} = \frac{q}{\epsilon_0} \quad (4.1)$$

If S_3 and S_4 are perpendicular to the equipotential surfaces S_1 and S_2 , E_3 and E_4 will be zero. This will allow us to write for Eq. (4.1)

$$\int_{S_2} E_2 dS = \frac{q}{\epsilon_0} - \int_{S_1} E_1 dS \quad (4.2)$$

where E_1 is specified on the boundary surface S_1 . We see that if we know the shape of the initial boundary surface S_1 , and the value of the electric field on that surface, and if we perform our calculations from one equipotential surface to the next, the values of the electric field on a neighboring equipotential surface can be calculated from a knowledge of the space charge between these two surfaces. This process can be performed from one equipotential surface to the next so as to trace out a section of the electric field without a knowledge of the rest of the field other than that it must be consistent everywhere with the traced out section. The conditions specified here will be met in the procedure and the equations used to solve screening problems.

CHAPTER V

THE DENSITY OF IONS AND ELECTRONS IN AN AXIALLY SYMMETRIC POTENTIAL FIELD FOR A RAPIDLY MOVING CHARGED BODY

A. The ion density N_+ . Assume that we have a negatively charged body moving rapidly through a plasma in which the relative velocity u between the body and the plasma is large compared to the velocity of the ions, but small compared to the velocity of the electrons. In a frame of reference at rest with respect to the charged body, the ions may be considered to be approaching the body with a velocity u parallel to the axis of symmetry and with impact parameter q (see Fig. (5.1)).

The accretion of particles through a ring element of area $2\pi q \Delta q$ in a plane perpendicular to the axis of symmetry, ΔA , is

$$\Delta A = 2 \pi q \Delta q N_0 U \quad (5.1)$$

where N_0 is the ambient density of ions. Now, at any later moment, the density N of these ions can be specified if we know the flux J of the particles at that time and if we know their velocity v :

$$N = J/v \quad (5.2)$$

The flux can be specified in terms of the component of the ring surface element ΔS through which these particles pass at some later position in space which is perpendicular to the velocity vector of the particles at that position in space. We can then write for the flux J :

$$J = \Delta A / \Delta S \quad (5.3)$$

In order to evaluate ΔS let us consider Fig. (5.2) which shows the section of the equipotential surface which test particles coming

from Δq cross. The projection of this surface perpendicular to the velocity vector of the particles is

$$\Delta S = 2 \pi r \sin \theta \Delta \ell \quad , \quad (5.4)$$

(r, θ) being the coordinates of the particles. The angle α is the angle between the radius vector \underline{r} and the velocity vector \underline{v} . The angle β is the angle between the radius vector and the normal to the equipotential surface (β is positive in the counterclock-wise direction). The angle $\Delta\theta_{2p}$ is the angle between two particle trajectory intersections with the equipotential surface. The value of $\Delta\ell$ in the limit as $\Delta\theta_{2p}$ approaches zero is

$$\Delta \ell = r \Delta\theta_{2p} (1 + \tan^2 \beta)^{\frac{1}{2}} \cos (\alpha + \beta) = r \Delta\theta_{2p} \cos (\alpha + \beta) / \cos \beta \quad . \quad (5.5)$$

Thus, substituting this expression for $\Delta\ell$ into Eq. (5.4) for ΔS we have

$$\Delta S = 2 \pi r^2 \sin \theta \Delta\theta_{2p} \cos (\alpha + \beta) / \cos \beta \quad . \quad (5.6)$$

Thus we have for the flux J on substituting Eq. (5.6) and Eq. (5.1) into Eq. (5.3)

$$J = \frac{q \Delta q N_0 U \cos \beta}{r^2 \Delta\theta_{2p} \sin \theta \cos (\alpha + \beta)} \quad (5.7)$$

and for the ion density N_+ we will have

$$N_+ = \frac{q \Delta q N_0 \cos \beta}{r^2 (1 + v/u)^{\frac{1}{2}} \Delta\theta_{2p} \sin \theta \cos (\alpha + \beta)} \quad , \quad (5.8)$$

since $v/u = (1 + v/u)^{\frac{1}{2}}$. In terms of the angle subtended by Δq we have

$$\sin \theta_0 = q/r_0 \quad ; \quad (5.9)$$

$$\cos \theta_0 \Delta\theta_0 = \Delta q/r_0 \quad . \quad (5.10)$$

Writing $\Delta\theta_0 \equiv (\Delta\theta_{2p})_0$ to emphasize the definition of the quantity, we have on substituting from Eqs. (5.9) and (5.10) into Eq. (5.8):

$$\frac{N_+}{N_0} \equiv n_+ = \frac{r_0^2 \sin \theta_0 \cos \theta_0 (\Delta\theta_{2p})_0 \cos \beta}{r^2 (1 + 1/U)^2 \sin \theta (\Delta\theta_{2p}) \cos (\alpha + \beta)} \quad (5.11)$$

Particular care must be exercised in the use of Eq. (5.11) if $\alpha + \beta$ approaches $\pi/2$.

Since we intend to use numerical methods to evaluate n_+ and since in that evaluation $\Delta\theta_{2p}$ will be finite, the derivation of $\Delta\ell$ which resulted in Eq. (5.5) is not satisfactory everywhere. We derive below the correct expression which takes into account the finite value of $\Delta\theta_{2p}$, the angular separation between the test particles.

Consider Fig. (5.3). Here we show a finite $\Delta\theta_{2p}$, which gives the angular separation between the test particles A and B. Since $\Delta\ell$ is finite, the variations in θ between A and B must be included. For a differential element of $\Delta\ell$, $d\Delta\ell$, we have that

$$d\Delta\ell = dS |\cos [(\alpha + \beta) - \Delta\theta_i]| \quad (5.12)$$

Now we see that

$$dS = r d(\Delta\theta_i) |(1 + \tan^2 \beta)^{\frac{1}{2}}| = r d(\Delta\theta_i) / |\cos \beta| \quad (5.13)$$

and thus on integrating $d\Delta\ell$ from 0 to $\Delta\ell$, and $d(\Delta\theta_i)$ from 0 to $\Delta\theta_{2p}$, we have

$$\Delta\ell = \int_0^{\Delta\theta_{2p}} \left| \frac{r}{\cos \beta} \cos [(\alpha + \beta) - \Delta\theta_i] \right| d(\Delta\theta_i) \quad (5.14)$$

Thus $\Delta\ell$ becomes

$$\Delta\ell = \left| \frac{r}{\cos \beta} [\sin (\alpha + \beta) - \sin (\alpha + \beta - \Delta\theta_{2p})] \right| \quad (5.15)$$

However, if $\alpha + \beta > \pi/2$, then particle A of Fig. (5.3) will be on the opposite side of B. We will then have to use the expression

$$\Delta\ell = \int_0^{\Delta\theta_{2p}} \left| \frac{r}{\cos \beta} \cos [(\alpha + \beta) + \Delta\theta_i] \right| d(\Delta\theta_i) \quad (5.16)$$

to replace Eq. (5.14); thus, when $\alpha + \beta > \pi/2$

$$\Delta\ell = \left| \frac{r}{\cos \beta} [\sin(\alpha + \beta) - \sin(\alpha + \beta + \Delta\theta_{2p})] \right| \quad (5.17)$$

Using Eqs. (5.15) and (5.17) for $\Delta\ell$, n_+ becomes

$$n_+ = \left| \frac{r_0^2 \sin \theta_0 \cos \theta_0 \cos \beta (\Delta\theta_{2p})_0}{r^2 (1 + \theta/U)^2 \sin \theta [\sin(\alpha + \beta) - \sin(\alpha + \beta + \Delta\theta_{2p})]} \right| \quad (5.18)$$

with (-) for $\alpha + \beta \leq \pi/2$

(+) for $\alpha + \beta > \pi/2$

As the angle θ approaches 0 or π the density of ions, according to Eq. (5.18) approaches infinity. This is the result of our neglect of the thermal velocities of the screening particles which in reality will prevent the ions from converging toward the axis of symmetry; i.e. although θ may reach $\theta = \pi$ along some of the ion trajectories, most of the ions will only approach π .

Let us now obtain a correction to Eq. (5.18) (specifically $\sin \theta$) which will introduce the thermal velocities as an approximate correction to the density calculations in the neighborhood of the axis. Consider a typical ion that is approaching the charged body but is still "outside" the field of the body. Its velocity relative to the charged body will be the vectorial sum of \underline{u} (the vector velocity between the plasma and the charged body) and \underline{w} , the thermal velocity of the ion. In Fig. (5.4) we show the sum of \underline{w} and $\underline{u} = u\underline{z}$ (where u is the scalar magnitude of \underline{u} and \underline{z} is the unit vector along

the axis of symmetry of the coordinate system. The three unit vectors for this coordinate system are \underline{z} , \underline{r} , $\underline{\theta}$.) The components of \underline{w} are also shown.

Now the fact that n_+ is not infinite for trajectories crossing the z axis is due only to w_θ , the θ component of the thermal velocities of the ions. The components w_r and w_z contribute only higher order corrections to the density calculations. But how is it that the w_θ component of the ion velocity results in a reduction in the density near the axis? Consider again Fig. (5.4) and assume that the thermal velocities are small compared to \underline{u} (i.e., $kT \ll U$). In order to calculate n_+ to first order we may set $\underline{u} + \underline{w} = \underline{u} + w_\theta \underline{\theta} = \underline{u}'$. With a velocity of \underline{u}' the axis of symmetry for the particle will be shifted from the coordinate axis z . A particle whose thermal velocity in the θ direction is w_θ will pass no closer to the z coordinate axis than $\rho w_\theta / u$ (where $w_\theta \ll u$). Thus no particle with $w_\theta > u(\pi - \theta)$ can reach a coordinate point ρ , θ ($\theta = 0$ being on the forward side of the body). We, therefore, obtain the first order correction to the density equations by excluding all such particles.

If $kT \ll U$, the density contribution of each particle reaching ρ , θ will be the same to first order. The density will be reduced in proportion to the reduction in the number of particles reaching ρ , θ . The density is thus reduced by a factor F .

$$F = 1 - \delta(w_\theta')$$
(5.19)

where $\delta(w_\theta')$ is the fraction of particles with w_θ greater than w_θ'

$$w_\theta' = u(\pi - \theta)$$
(5.20)

If we assume the ambient ions to have a Maxwellian velocity

distribution, then the function $\delta(w_{\theta'})$ is given by

$$\delta(w_{\theta'}) = \sqrt{\frac{2m}{\pi kT}} \int_{w_{\theta'}}^{\infty} e^{-\frac{mw_{\theta'}^2}{2kT}} dw_{\theta'} = \frac{2}{\sqrt{\pi}} \int_{x'}^{\infty} e^{-x^2} dx \quad (5.21)$$

where

$$x' = \sqrt{\frac{m}{2kT}} w_{\theta'} \quad (5.22)$$

F becomes, using Eq. (5.21) in (5.19)

$$F = 1 - \frac{2}{\sqrt{\pi}} \int_{\sqrt{\frac{m}{2kT}} w_{\theta'}}^{\infty} e^{-x^2} dx \quad (5.23)$$

Using Eq. (5.20) in (5.23) we have

$$F = 1 - \frac{2}{\sqrt{\pi}} \int_{\sqrt{U/kT} (\pi - \theta)}^{\infty} e^{-x^2} dx \quad (5.24)$$

Using the conditions of Eq. (5.24), the expression for n_+ , Eq. (5.18), will become

$$n_+ = \left| \frac{r_0^2 \sin \theta_0 \cos \theta_0 \cos \beta (\Delta \theta_{2p})_0}{r^2 (1 + \theta/U)^{\frac{1}{2}} [\sin (\alpha + \beta) - \sin (\alpha + \beta \mp \Delta \theta_{2p})] \sin \theta} \right| \cdot \left[1 - \frac{2}{\sqrt{\pi}} \int_{\sqrt{U/kT} (\pi - \theta)}^{\infty} e^{-x^2} dx \right] \quad (5.25)$$

with (-) for $\alpha + \beta \leq \pi/2$

(+) for $\alpha + \beta > \pi/2$

Where $\theta_0 = 0$ for any of the test particles, Eqs. (5.18) and (5.25) must be supplemented by the expression

$$n_+ = \frac{r_0^2 (\Delta \theta_{2p})_0}{r^2 (1 + \theta/U)^{\frac{1}{2}} \Delta \theta_{2p}} \quad (5.26)$$

This results from the observation that for a particle initially moving along the axis of symmetry, for which β must be zero, α must always be zero as well. Thus, the value of θ will also remain zero. One, therefore, can take the limit of Eq. (5.18), which yields Eq. (5.26).

Finally, note that Eqs. (5.18), (5.25), and (5.26) can be rendered in non-dimensional form merely by substituting ρ , ρ_0 and ψ for r , r_0 and θ/U .

B. The electron density N_- . The density of the electrons in the repulsive electric field can be obtained from general considerations alone. In the case of a stationary gas of non-interacting particles in which the particles are subject to an external force, the Maxwell-Boltzmann statistics derivation using Lagrange multipliers yields for the distribution function in phase space²⁴

$$d^6N = \frac{N}{V_e} e^{-|\theta|/kT} dx dy dz \left(\frac{m}{2\pi kT}\right)^{\frac{3}{2}} e^{-mv^2/2kT} dv_x dv_y dv_z \quad (5.27)$$

where V_e is an integral over a volume V

$$V_e = \iiint_V e^{-|\theta|/kT} dx dy dz \quad (5.28)$$

x , y , z , v_x , v_y , v_z are the phase space coordinates and m is the particular mass.

If one integrates Eq. (5.27) over all v_x , v_y , v_z , one obtains

$$N_- = \frac{dN}{dV} = \frac{N}{V_e} e^{-|\theta|/kT} \quad (5.29)$$

Since V_e includes all space

$$\frac{N}{V_e} = \frac{\text{All particles in space}}{\text{All space}} \equiv N_0 \quad , \quad (5.30)$$

we have

$$N_- = N_0 e^{-|\phi|/kT} \quad (5.31)$$

There are, however, certain considerations that need more careful consideration. The integral over all v_x, v_y, v_z , is only allowable if all values are permitted. If the field is attractive, then there will be a cone of angles for the velocity vectors specified by energy and angular momentum considerations that are allowable. It is impossible for a particle to arrive at this particular point in space with a velocity vector lying outside this cone of angles. Thus, under these conditions, the integration of Eq. (5.27) will not yield Eq. (5.29). In general, the result will be quite complicated and may depend upon the paths of the particles. It is this fact which dictated the approach in section A of this chapter for the derivation of the ion density.

When the field is repulsive everywhere in space, then the allowed cone of velocity vectors fills the whole velocity space (i.e. all values of v_x, v_y, v_z are permitted). Thus, for a specularly reflecting, negatively charged body, the electrons will have a density at any point in space given by Eq. (5.31) if one neglects their drift velocity.

To allow for the drift of the electron gas relative to the charged body, transform the coordinate v_x into $v_x - u_s$, in Eq. (5.27) where u_s is the drift velocity of the gas relative to the body

$$d^6N = \frac{N}{V_e} e^{-|\phi|/kT} dx dy dz \left(\frac{m}{2\pi kT}\right)^{\frac{3}{2}} \cdot \exp\left\{-\frac{m}{2kT} [(v_x - u_s)^2 + v_y^2 + v_z^2]\right\} dv_x dv_y dv_z \quad (5.32)$$

If we choose a position in space far removed from the charged body and if the potential energy for the electrons at that point is ϕ , then we would obtain upon integrating Eq. (5.32) over all allowable v_x, v_y, v_z :

$$n_- = e^{-|\phi|/kT} \left(\frac{m}{2\pi kT}\right)^{\frac{3}{2}} \int_{-\infty}^{\infty} \int_{-\infty}^{\infty} \int_{-\infty}^{\infty} e^{(-m/2kT) [(v_x - u_s)^2 + v_y^2 + v_z^2]} \cdot dv_x dv_y dv_z = e^{-|\phi|/kT} \quad (5.33)$$

If, however, the charged body is very large and nearby and if electrons are specularly reflected off the body, then along the axis of the body, we can write

$$n_- = e^{-|\phi|/kT} \left(\frac{m}{2\pi kT}\right)^{\frac{3}{2}} \left[\int_{-\infty}^{\infty} \int_{-\infty}^{\infty} e^{(-m/2kT) (v_y^2 + v_z^2)} dv_y dv_z \right] \cdot \left[2 \int_{-\infty}^{u_s} e^{(-m/2kT) (v_x - u_s)^2} dv_x \right] \quad (5.34)$$

The factor 2 before the integral over v_x is the return factor Q .

The limits on the integral over v_x are from $-\infty$ to u_s since any electron with a higher velocity will run away from the charged body on the frontside, and on the back side it is prevented from reaching any point on the frontside due to the presence of the charged body. If we transform coordinates in Eq. (5.34) so that $w = v_x - u_s$ we obtain:

$$n_- = e^{-|\phi|/kT} \left(\frac{m}{2\pi kT}\right)^{\frac{3}{2}} \left[\int_{-\infty}^{\infty} \int_{-\infty}^{\infty} e^{(-m/2kT) (v_y^2 + v_z^2)} dv_y dv_z \right] \cdot \left[2 \int_{-\infty}^0 e^{-mw^2/2kT} dw \right] = e^{-|\phi|/kT} \quad (5.35)$$

We again, have obtained the same simple relation for n_- .

If the electrons are not reflected from the surface of the

charged body, then the return factor will be $Q = 2$ only for those electrons that do not reach the surface of the body; i.e., for particles of velocity v_x with $\frac{1}{2}mv_x^2 < |\phi_s|$. For those that reach the surface $Q = 1$. In this case, Eq. (3.34), which already excludes all particles that do not approach the surface of the body, becomes

$$n_- = e^{-|\phi|/kT} \left(\frac{m}{2\pi kT} \right)^{\frac{1}{2}} \left[2 \int_{-\infty}^{u_s} e^{-(m/2kT)(v_x - u_s)^2} dv_x - \int_{-\infty}^{-v_\phi} e^{-(m/2kT)(v_x - u_s)^2} dv_x \right] \quad (5.36)$$

where v_ϕ is

$$v_\phi = (2|\phi_s|/m)^{\frac{1}{2}} \quad (5.37)$$

and ϕ is the potential (energy) of the surface. If we make the substitution

$$\omega = \sqrt{\frac{m}{2kT}} (v_x - u_s) \quad (5.38)$$

and replace u_s with $v_s = u_s \cos \theta_0$ (θ_0 is the initial polar angle coordinate) in Eq. (5.36), we obtain

$$n_- = e^{-|\phi|/kT} \left[1 - \frac{1}{\sqrt{\pi}} \int_{(v_\phi + v_s)\sqrt{m/2kT}}^{\infty} e^{-\omega^2} d\omega \right] \quad (5.39)$$

where m is the mass of the repelled particle (the electronic mass in our case).

A similar expression has been obtained by Lundgren and Chang⁷. The validity of Eq. (5.39) is seriously limited, however, since the potential is assumed to vary in only one dimension; the expression is not even valid for an uncharged body, except near the surface. Equation (5.39) holds only if the radii of curvature of the body and

of the equipotential surface ϕ are large compared with the distance between these two surfaces.

If u_s is small compared to the mean velocity of the electrons, the lower limit on the integral in Eq. (5.39) becomes simply $\sqrt{|\phi_s|/kT}$. If in addition, $|\phi_s| \gg kT$, Eq. (5.39) will become

$$n_- = e^{-|\phi|/kT} \quad (5.40)$$

as before (Eqs. (5.35), (5.33), (5.31)).

For the problems that we will investigate numerically, u_s is small compared with the mean velocity of the electrons and we will therefore neglect it. There is also some experimental evidence that $|\phi_s| \gg kT$, at least for some cases. We will, therefore, use Eq. (5.40) for the electron density. In order to make use of Eq. (5.39) one must concentrate on a specific problem. The use of Eq. (5.39) would greatly increase the computation time and is not essential to the present purposes.

Although we obtained Eq. (5.40) from Eq. (5.39) by assuming that $|\phi_s| \gg kT$, this condition is effectively satisfied even if we set $\phi_s = \phi_e$, the equilibrium value of the potential. For $\phi_s = \phi_e$ the error in the calculation of $n_+ - n_-$ using Eq. (5.40) as compared with using Eq. (5.39) will be at most about 1%.

CHAPTER VI

OTHER EQUATIONS FOR FOLLOWING TRAJECTORIES

A. Calculation of new orbit coordinates (ρ, θ). The solution of screening problems requires only the Poisson equation and expressions for the ion and electron densities. In Chapter V we obtained expressions for the ion and electron densities which allow us to compute the electric field along test particle trajectories. We must, now, obtain equations for particle trajectories. In addition we will need an expression for the normal to the equipotential surface, and we must express the Poisson equation in convenient coordinates.

We consider first the question of trajectory calculations. The trajectory is obtained by "updating" the test particle coordinates as the test particle traces out the field. The current coordinate position of a particle can be determined by extrapolating its trajectory using the current value of α , the pitch angle of the particle's velocity vector. In Fig. (6.1), the parameters for this extrapolation are indicated. We assume initially that the particle is located at r_1, θ_1 . An extrapolation of the particle coordinates by a distance Δe parallel to the velocity vector will bring the particle to r_2, θ_2 . By trigonometric relations, we obtain for r_2

$$r_2 = [r_1^2 + (\Delta e)^2 - 2r_1 \Delta e \cos \alpha]^{\frac{1}{2}} \quad (6.1)$$

and for θ_2 :

$$\theta_2 = \theta_1 + \Delta\theta \quad (6.2)$$

where

$$\sin \Delta\theta = \frac{\Delta e}{r_2} \sin \alpha \quad (6.3)$$

If $r_1 \gg \Delta e$, we can simplify Eq. (6.1) to

$$r_2 = r_1 \sqrt{1 + (\Delta e/r_1)^2 - 2\Delta e \cos \alpha / r_1} \approx r_1 - \Delta e \cos \alpha. \quad (6.4)$$

The equation for $\Delta\theta$, equation (6.3), can be written approximately as

$$\Delta\theta \approx \frac{\Delta e}{r_2} \sin \alpha. \quad (6.5)$$

Approximate expressions such as Eqs. (6.4) and (6.5) can be used to reduce the computation time without affecting significantly the accuracy of the calculations. Equations (6.4) and (6.5) can be written in a nondimensional form by substituting ρ_2 for r_2 , ρ_1 for r_1 , and $\Delta\eta$ for Δe .

B. Calculation of the particle's pitch angle α . In Fig. (6.2), we have shown the position of a particle at two points along its trajectory separated by the incremental angle $\Delta\theta$. The value of the angles between the velocity vectors v_1 and v_2 and the respective radius vectors are α_1 and α_2 . The angle $\Delta\gamma$ represents the angular change from a straight line trajectory (positive in the direction of increasing α). In terms of these quantities, we have the geometric relation

$$\alpha_2 - \Delta\gamma = \alpha_1 + \Delta\theta. \quad (6.6)$$

If we consider that the change in β will enter only as a higher order term, we may consider the equipotential surfaces to be parallel at these two points. Thus, the components of the velocity vectors normal to the electric field will not be affected in going from P to Q. We, therefore, have

$$v_1 \sin(\alpha_1 + \beta_1) = v_2 \sin(\alpha_2 + \beta_1 - \Delta\theta). \quad (6.7)$$

Substituting from Eq. (6.6) for α_2 we obtain

$$\begin{aligned} \frac{v_1}{v_2} \sin (\alpha_1 + \beta_1) &= \sin (\alpha_1 + \beta_1) \cos \Delta \gamma + \cos (\alpha_1 + \beta_1) \sin \Delta \gamma \\ &\approx \sin (\alpha_1 + \beta_1) + \cos (\alpha_1 + \beta_1) \Delta \gamma \quad . \quad (6.8) \end{aligned}$$

Thus $\Delta \gamma$ becomes

$$\Delta \gamma = \left(\frac{v_1}{v_2} - 1 \right) \tan (\alpha_1 + \beta_1) \quad . \quad (6.9)$$

Substituting from Eq. (6.9) into Eq. (6.6) yields

$$\alpha_2 = \alpha_1 + \Delta \theta - \left(1 - \frac{v_1}{v_2} \right) \tan (\alpha_1 + \beta_1) \quad . \quad (6.10)$$

Substituting for v_1 and v_2 in terms of θ_1 , θ_2 and U , we have

$$\alpha_2 = \alpha_1 + \Delta \theta - \left[1 - \frac{\sqrt{1 + \theta_1/U}}{\sqrt{1 + \theta_2/U}} \right] \tan (\alpha_1 + \beta_1) \quad . \quad (6.11)$$

C. Calculation of β from the coordinates of two test particles.

The angle between the normal to the equipotential surface and the radius vector plays an important part in the expression for the ion density and in the second derivative of the potential. In the calculational procedure which we have adopted, the quantity β will be determined by following a pair of test particles so that their coordinate positions on the same equipotential surface can be used to evaluate β . It is possible to do this using the same pair of test particles that are used to obtain $\Delta \theta_{2p}$. The equation for β in terms of the coordinate positions r_1 , θ_1 and r_2 , θ_2 is immediately obtainable from Fig. (6.3).

$$\beta = \arctan \frac{(r_1 - r_2)}{r_2 (\theta_2 - \theta_1)} \quad (6.12)$$

where β is positive in the direction shown in Fig. (6.3).

D. The transformation of the Laplacian. In order to achieve simplicity in the point by point computations of the electric and potential fields using Poisson's equation

$$\nabla^2 \psi = n_- - n_+ \quad (6.13)$$

let us consider the form of $\nabla^2 \psi$ expressed in terms of local coordinates for which the electric field is parallel to the radius vector. The geometric relationship of these local coordinates λ, Θ, θ to the coordinates ρ, θ, θ are shown for a constant θ plane in Fig. (6.4). In addition, we will introduce the coordinates $\lambda', \Theta', \theta$ for which λ' is parallel to λ but the center of these coordinates is located at the center of curvature of the equipotential surface.

Since we will be following several particle trajectories at the same time and will be incrementing their paths from equipotential surface to equipotential surface, it will be convenient to express the electric field vector in terms of local coordinates. For an appropriate choice of local coordinates (λ', Θ') the variation in β along $\psi = \text{constant}$ (in the ρ, θ coordinates) will vanish (in the λ', Θ' coordinates).

These coordinates will allow us to update the trajectory of the ions from one point to the next in terms of the coordinate ρ, θ and to update the electric and potential fields in the coordinates λ', Θ' . The choice of the λ', Θ' coordinates makes transformations between the two systems quite straightforward as shown below.

The Laplacian $\nabla^2 \psi$ expressed in terms of the coordinates λ, Θ, θ is

$$\nabla^2 \psi = \frac{1}{\lambda^2} \frac{\partial}{\partial \lambda} \left(\lambda^2 \frac{\partial \psi}{\partial \lambda} \right) + \frac{1}{\lambda^2 \sin \Theta} \frac{\partial}{\partial \Theta} \left(\sin \Theta \frac{\partial \psi}{\partial \Theta} \right) + \frac{1}{\lambda^2 \sin^2 \Theta} \frac{\partial^2 \psi}{\partial \theta^2} . \quad (6.14)$$

Since we have axial symmetry with respect to θ , the last term can be dropped. According to Fig. (6.4), we can express λ in terms of ρ by:

$$\frac{\lambda}{\sin \theta} = \frac{\rho}{\sin \theta} = \frac{\rho}{\sin (\theta + \beta)} \quad . \quad (6.15)$$

Thus Eq. (6.14) becomes

$$\nabla^2 \psi = \frac{\partial^2 \psi}{\partial \lambda^2} + \frac{2 \sin (\theta + \beta)}{\rho \sin \theta} \frac{\partial \psi}{\partial \lambda} + \frac{\sin^2 \theta}{\rho^2 \sin^2 \theta} \left(\cot \theta \frac{\partial \psi}{\partial \theta} + \frac{\partial^2 \psi}{\partial \theta^2} \right) \quad . \quad (6.16)$$

Now consider the variation of the electric field along an equipotential surface (which by definition is concentric with λ'). Since the electric field is perpendicular to the equipotential surface at all points, $\partial \psi / \partial \theta' = 0$ in the neighborhood of the point and, also, $\partial \psi / \partial \theta = 0$.

Let us next consider the value of $\partial^2 \psi / \partial \theta^2$. This of course, is the rate at which $\partial \psi / \partial \theta$ varies as θ increases. Since there is no "angle" component of the electric field in the coordinates λ' , θ' (i.e. $\partial \psi / \partial \theta' = 0$), the "angle" component of the electric field in the coordinates λ , θ (i.e. $\partial \psi / \partial \theta$) is simply a component of $\partial \psi / \partial \lambda'$. Thus, as shown in Fig. (6.5), the value of $\partial \psi / \partial \theta$ at point 2 is given by:

$$\frac{1}{\lambda} \frac{\partial \psi}{\partial \theta} = \sin \delta \gamma \left(\frac{\partial \psi}{\partial \lambda'} \right)_2 \quad . \quad (6.17)$$

Now $(\partial \psi / \partial \lambda')_2$ is given by

$$\left(\frac{\partial \psi}{\partial \lambda'} \right)_2 = \left(\frac{\partial \psi}{\partial \lambda'} \right) + \frac{\partial}{\partial \theta'} \left(\frac{\partial \psi}{\partial \lambda'} \right) \delta \theta' \quad , \quad (6.18)$$

so that Eq. (6.17) gives

$$\frac{\partial \psi}{\partial \theta} = \lambda \sin \delta \gamma \left[\left(\frac{\partial \psi}{\partial \lambda'} \right)_1 + \frac{\partial}{\partial \theta'} \left(\frac{\partial \psi}{\partial \lambda'} \right) \delta \theta' \right] \quad . \quad (6.19)$$

Since $\partial \psi / \partial \theta = 0$ at point 1, we obtain for $\partial^2 \psi / \partial \theta^2$

$$\frac{\partial^2 \psi}{\partial \theta^2} = \frac{\delta}{\delta \theta} \left(\frac{\partial \psi}{\partial \theta} \right) = \lambda \left[\left(\frac{\partial \psi}{\partial \lambda'} \right)_1 + \frac{\partial^2 \psi}{\partial \theta' \partial \lambda'} \delta \theta' \right] \frac{\delta \gamma}{\delta \theta} = \lambda \left(\frac{\partial \psi}{\partial \lambda'} \right)_1 \frac{\delta \gamma}{\delta \theta}. \quad (6.20)$$

To obtain $\delta \gamma / \delta \theta$ consider the triangle ABC in Fig. (6.5). We have:

$$(\lambda - \lambda') \sin \delta \theta = \lambda' \sin \delta \gamma \quad (6.21)$$

so that

$$\frac{\delta \gamma}{\delta \theta} = \frac{\lambda}{\lambda'} - 1 \quad (6.22)$$

To obtain λ / λ' , we see from Fig. (6.6) that λ' can be expressed in terms of ρ by

$$\lambda' \Delta \theta' \cos \beta = \rho \Delta \theta \quad (6.23)$$

From Fig. (6.4) we see that $\theta' = \theta + \beta$; a variation along an equipotential surface gives

$$\Delta \theta' = \Delta \beta + \Delta \theta \quad (6.24)$$

Substituting Eq. (6.24) for $\Delta \theta'$ and Eq. (6.15) for ρ into Eq. (6.23) we have

$$\frac{\lambda}{\lambda'} = \frac{\sin \theta \cos \beta}{\sin (\theta + \beta)} \left(1 + \frac{\Delta \beta}{\Delta \theta} \right) \quad (6.25)$$

Since the variations in Eq. (6.23) and (6.24) are along an equipotential surface, Eq. (6.25) becomes in the limit as $\Delta \theta \rightarrow 0$

$$\frac{\lambda}{\lambda'} = \frac{\sin \theta \cos \beta}{\sin (\theta + \beta)} \left[1 + \left(\frac{\partial \beta}{\partial \theta} \right)_\psi \right] \quad (6.26)$$

If we now use Eq. (6.26) for λ / λ' in Eq. (6.22) and substitute the resulting expression into Eq. (6.20) we obtain for $\partial^2 \psi / \partial \theta^2$

$$\frac{\partial^2 \psi}{\partial \theta^2} = \lambda \left\{ \frac{\sin \theta \cos \beta}{\sin (\theta + \beta)} \left[1 + \left(\frac{\partial \beta}{\partial \theta} \right)_\psi \right] - 1 \right\} \left(\frac{\partial \psi}{\partial \lambda'} \right)_1 \quad (6.27)$$

Since the coordinates λ and λ' are always parallel, we have that

$$\left(\frac{\partial \psi}{\partial \lambda'} \right)_1 = \frac{\partial \psi}{\partial \lambda} \quad (6.28)$$

and thus

$$\frac{\partial^2 \psi}{\partial \theta^2} = \lambda \left\{ \frac{\sin \theta \cos \beta}{\sin (\theta + \beta)} \left[1 + \left(\frac{\partial \beta}{\partial \theta} \right)_{\psi} \right] - 1 \right\} \frac{\partial \psi}{\partial \lambda} \quad (6.29)$$

If we substitute Eq. (6.29) for $\partial^2 \psi / \partial \theta^2$ into Eq. (6.16), we obtain

$$\nabla^2 \psi = \frac{\partial^2 \psi}{\partial \lambda^2} + \frac{\sin (\theta + \beta)}{\rho \sin \theta} \left\{ 1 + \frac{\sin \theta \cos \beta}{\sin (\theta + \beta)} \left[\left(\frac{\partial \beta}{\partial \theta} \right)_{\psi} + 1 \right] \right\} \frac{\partial \psi}{\partial \lambda} \quad (6.30)$$

It must be remembered that Eq. (6.30) does not express $\nabla^2 \psi$ in terms of coordinates moving with the particles, but merely represents a geometric relationship between the coordinates ρ , θ and λ , θ which allows us to deal with the total electric field intensity (actually the electric force on a charge) $\partial \psi / \partial \lambda$ rather than the components $\partial \psi / \partial \rho$ and $\partial \psi / \rho \partial \theta$. Since the electric field must be invariant under coordinate transformations, it is immaterial what coordinates are chosen; Eq. (6.30) is employed only because it expresses $\nabla^2 \psi$ in the most convenient terms for our purposes.

Equation (6.30) will be used for "updating" the electric field. Because of the particular choice of coordinates used to calculate $\nabla^2 \psi$, the electric field will lie along the radius vector. The updating equation is then, simply,

$$\left(\frac{\partial \psi}{\partial \lambda} \right)_2 = \left(\frac{\partial \psi}{\partial \lambda} \right)_1 + \left(\frac{\partial^2 \psi}{\partial \lambda^2} \right) \Delta \lambda \quad (6.31)$$

CHAPTER VII

GROWTH OF ERRORS IN NUMERICAL CALCULATIONS

Although some special cases of the screening problem can be treated by analytical means, complete solutions can be obtained only by recourse to digital computers, as already mentioned. However, the numerical calculations of a solution is of practical necessity limited in accuracy. Since single precision floating point calculations on an IBM 7090, as employed in our calculations, use 27 bit mantissas and double precision 54 bits, each single precision calculation will involve an error in the 9th digit and each double precision calculation will involve an error in the 17th digit. Each step in the integration of the screening equations (see Chapters V and VI) involves the calculation of various quantities in terms of their values on the previous step. It should appear obvious that a small error introduced early in the trajectory calculations can become quite significant at a later point. There exists also the possibility that the error will not become important.

It is quite possible to calculate whether the error involved in updating a particular quantity will grow or be removed; whether the series of such errors is divergent or convergent. The procedure for deriving the criterion is simple but may require considerable effort for involved equations, such as we have. In most cases it is simplest merely to experiment with various parameters, such as the step size and or particle separation, to see if the results depend upon their value. In some cases, however, such a trial and error procedure is not satisfactory due to the large amount of computation time that may be involved. There is, also, the danger that the

erratic results obtained from the computations arise from other shortcomings. For these reasons, a formulation of the behavior of the errors will be obtained here.

The procedure involved is simply to assume that in the step-by-step calculations a variable X is updated according to the relation

$$X_{\text{new}} = X_{\text{old}} + f(X_{\text{old}}) \quad . \quad (7.1)$$

We then assume that the true value of X is replaced by \bar{X} (which includes an error δ)

$$\bar{X} = X + \delta \quad (7.2)$$

where δ is the round-off error in the value of X . We thus find that

$$X_{\text{new}} + \delta_{\text{new}} = X_{\text{old}} + \delta_{\text{old}} + f(X_{\text{old}} + \delta_{\text{old}}) \quad (7.3)$$

$$= X_{\text{old}} + \delta_{\text{old}} + f(X_{\text{old}}) + f'(X_{\text{old}}) \delta_{\text{old}} \quad (7.4)$$

Thus for δ we have,

$$\delta_{\text{new}} = \delta_{\text{old}} [1 + f'(X)] \quad . \quad (7.5)$$

Equation (7.5) shows that if $|1 + f'(X)|$ is less than one, then any error δ introduced at any point in the calculations will be removed exponentially; if it is greater than one, the error will grow exponentially. Thus, the convergence of the series of errors can be effected only by changing the values of the parameters in $f'(X)$.

Early attempts at obtaining numerical solutions in the problem of the screening of a rapidly moving charged body showed that the angle β between the normal to the equipotential surface and the radius vector is highly unstable for small values of θ_{10} , the initial angle for the first particle (i.e., near the axis). (The reader should remember that the field is traced using four test particles divided

into pairs; each pair is used to obtain a value of β on the equipotential surface. The resulting pair of values for β is used to obtain $\partial\beta/\partial\theta$.)

The equation for β for the first two particles is, from Eq. (6.12),

$$\beta = \arctan \frac{\rho_{12} - \rho_{22}}{\rho_{22} (\theta_{22} - \theta_{12})} \quad (7.6)$$

where the first subscript on ρ and θ specifies the particle and the second subscript specifies whether the value of ρ and θ is for the current step (2) or the last step (1), corresponding to the subscripts new and old in Eqs. (7.1) through (7.5). For small values of β , Eq. (7.6) can be approximated by

$$\beta = \frac{1}{\delta\theta_{12}} (\frac{\rho_{12}}{\rho_{22}} - 1) \quad (7.7)$$

where $\delta\theta_{12} = (\theta_{22} - \theta_{12})$, the subscript 12 on $\delta\theta$ referring to the first pair of particles (used to calculate β) on the current step.

If we write

$$\rho_{12} = \rho_{11} + \Delta\rho_1 \quad , \quad (7.8)$$

$$\rho_{22} = \rho_{21} + \Delta\rho_2 \quad (7.9)$$

and

$$\delta\theta_{12} = \delta\theta_{11} + \Delta\delta\theta_1 \quad , \quad (7.10)$$

we can write for β , where β is small

$$\beta_{\text{new}} = \beta_{\text{old}} + \Delta\beta \quad (7.11)$$

where

$$\Delta\beta = \frac{1}{\delta\theta_{11}} \left[\frac{\Delta\rho_1}{\rho_{21}} - \frac{\rho_{11} \Delta\rho_2}{\rho_{21}^2} + \frac{\Delta\delta\theta_1}{\delta\theta_{11}} \left(1 - \frac{\rho_{11}}{\rho_{21}} \right) \right] \quad (7.12)$$

If $\Delta\beta$ is defined to be $f(\beta)$

$$\Delta\beta \equiv f(\beta) \quad , \quad (7.13)$$

then Eq. (7.11) will take the form of Eq. (7.1). We thus can write according to Eq. (7.5)

$$\delta_{\text{new}} = \delta_{\text{old}} [1 + f'(\beta)] \quad . \quad (7.14)$$

Thus, we require the quantity $f'(\beta)$. Let us write, therefore

$$f(\beta) = f_1 - f_2 + f_3 \quad (7.15)$$

where

$$f_1 = \frac{\Delta\rho_1}{\delta\theta_{11} \rho_{21}} \quad (7.16)$$

$$f_2 = \frac{\rho_{11}}{\delta\theta_{11} \rho_{21}^2} \Delta\rho_2 \quad (7.17)$$

$$f_3 = \frac{1}{(\delta\theta_{11})^2} (1 - \frac{\rho_{11}}{\rho_{21}}) \Delta\delta\theta_1 \quad . \quad (7.18)$$

Here the quantities $\Delta\rho_1$, $\Delta\rho_2$ and $\Delta\delta\theta_1$ are expressed in terms of the quantities from step (1) (i.e., the old values). From Eq. (6.4), we can write for $\Delta\rho_1$

$$\Delta\rho_1 = - \Delta\eta_1 \cos \alpha_{12} \quad (7.19)$$

so that Eq. (7.16) for f_1 , becomes

$$f_1 = - \frac{\Delta\eta_1 \cos \alpha_{12}}{\delta\theta_{11} \rho_{21}} \quad ; \quad (7.20)$$

therefore,

$$f_1' = \frac{\Delta\eta_1 \sin \alpha_{12}}{\delta\theta_{11} \rho_{21}} \frac{\partial \alpha_{12}}{\partial \beta} \quad . \quad (7.21)$$

From Eq. (6.11) for α and Eq. (6.5) for $\Delta\theta$ we have for α_{12}

$$\alpha_{12} = \alpha_{11} + \frac{\Delta\eta_1 \sin \alpha_{11}}{\rho_{12}} + [- \frac{\Delta\psi}{2(1+\psi)}] \tan(\alpha_{11} + \beta_1) \quad (7.22)$$

so that

$$\frac{\partial \alpha_{12}}{\partial \beta} = - \frac{\Delta \psi}{2 (1 + \psi) \cos^2 (\alpha_{11} + \beta_1)} \quad (7.23)$$

and Eq. (7.21) for f_1' becomes:

$$f_1' = - \frac{\Delta \psi \Delta \eta_1 \sin \alpha_{12}}{2 (1 + \psi) \cos^2 (\alpha_{11} + \beta_1) \delta \theta_{11} \rho_{21}} \quad (7.24)$$

For f_2 we have, using Eq. (6.4) to obtain $\Delta \rho_2$:

$$f_2 = - \frac{\rho_{11}}{\delta \theta_{11} \rho_{21}^2} [\frac{\psi_{12}' \Delta \eta_1 \cos (\alpha_{12} + \beta_1)}{\psi_{22}' \cos (\alpha_{22} + \beta_1)} \cos \alpha_{22}] \quad (7.25)$$

Thus, for the derivative of f_2 with respect to β , we can write

$$\begin{aligned} f_2' = & - \frac{\rho_{11} \Delta \eta_1}{\theta_{11} \rho_{21}^2} \left\{ \frac{\cos (\alpha_{12} + \beta_1) \cos \alpha_{22}}{\psi_{22}' \cos (\alpha_{22} + \beta_1)} \frac{\partial}{\partial \beta} (\psi_{12}') \right. \\ & - \frac{\psi_{12}' \cos (\alpha_{12} + \beta_1) \cos \alpha_{22}}{\psi_{22}'^2 \cos (\alpha_{22} + \beta_1)} \frac{\partial}{\partial \beta} (\psi_{22}') \\ & - \frac{\psi_{12}' \cos \alpha_{22} \sin (\alpha_{12} + \beta_1)}{\psi_{22}' \cos (\alpha_{22} + \beta_1)} \frac{\partial \alpha_{12}}{\partial \beta} \\ & - \frac{\psi_{12}' \cos (\alpha_{12} + \beta_1)}{\psi_{22}' \cos (\alpha_{22} + \beta_1)} [\cos (\alpha_{22} + \beta_1) \sin \alpha_{22} \\ & - \cos \alpha_{22} \sin (\alpha_{22} + \beta_1)] \frac{\partial \alpha_{22}}{\partial \beta} \\ & + \frac{\psi_{12}' \cos \alpha_{22}}{\psi_{22}' \cos^2 (\alpha_{22} + \beta_1)} [\cos (\alpha_{12} + \beta_1) \sin (\alpha_{22} + \beta_1) \\ & \left. - \cos (\alpha_{22} + \beta_1) \sin (\alpha_{12} + \beta_1)] \right\} \quad (7.26) \end{aligned}$$

From the equation for updating ψ' , Eq. (6.31), we obtain

$$\begin{aligned} \frac{\partial}{\partial \beta} (\psi_{12}') = & \left\{ n_{+11} [\tan (\alpha_{11} + \beta_1) - \tan \beta_1] + \left[\frac{\cos (\theta_{11} + \beta_1)}{\rho_{11} \sin \theta_{11}} \right. \right. \\ & \left. \left. - \frac{\sin \beta_1}{\rho_{11}} (1 + \beta') \right] \psi_{11}' \right\} \Delta \eta_1 \cos (\alpha_{11} + \beta_1) + \left\{ n_{-11} - n_{+11} \right. \\ & \left. - \left[\frac{\sin (\theta_{11} + \beta_1)}{\rho_{11} \sin \theta_{11}} + \frac{\cos \beta_1}{\rho_{11}} (1 + \beta') \right] \psi_{11}' \right\} \Delta \eta_1 \sin (\alpha_{11} + \beta_1) \quad (7.27) \end{aligned}$$

and

$$\begin{aligned} \frac{\partial}{\partial \beta} (\psi_{22}') = & \left\{ n_{+21} [\tan (\alpha_{21} + \beta_1) - \tan \beta_1] + \frac{\cos (\theta_{21} + \beta_1)}{\rho_{21} \sin \theta_{21}} \right. \\ & \left. - \frac{\sin \beta_1}{\rho_{21}} (1 + \beta') \right\} \Delta \eta_2 \cos (\alpha_{21} + \beta_1) \\ & + \left\{ n_{-21} - n_{+21} - \frac{\sin (\theta_{21} + \beta_1)}{\rho_{21} \sin \theta_{21}} + \frac{\cos \beta_1}{\rho_{21}} \right. \\ & \left. \cdot (1 + \beta') \right\} \Delta \eta_2 \sin (\alpha_{21} + \beta_1) \quad . \quad (7.28) \end{aligned}$$

We also have corresponding to Eq. (7.23) for $\partial \alpha_{12} / \partial \beta$

$$\frac{\partial \alpha_{22}}{\partial \beta} = - \frac{\Delta \psi}{2 (1 + \psi) \cos^2 (\alpha_{21} + \beta_1)} \quad . \quad (7.29)$$

Thus for f_2' we obtain

$$\begin{aligned} f_2' = & - \frac{\rho_{11} \Delta \eta_1}{\delta \theta_{11} \rho_{21}^2} \left\{ \frac{\cos (\alpha_{12} + \beta_1) \cos \alpha_{22}}{\psi_{22}' \cos (\alpha_{22} + \beta_1)} [n_{+11} (\tan (\alpha_{11} + \beta_1) \right. \\ & - \tan \beta_1) \Delta \eta_1 \cos (\alpha_{11} + \beta_1) - n_{+21} (\tan (\alpha_{21} + \beta_1) \\ & - \tan \beta_1) \left(\frac{\psi_{12}'}{\psi_{22}'} \right) \Delta \eta_2 \cos (\alpha_{21} + \beta_1) + \frac{\cos (\theta_{11} + \beta_1)}{\rho_{11} \sin \theta_{11}} \\ & \cdot \Delta \eta_1 \cos (\alpha_{11} + \beta_1) \psi_{11}' - \left(\frac{\psi_{12}'}{\psi_{22}'} \right) \frac{\cos (\theta_{21} + \beta_1)}{\rho_{21} \sin \theta_{21}} \Delta \eta_2 \\ & \cdot \cos (\alpha_{21} + \beta_1) \psi_{21}' + \psi_{11}'' \Delta \eta_1 \sin (\alpha_{11} + \beta_1) - \left(\frac{\psi_{12}'}{\psi_{22}'} \right) \\ & \cdot \psi_{22}'' \Delta \eta_2 \sin (\alpha_{21} + \beta_1)] + \left(\frac{\psi_{12}'}{\psi_{22}'} \right) \\ & \cdot \frac{\cos \alpha_{22} \sin (\alpha_{12} + \beta_1) \Delta \psi}{\cos (\alpha_{22} + \beta_1) 2 (1 + \psi) \cos^2 (\alpha_{11} + \beta_1)} + \left(\frac{\psi_{12}'}{\psi_{22}'} \right) \\ & \cdot \frac{\cos (\alpha_{12} + \beta_1)}{\cos (\alpha_{22} + \beta_1)} [\cos (\alpha_{22} + \beta_1) \sin \alpha_{22} - \cos \alpha_{22} \\ & \cdot \sin (\alpha_{22} + \beta_1)] \frac{\Delta \psi}{2 (1 + \psi) \cos^2 (\alpha_{21} + \beta_1)} - \left(\frac{\psi_{12}'}{\psi_{22}'} \right) \end{aligned}$$

$$\left. \begin{aligned} & \cdot \frac{\cos \alpha_{22}}{\cos^2 (\alpha_{22} + \beta_1)} [\cos (\alpha_{12} + \beta_1) \sin (\alpha_{22} + \beta_1) \\ & - \cos (\alpha_{22} + \beta_1) \sin (\alpha_{12} + \beta_1)] \end{aligned} \right\} \quad (7.30)$$

Consider typical values for the variables. Take $\Delta\eta$, θ , $\delta\theta$, ψ' , ψ , α of the order of magnitude of 10^{-3} , $\rho \approx 1$, $\psi \approx 10^{-6}$ and finally β less than α . We find that the only large terms in f_2' are:

$$\begin{aligned} f_2' = & - \frac{\rho_{11} \Delta\eta_1 \cos (\alpha_{12} + \beta_1) \cos \alpha_{22}}{\delta\theta_{11} \rho_{21} \psi_{22}' \cos (\alpha_{22} + \beta_1)} \left[\frac{\cos (\theta_{11} + \beta_1)}{\rho_{11} \sin \theta_{11}} \right. \\ & \cdot \Delta\eta_1 \cos (\alpha_{11} + \beta_1) \psi_{11}' - \left(\frac{\psi_{12}'}{\psi_{22}'} \right) \frac{\cos (\theta_{21} + \beta_1)}{\rho_{21} \sin \theta_{21}} \\ & \cdot \Delta\eta_2 \cos (\alpha_{21} + \beta_1) \psi_{21}' \left. \right] \quad (7.31) \end{aligned}$$

We also find that f_1' as expressed in Eq. (7.24) is small compared to f_2' in this range of values for the variables. Considering f_3 we have

$$\begin{aligned} f_3 = & \frac{1}{(\delta\theta_{11})^2} \left(1 - \frac{\rho_{11}}{\rho_{21}} \right) \left[- \frac{\Delta\eta_1 \sin \alpha_{12}}{\rho_{12}} + \frac{\sin \alpha_{22}}{\rho_{22}} \left(\frac{\psi_{12}'}{\psi_{22}'} \right) \right. \\ & \cdot \frac{\Delta\eta_1 \cos (\alpha_{12} + \beta_1)}{\cos (\alpha_{22} + \beta_1)} \left. \right] \quad (7.32) \end{aligned}$$

This expression is very similar to that for f_2 . As we have seen, those terms involving the derivation of α_{12} and α_{22} , with respect to β are not as important as those for ψ_{12}' and ψ_{22}' . Therefore, we can write for f_3' , approximately:

$$\begin{aligned} f_3' = & \frac{\Delta\eta_1}{(\delta\theta_{11})^2} \left(1 - \frac{\rho_{11}}{\rho_{21}} \right) \cdot \frac{\cos (\alpha_{12} + \beta_1) \sin \alpha_{22}}{\rho_{22} \psi_{22}' \cos (\alpha_{22} + \beta_1)} \\ & \cdot \left[\frac{\cos (\theta_{11} + \beta_1)}{\rho_{11} \sin \theta_{11}} \Delta\eta_1 \cos (\alpha_{11} + \beta_1) \psi_{11}' - \left(\frac{\psi_{12}'}{\psi_{22}'} \right) \right. \\ & \cdot \frac{\cos (\theta_{21} + \beta_1)}{\rho_{21} \sin \theta_{21}} \Delta\eta_2 \cos (\alpha_{21} + \beta_1) \psi_{21}' \left. \right] \quad (7.33) \end{aligned}$$

Thus, including only the largest terms:

$$\begin{aligned}
 f'(\beta) = & \frac{\Delta\eta_1 \cos(\alpha_{12} + \beta_1)}{\delta\theta_{11} \psi_{22}' \cos(\alpha_{22} + \beta_1)} \left[\frac{(1 - \rho_{11}/\rho_{21}) \sin \alpha_{22}}{\rho_{22} \delta\theta_{11}} \right. \\
 & + \left. \frac{\rho_{11}}{\rho_{21}^2} \cos \alpha_{22} \right] \cdot \left[\frac{\cos(\theta_{11} + \beta_1)}{\rho_{11} \sin \theta_{11}} \Delta\eta_1 \cos(\alpha_{11} + \beta_1) \right. \\
 & \cdot \left. \psi_{11}' - \frac{\psi_{12}'}{\psi_{22}'} \frac{\cos(\theta_{21} + \beta_1)}{\rho_{21} \sin \theta_{21}} \Delta\eta_2 \cos(\alpha_{21} + \beta_1) \psi_{21}' \right] \quad (7.34)
 \end{aligned}$$

It is the sign and magnitude of this term that will ordinarily determine how fast β will accumulate errors. A further approximation in $f'(\beta)$ in which we ignore the $(1 - \rho_{11}/\rho_{21}) \sin \alpha_{22}/\rho_{22} \delta\theta_{11}$ term compared with $\rho_{11} \cos \alpha_{22}/\rho_{21}^2$, approximate $\cos(\alpha + \beta) \approx 1$ to first order, take $\psi_{12}' = \psi_{21}' = \psi_{22}'$, and set $\rho_{11} = \rho_{21}$ gives

$$f'(\beta) = \frac{(\Delta\eta_1)^2}{\delta\theta_{11} \rho^2} \left(\frac{1}{\sin \theta_{11}} - \frac{1}{\sin \theta_{21}} \right) \quad (7.35)$$

From Eq. (7.5), we have

$$\delta_{\text{new}} = \delta_{\text{old}} \left(1 + \frac{\Delta\eta_1^2}{\delta\theta_{11} \rho^2} \left[\frac{1}{\sin \theta_{11}} - \frac{1}{\sin(\theta_{11} + \delta\theta_{11})} \right] \right) \quad (7.36)$$

If we assume that θ , and $\delta\theta_{11}$ vary slowly compared to ρ , as will be the case for small angles, and if we write $\Delta\rho = \Delta\eta_1$, then

$$\frac{d\delta}{\delta} = \frac{\Delta\eta_1}{\delta\theta_{11}} \left[\frac{1}{\sin \theta_{11}} - \frac{1}{\sin(\theta_{11} + \delta\theta_{11})} \right] \frac{d\rho}{\rho^2} \quad (7.37)$$

Integrating, we obtain

$$\delta = \delta_0 \exp \left[\frac{\Delta\eta_1}{\delta\theta_{11}} \left(\frac{1}{\sin \theta_{11}} - \frac{1}{\sin(\theta_{11} + \delta\theta_{11})} \right) \left(\frac{1}{\rho} - \frac{1}{\rho_0} \right) \right] \quad (7.38)$$

or approximately

$$\delta = \delta_0 \exp \left[\frac{\Delta\eta_1}{\theta_{11}^2} \left(\frac{1}{\rho} - \frac{1}{\rho_0} \right) \right] \quad (7.39)$$

Thus, we see that the error δ will grow exponentially. For given ρ_0

and ρ_0 , i. e., a given distance over which we require a valid solution, we can make δ small by making $\Delta\eta_1$ small, θ_{11} large or δ_0 small. To make $\Delta\eta_1$ smaller will increase proportionately the computing time; increasing θ_{11} , of course, will exclude information regarding the field near the axis of symmetry. Making δ_0 smaller is equivalent to requiring greater precision in the calculations, for example by means of "double precision" calculations. For larger values of ρ_0 , the problem becomes less acute.

CHAPTER VIII

RESULTS OF THE NUMERICAL SOLUTION FOR THE SCREENING OF A RAPIDLY MOVING CHARGED BODY

A. The problems treated. In Chapters V and VI we have obtained the equations necessary for a numerical solution of the screening problem. In the Poisson equation, Eq. (6.13), we will use Eq. (5.18) for the ion density n_+ in the monoenergetic case and Eq. (5.25) in the Maxwellian velocity distribution case, and Eq. (5.31) for the electron density n_- . The Laplacian operator is re-expressed in the form of Eq. (6.30). Equations (6.2), (6.4), (6.5) and (6.11) will be used to follow the trajectory of the particles and Eq. (6.12) to calculate β , the angle between the radius vector and the normal to the equipotential surface. We will write the potential in the non-dimensional form $\psi = \phi/U$ and the radius as $\rho = r/h$ where

$$\begin{aligned} h &= \sqrt{U/4\pi e^2 N_0} \quad (\text{in cgs units}) \\ &= \sqrt{\epsilon_0 U / e^2 N_0} \quad (\text{in MKS units}) \end{aligned} \quad (8.1)$$

Let us restate here the limitations on the use of the above equations for the solution of screening problems for rapidly moving bodies. First of all, the shape of the body depends on the choice of the boundary conditions. If practical considerations permit (i.e., available time, etc.) one can obtain a solution for any axially symmetric shape by making successive approximations or by trial and error procedures. However, this should not be confused with an approach using successive iterations of the potential field (as employed by Davis and Harris¹⁸).

In the solutions calculated here (see below) no effort has

been made to obtain solutions for a body of a specific shape and surface potential. The problems treated have been chosen for their value in exemplifying the procedure and yielding a general understanding of the nature of the screening. In addition, no effort has been made here to introduce the effects of intersecting trajectories (such as ions intersecting trajectories from the lower half plane when they cross the axis). Their neglect, however, is not an inherent limitation of the method, but does require more elaborate calculational techniques (see Chapter IV); in addition, for bodies large compared to a Debye length the ion density is so low behind the body that the neglect of intersecting trajectories is unimportant.

With these reservations let us now consider a few specific problems. In the case of a spherically symmetric problem of a stationary sphere, we incorporate the ambient density N_0 and temperature T in the potential and radius variables by using a nondimensional radius. By solving the equations for various values of ρ_0 and of ψ_0 we obtained a set of solutions that were applicable to any specific value of N_0 and T . In the case of a moving body we must also specify kT/U , the ratio of the thermal energy of the electrons to the kinetic energy of the ions. In the numerical calculation given here let us set $kT/U = 0.031812$, a value corresponding to an electron temperature of 1500° K and a relative velocity of 7km/sec between the charged body and a plasma of singly ionized oxygen. These calculations thus correspond to the motion of a satellite through the earth's upper atmosphere.

As in the screening of a stationary sphere (Chapter I and II) we must begin at a distance from the charged body ρ_0 with a potential

ψ_0 . If ρ_0 is sufficiently large, we can establish with some certainty the boundary conditions. We will use here for the boundary a hemisphere axially symmetric and opening to the rear on which we have for the potential $\psi_0 = 0.001$; we will take, variously, $\rho_0 = 5, 10, 20$ for the radius of this boundary surface. For the value of ψ' on the boundary surface we again use Eq. (2.30).

B. Results of the numerical calculations and general observations. In Figs. (8.1), (8.2), and (8.3) we show plots of trajectories and equipotential surfaces where $\rho_0 = 5, 10, 20$, respectively. Figures (8.4), (8.5) and (8.6) show the corresponding equidensity curves. In these calculations we have assumed the ions to be without any significant thermal motions so that the velocity vector of each ion will be parallel to the axis of symmetry.

The trajectories and equipotential curves shown in Figs. (8.1), (8.2), and (8.3) are superficially quite what might be expected, except that the trajectories turn more directly toward the body and the sheath is thicker than might have been thought. The slow spatial variation of the potential shows that the Debye length is not a satisfactory indicator of the sheath thickness. The tail-like appearance of the equipotential curves behind the body is due primarily to the convergence of ions toward the axis. We will show later that a Maxwellian velocity distribution will remove these tail-like areas except for small bodies.

The most interesting information is shown in the equidensity curves, Figs. (8.4), (8.5), and (8.6). We find that there is no rise in the density as particles enter the field but rather, a drop in the density. This drop in ion density results from the acceleration

of the particles by the electric field. Near the axis on the front of the body the density drops steadily as the ions approach the body. Slightly further from the front there is a trough in the equidensity surface caused by the convergence of the ion trajectories toward the origin. On the side of the body the density becomes quite low giving a wide, low density trough. Behind this position lies a point of minimum density; the minimum, therefore, does not lie directly behind the body. Near the axis behind the body the density becomes quite large, due to the convergence of the trajectories toward the axis. This high density, of course, arises from the neglect of the ions' thermal motion.

Figures (8.7), (8.8), and (8.9) give the trajectories and equipotential curves obtained using a Maxwellian velocity distribution for the ambient ions; all other parameters are the same as in Figs. (8.1) through (8.6). These calculations assume that the ion temperature equals the electron temperature in the ambient plasma, although such an assumption is not necessary. The resulting equipotential surfaces are much more nearly spherical.

Figures (8.10), (8.11), and (8.12) show the equidensity surfaces corresponding respectively, to the trajectory and equipotential curves of Fig. (8.7), (8.8), and (8.9). The two most interesting changes are: the trough in the equidensity surface extends across the axis behind the body, with the trough nearly encircling the body, and the density of particles crossing the axis behind the body no longer reaches the unduly high values found in Figs. (8.4), (8.5), and (8.6). Nevertheless, there is a considerable concentration for small bodies (of about one Debye length) with large potentials, as

shown in Fig. (8.10). For large bodies the density along the axis is small. This shows that the intersection of trajectories becomes fairly unimportant for large bodies.

The equidensity curves computed by Davis and Harris¹⁸ show some similarity with our results. They show a large concentration of ions near the axis (the ions are cold) and a depression in the equidensity surface behind and to the side of the body. However, in their work there is no drop in ion density along the front of the body but rather a slight increase in density before the density drops. Also, there is no trough in the equidensity surface although it must exist. Nevertheless, an iterative method of solution using a large number of trajectories and a good first approximation to the potential might prove quite satisfactory. It appears, however, that one would need a much finer mesh than the 441 density points used by Davis and Harris to calculate the electric field.

In addition to the previous graphical displays of our data (Figs. (8.1) through (8.12)) it is useful to plot the radial variation in ψ and n_+ for several different directions from the body. Plots of this kind are shown in Figs. (8.13) through (8.24). Figures (8.13), (8.14), and (8.15) show the variation of the potential starting at a value equal to the maximum potential shown in the corresponding Figs. (8.1), (8.2), and (8.3). The density variations plotted in this manner are shown in Figs. (8.16), (8.17), and (8.18) and correspond to Figs. (8.4), (8.5), and (8.6). Figures (8.13) through (8.18) are for ions with no thermal motion. For the case where the ions have a Maxwellian velocity distribution superimposed on their velocity toward the charged body, we show the radial variations in ψ and n_+ in

Figs. (8.19) through (8.24) corresponding to the curves shown in Figs. (8.7) through (8.12), respectively.

Most all of the particle trajectories are shown in Figs. (8.1), (8.2), (8.3) and (8.7), (8.8), (8.9) are spiral rather than pseudo-hyperbolic. This fact is quite consistent with the electric fields that we obtain. Notice that Figs. (8.13), (8.14), (8.15), (8.19), (8.20), and (8.21) show a radical variation of the potential ψ with an exponent $n > 2$ (where $\psi = K\rho^{-n}$) everywhere except close to the axis behind the body. As we stated in Chapter II, particle trajectories are in general spirals, if the exponent $n > 2$ in a central force field. (In the present case, of course, the fields only approximate central force fields over certain regions of space.)

CHAPTER IX

PARTICLE ACCRETION AND DRAG ON A RAPIDLY MOVING CHARGED BODY

A. The ion and electron currents to the surface of a rapidly moving charged body. The numerical solution of the screening problem for a rapidly moving charged body (see Chapter VIII) yields the data necessary for the calculation of the ion current to the surface of charged bodies and the drag on the bodies. The calculation of the ion current to the surface of the charged body requires merely that we integrate the particle flux to the surface and multiply by the electronic charge on the individual ions of the plasma. The flux per unit area is given by the density at the surface multiplied by the velocity component normal to the surface. If we assume the surface of the body to be an equipotential surface (as it will be if it is a conductor), then the ion current I_+ to the body is given by

$$I_+ = 2\pi e N_0 \int_0^\pi n_+ v r^2 \cos(\alpha + \beta) \left| \frac{\sin \theta}{\cos \beta} \right| d\theta \quad (9.1)$$

where $2\pi r^2 \left| \sin \theta d\theta / \cos \beta \right|$ is the element of area supported by $d\theta$, and $v \cos(\alpha + \beta)$ is the component of the velocity vector normal to the surface element as shown in Fig. (9.1). Also, e is the electronic charge, N_0 is the ambient ion density, n_+ is the ratio of the ion density at the point r, θ to the ambient density, v is the ion velocity at this point on the surface, α is the angle between the velocity vector and the radius vector, and β is the angle between the radius vector and the normal to the equipotential surface.

If u is the drift velocity between the body and the ambient plasma, energy considerations give

$$v = u \sqrt{1 + \psi} \quad (9.2)$$

where $\psi = D/U$; $U = \frac{1}{2} mu^2$.

Using Eq. (9.2) in Eq. (9.1) and writing $\rho = r/h$, where h is the Debye length expressed in terms of U (see Eq. (9.20)) we have

$$I_+ = 2\pi e N_0 u h^2 \int_0^\pi n_+ \rho^2 \sqrt{1 + \psi} \left| \frac{\sin \theta}{\cos \beta} \right| \cos(\alpha + \beta) d\theta \quad (9.3)$$

Let us re-express Eq. (9.3) in terms of the current intersecting an uncharged area having a geometric cross section, πr^2 , equal to that of the body:

$$i_+ = I_+ / \pi e N_0 u h^2 \rho_g^2 \quad (9.4)$$

where ρ_g is the distance from the axis of symmetry of the body to the furthest point on the body measured in Debye lengths. Substituting for I_+ from Eq. (9.3) in Eq. (9.4) gives:

$$i_+ = \frac{2}{\rho_g^2} \int_0^\pi n_+ \rho^2 \sqrt{1 + \psi} \left| \frac{\sin \theta}{\cos \beta} \right| \cos(\alpha + \beta) d\theta \quad (9.5)$$

Figure (9.2) shows the results of integrating Eq. (9.5) using the numerical solutions of the screening problem given in Chapter VIII. Only those screening calculations that include the first order correction for the Maxwellian velocity distribution have been used to obtain the results of Fig. (9.2). It should be noted that the parameter $U/kT = 31.43$ for the family of curves in Fig. (9.2); however, except for small values of ψ ($\lesssim 0.03$) the results should not be strongly dependent on the value of U/kT .

B. The drag on the charged body. We wish now to obtain the drag characteristics for a charged body embedded in a plasma and moving rapidly with respect to the ions of the plasma. It is assumed

that there is no magnetic field pervading the plasma, that the surface of the body is a conductor or is otherwise made to conform to an equipotential surface, and that the electric field and the space charge distribution is in an equilibrium configuration.

There are two ways in which one can calculate the drag on the charged body, given the solution to the screening problem. If we completely enclose the charged body in a boundary surface which is remote from the electric field of the body, then, all momentum transfer must appear as the difference between the momentum of the particles entering the boundary and of the particles leaving the boundary. The drag force is then given as the rate at which momentum enters the boundary minus the rate at which it leaves. The difficulty with this approach is that the solution to the problem that we have may not extend sufficiently far into the wake (or other areas).

We may, however, have data that is complete at the surface of the charged body. This allows us to use the second method which employs a calculation of the forces acting directly at the surface of the body. The forces acting directly on a surface element of the body are the impact forces, given by the rate of momentum transfer on the surface element, and the electrostatic forces given by the appropriate component of the Maxwell stress tensor. Let us consider first the impact forces.

The impact force on the body arises from the collision of the ions with the body. These ions will, for the most part, experience Auger neutralization on impact and may then recoil elastically or remain attached to the surface either temporarily or permanently. We will consider the two extreme cases; completely elastic impact

and recoil resulting in a force F on the body, or completely inelastic impact resulting in a force F' on the body. The differential force dF on an axially symmetric surface element subtended by $d\theta$ (see Fig.

(9.1)) will be given by the product

$$dF = (\text{surface element area}) \cdot (\text{particle flux through the component of the surface element normal to } \underline{v}) \cdot (\text{momentum transferred per impact}) \cdot (\text{component of force parallel to axis}) \quad (9.6)$$

For completely elastic impacts Eq. (9.6) gives

$$\begin{aligned} dF &= 2\pi r^2 \left| \frac{\sin \theta}{\cos \beta} \right| d\theta \cdot N_+ v \cos(\alpha + \beta) \cdot 2mv \cos(\alpha + \beta) \\ &\quad \cdot \cos(\theta + \beta) \\ &= 4\pi m v^2 N_+ r^2 \left| \frac{\sin \theta}{\cos \beta} \right| \cos^2(\alpha + \beta) \cos(\theta + \beta) d\theta \quad (9.7) \end{aligned}$$

where m and v are the mass and velocity of the ion and N_+ is the ion density at the point r , θ as shown in Fig. (9.1). For completely inelastic impacts Eq. (9.6) gives

$$\begin{aligned} dF' &= 2\pi r^2 \left| \frac{\sin \theta}{\cos \beta} \right| d\theta \cdot N_+ v \cos(\alpha + \beta) \cdot mv \cdot \cos(\theta - \alpha) \\ &= 2\pi m v^2 N_+ r^2 \left| \frac{\sin \theta}{\cos \beta} \right| \cos(\alpha + \beta) \cos(\theta - \alpha) d\theta \quad (9.8) \end{aligned}$$

Let us express

$$n_+ = N_+/N_0 \quad (9.9)$$

where N_0 is the ambient density and write for the velocity of the ions at the surface $v = u \sqrt{1 + \psi}$ (see Eq. (9.2)). Substituting Eqs. (9.9) and (9.2) into Eqs. (9.7) and (9.8) we obtain

$$dF = 4\pi N_0 m u^2 (1 + \psi) n_+ r^2 \left| \frac{\sin \theta}{\cos \beta} \right| \cos^2(\alpha + \beta) \cos(\theta + \beta) d\theta \quad (9.10)$$

and

$$dF' = 2\pi N_0 \mu u^2 (1 + \psi) n_+ r^2 \left| \frac{\sin \theta}{\cos \beta} \right| \cos(\alpha + \beta) \cos(\theta - \alpha) d\theta . \quad (9.11)$$

If we divide dF and dF' by the drag force F_g due to inelastic impacts acting on the uncharged body, that is, the geometric drag

$$F_g = \pi h^2 \rho_g^2 N_0 \mu u^2 \quad (9.12)$$

and define dD to be dF/F_g and dD' to be dF'/F_g , we obtain:

$$dD = 4n_+ \left(\frac{\rho}{\rho_g} \right)^2 (1 + \psi) \left| \frac{\sin \theta}{\cos \beta} \right| \cos^2(\alpha + \beta) \cos(\theta + \beta) d\theta \quad (9.13)$$

$$dD' = 2n_+ \left(\frac{\rho}{\rho_g} \right)^2 (1 + \psi) \left| \frac{\sin \theta}{\cos \beta} \right| \cos(\alpha + \beta) \cos(\theta - \alpha) d\theta . \quad (9.14)$$

Let us consider, now, the Maxwell stress tensor acting at the surface of the charged conductor. In the present case no dielectrics are present since the problem has been reduced to an electrostatic problem containing a space charge distribution only. The Maxwell stress tensor $\sigma_{\alpha\beta}$ is, therefore, (MKS units)

$$\sigma_{\alpha\beta} = \epsilon_0 E_\alpha E_\beta - \frac{1}{2} \epsilon_0 \delta_{\alpha\beta} E_\gamma E_\gamma \quad \alpha, \beta = 1, 2, 3 \quad (9.15)$$

When the surface is a negatively charged equipotential surface, Eq. (9.15) becomes

$$\sigma = - \frac{1}{2} \epsilon_0 E^2 \quad (9.16)$$

along the outward normal. Expressing Eq. (9.16) in terms of ψ' we obtain

$$\sigma = - \frac{1}{2} \epsilon_0 \left(\frac{U}{eh} \psi' \right)^2 \quad (9.17)$$

Taking the component of σ that is parallel to the axis of symmetry of the charged body (see Fig. (9.1)) and multiplying by the surface element supported by the angle $d\theta$ we have for the electrostatic force on the element of area

$$dF_E = -\pi\epsilon_0 \left(\frac{U}{e} \rho\psi'\right)^2 \left|\frac{\sin \theta}{\cos \beta}\right| \cos(\theta + \beta) d\theta \quad (9.18)$$

Dividing Eq. (9.18) by Eq. (9.12) we have

$$dD_E = -\frac{\epsilon_0}{N_0 \mu u^2} \left(\frac{U\rho\psi'}{eh\rho_g}\right)^2 \left|\frac{\sin \theta}{\cos \beta}\right| \cos(\theta + \beta) d\theta \quad (9.19)$$

Now h , the Debye length, is expressed in terms of the ambient energy of the ions relative to the charged body: $U = \frac{1}{2} \mu u^2$ and is given by

$$h = \sqrt{\frac{\epsilon_0 U}{e^2 N_0}} \quad (\text{MKS units}) \quad (9.20)$$

Substituting for h in Eq. (9.19) from (9.20) we obtain

$$dD_E = -\frac{1}{2} \left(\frac{\rho\psi'}{\rho_g}\right)^2 \left|\frac{\sin \theta}{\cos \beta}\right| \cos(\theta + \beta) d\theta \quad (9.21)$$

If we express Eqs. (9.13), (9.14) and (9.21) in integral form we obtain:

$$D = \frac{4}{\rho_g^2} \int_0^\pi n_+ \rho^2 (1 + \psi) \left|\frac{\sin \theta}{\cos \beta}\right| \cos^2(\alpha + \beta) \cos(\theta + \beta) d\theta \quad (9.22)$$

$$D' = \frac{2}{\rho_g^2} \int_0^\pi n_+ \rho^2 (1 + \psi) \left|\frac{\sin \theta}{\cos \beta}\right| \cos(\alpha + \beta) \cos(\theta - \alpha) d\theta \quad (9.23)$$

$$D_E = -\frac{1}{2\rho_g^2} \int_0^\pi (\rho\psi')^2 \left|\frac{\sin \theta}{\cos \beta}\right| \cos(\theta + \beta) d\theta \quad (9.24)$$

Finally, the total (nondimensional) drag forces D_T for completely elastic impacts and D_T' for completely inelastic impacts will be

given by the sums

$$D_T = D + D_E \quad (9.25)$$

and

$$D_T' = D' + D_E \quad (9.26)$$

Figure (9.3) shows a plot of the drag characteristics that we obtain using the data of Chapter VIII. For clarity, we have plotted the quantities $D_T \rho_g^2$ and $D_T' \rho_g^2$ against $(-\psi)$, with the cross section radius ρ_g as the parameter. It is at first quite startling to find that D_T can become negative as $|\psi|$ increases. The explanation is not difficult to discover, however.

Consider a test particle of mass m moving with velocity $u = 7\text{km/sec}$ toward a body charged to a potential $\psi = 24$. The particle has a velocity $v = u \sqrt{1 + \psi}$ (see Eq. (9.2)) or 35km/sec upon reaching the surface. Since the test particle is Auger neutralized and (by assumption) specularly reflected at the surface, it will not be decelerated as it moves away from the body. If the particle moves away from the body in the rearward direction ($\underline{v} \parallel \underline{u}$), then the net momentum transfer ΔP will be

$$\begin{aligned} \Delta P &= m (7\text{km/sec} - 35\text{km/sec}) \\ &= -m \cdot 28\text{km/sec} \end{aligned} \quad (9.27)$$

thereby increasing the momentum of the body. For the body as a whole there will only be a net increase in the momentum of the body if there are more particles reflected in the rearward direction than in the forward direction. If the "sheath thickness" s is sufficiently large so that $s^2 - \rho_g^2 \gg \rho_g^2$, then we might expect to find a greater flux of particles scattering rearwards than forwards. Under such conditions a negative drag becomes possible.

Since the geometry of the body is important in determining both the shape of the equipotential surfaces and the reflection angles of the particles, it follows that the geometry is also quite important in determining the drag. We can probably conclude, therefore, that needle-shaped, cylindrical or cone-shaped (with a small apex angle) bodies moving parallel to their longest dimension are the shapes most likely to satisfy the (approximate) condition $s^2 \gg 2\rho_g^2$ and to favor rearward reflections. Of course, the energy source that a negative drag demands must be provided by whatever mechanism is used to maintain the high negative potential. In addition, as the velocity of the body increases, $U = \frac{1}{2} \mu u^2$ becomes larger, making $|\psi|$ and $|D_T|$ smaller. Thus a body experiencing negative drag will approach a terminal velocity that will make the drag zero.

The curves in Fig. (9.3) for the product $D_T' \rho_g^2$ (D_T' being the completely inelastic drag as given by Eqs. (9.23), (9.24), and (9.26)) increase monotonically with the potential. These curves show a marked similarity to the current-voltage characteristic curves for stationary spheres, Fig. (2.17) and for moving bodies, Fig. (9.2). It is reasonable to expect that we can obtain an a posteriori equation for D_T' similar to the one for T_+ using Eqs. (2.70) and (2.75).

In addition to the obvious complications arising for the case of a rapidly moving body, we must consider the effect of the energy difference between the ions and electrons. Since the electron energy kT is ordinarily small compared to U , there will be a region of high electric field beginning at the edge of the ion sheath that arises from the rapid change in the electron density. This latter region is the electron-dominated region of the ion sheath. If σ_i and σ_e

are the nondimensional thicknesses of the ion and electron-dominated regions of the ion sheath, we have for the total sheath σ , adapting Eq. (2.75),

$$\begin{aligned}\sigma &= \sigma_i + \sigma_e \\ &= 0.83 \rho_g^{\frac{1}{2}} \psi_s^{\frac{1}{2}} + 0.83 (\rho_g + \sigma_i)^{\frac{1}{2}} \psi_{\text{eff}}^{\frac{1}{2}} \quad ; \quad (9.28)\end{aligned}$$

ψ_{eff} is the value of ψ where the density variation of the electrons becomes less important than the ion density variation (moving toward the body's surface). Now for the electrons

$$n_- = e^{-|\psi|U/kT} \quad (9.29)$$

Assume the ion density to vary approximately as

$$n_+ = e^{|\psi|} \quad \text{for } |\psi| \lesssim |\psi_{\text{eff}}| \quad (9.30)$$

in the electron dominated region, we obtain ψ_{eff} by requiring

$$\frac{dn_-}{d\psi} + \frac{dn_+}{d\psi} = 0 \quad \text{for } |\psi| = \psi_{\text{eff}} \quad (9.31)$$

Substituting Eqs. (9.29) and (9.30) into Eq. (9.31), we obtain for ψ_{eff}

$$\psi_{\text{eff}} = \frac{\ln(U/kT)}{(1 + U/kT)} \quad (9.32)$$

In the present case we have taken $U/kT = 31.43$ which gives $\psi_{\text{eff}} = 0.1063$.

Adapting Eq. (2.70), we can write

$$\begin{aligned}T_+^1 &= D_T^1 \rho_g^2 \\ &= \alpha^2 [1 - (1 - \rho_g^2/\alpha^2) \exp(-\frac{\rho_g^2 |\psi_s|}{\alpha^2 - \rho_g^2})] \quad (9.33)\end{aligned}$$

where

$$\alpha = \rho_g + \sigma \quad , \quad (9.34)$$

σ being given by Eqs. (9.28) and (9.32). The agreement of Eq. (9.33) with the curves in Fig. (9.3) is fairly good considering the obvious limitations of both the equation and of the curves which obtains from prolate spheroidal bodies. It is also found that Eq. (9.33) is in fair agreement with the curves in Fig. (9.2) if we write

$$T_+' = i_+ \rho_g^2 \quad (9.35)$$

REFERENCES

1. E. J. ["]Opik and S. F. Singer, "Distribution of Density in a Planetary Exosphere," *Phys. Fluids* 2, 653 (1959).
2. S. F. Singer, "Distribution of Dust in Cislunar Space, Possible Existence of a Terrestrial Dust Belt;" Lunar Explorations and Spacecraft Systems; ed. by R. Fleisig (Plenum Press, New York, 1962), pp. 11-24.
3. S. F. Singer, "Interplanetary Dust Near the Earth," *Nature* 192, 321 (1961).
4. H. M. Mott-Smith and I. Langmuir, "The Theory of Collectors in Gaseous Discharge," *Phys. Rev.* 28, 727 (1926).
5. I. B. Bernstein and I. N. Rabinowitz, "Theory of Electrostatic Probes in a Low Density Plasma," Project Matterhorn Report PM-S-38, October 1958.
6. S. F. Singer, "Measurements of Interplanetary Dust;" Scientific Uses of Earth Satellites; ed. by J. A. Van Allen (Univ. of Michigan Press, Ann Arbor, 1956), pp. 301-316.
7. S. F. Singer, "Interaction of West Ford Needles with the Earth's Magnetosphere," *Nature* 192, 303 (1961).
8. S. F. Singer, "Interaction of West Ford Needles with the Earth's Magnetosphere and their Lifetime," *Nature* 192, 1061 (1961).
9. S. F. Singer and E. H. Walker, "Photoelectric Screening of Bodies in Interplanetary Space," *ICARUS* 1, 7 (1962).
10. R. Jastrow and C. A. Pearse, "Atmospheric Drag on the Satellite," *J. Geophys. Research* 62, 3 (1957).
11. D. B. Beard and F. S. Johnson, "Charge and Magnetic Field Interaction with Satellites," *J. Geophys. Research* 65, 1 (1960).
12. D. B. Beard and F. S. Johnson, "Ionospheric Limitations on Attainable Satellite Potentials," *J. Geophys. Research* 66, 12 (1961).
13. E. J. ["]Opik, Interactions of Space Vehicles with an Ionized Atmosphere (Am. Astronaut. Soc. Symp. March 1961); ed. by S. F. Singer (Pergamon Press, New York, 1964).
14. L. Kraus and K. M. Watson, "Plasma Motion Induced by Satellites in the Ionosphere," *Phys. Fluids* 1, 480 (1958).
15. L. P. Pitaevskii, "Perturbations Produced in a Plasma by a Rapidly Moving Body," *AIAA* 1, 994 (1963).

16. S. Rand, "Structure of the Satellite," Phys. Fluids 2, 265 (1959).
17. T. S. Lundgren and C. C. Chang, "Some Details of the Satellite Potential Sheath," Aerospace Corporation Report No. ATN-63(9226)-2 (1963).
18. A. H. Davis and I. Harris, "Interaction of a Charged Satellite with the Ionosphere;" Rarefied Gas Dynamics; ed. by L. Talbot (Academic Press, New York, 1961), pp. 691-699.
19. H. Hagstrum, "Auger Ejection of Electrons from Tungsten," Phys. Rev. 96, 325 (1954a).
20. H. Hagstrum, "Theory of Auger Ejection of Electrons from Metals by Ions," Phys. Rev. 96, 336 (1954b).
21. H. Hagstrum, "Auger Ejections of Electrons from Molybdenum by Noble Gas Ions," Phys. Rev. 104, 672 (1956).
22. H. A. Fowler and L. E. Farnsworth, "Reflection of Very Slow Electrons," Phys. Rev. 111, 103 (1958).
23. R. T. Bettinger and E. H. Walker, "A Relationship for Plasma Sheaths About Langmuir Probes," University of Maryland, Physics Department, Technical Report 350 (1964).
24. W. P. Allis and M. A. Herlin, Thermodynamics and Statistical Mechanics (McGraw-Hill, New York, 1952), p. 196.

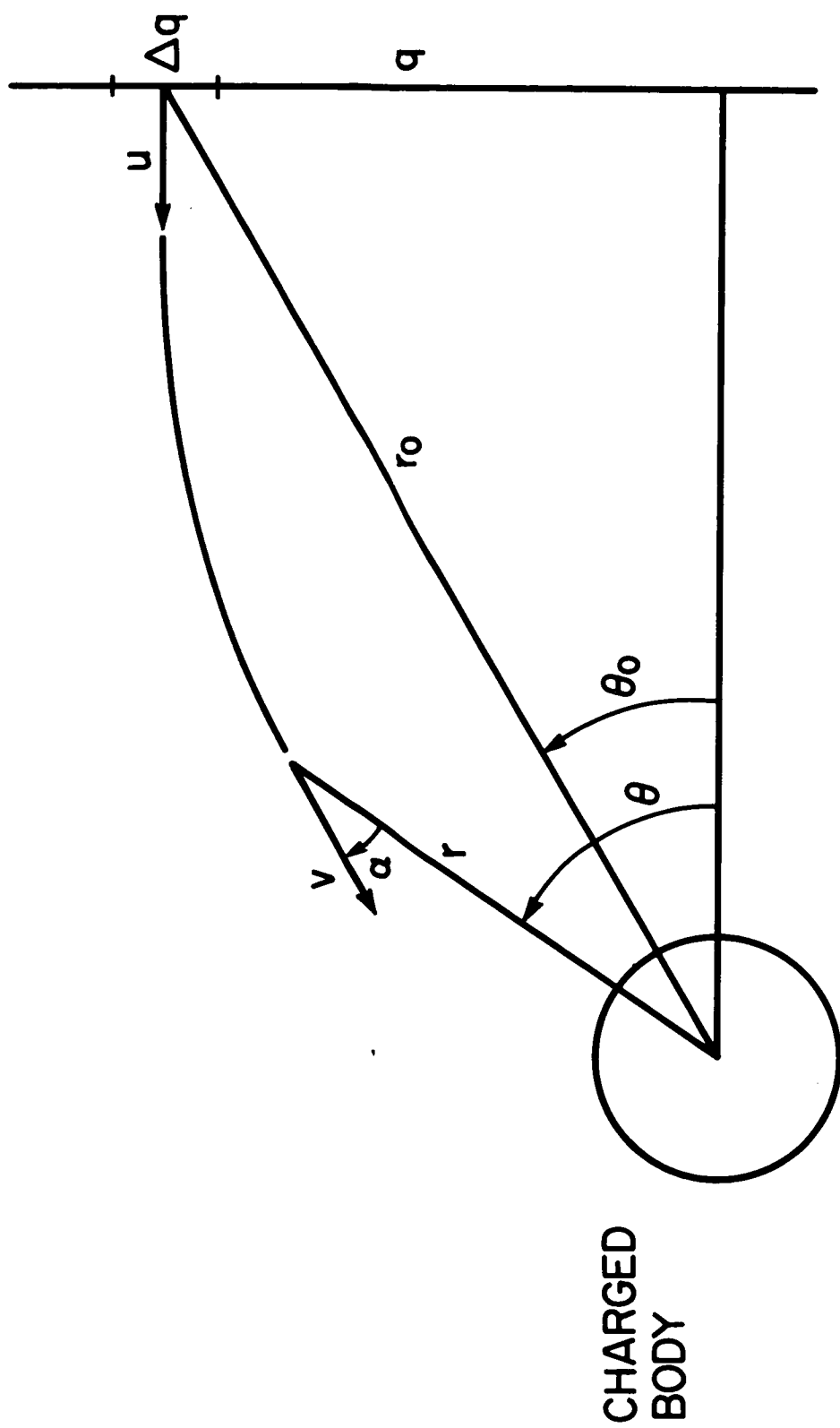


FIG. 2.1

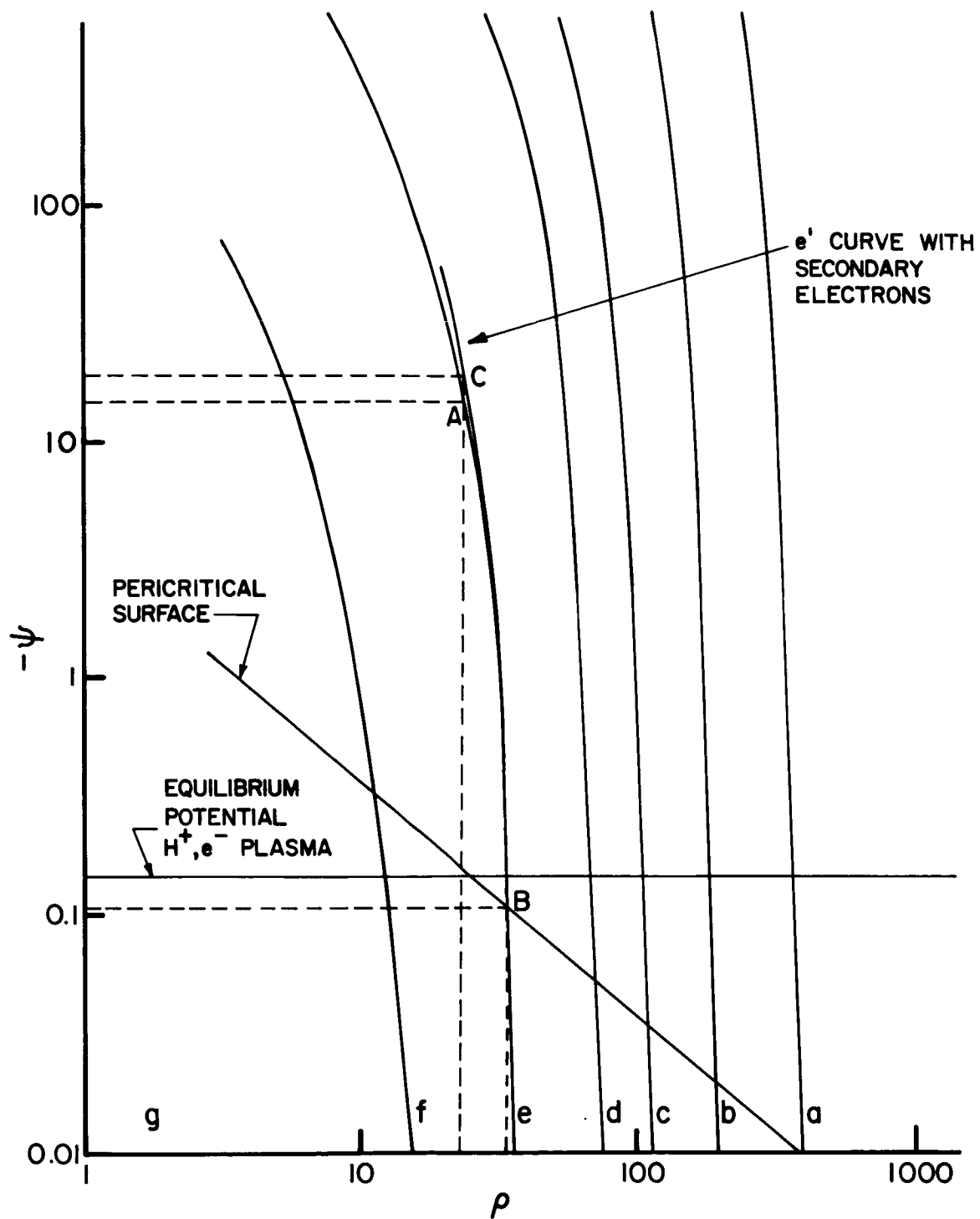


FIG. 2.2

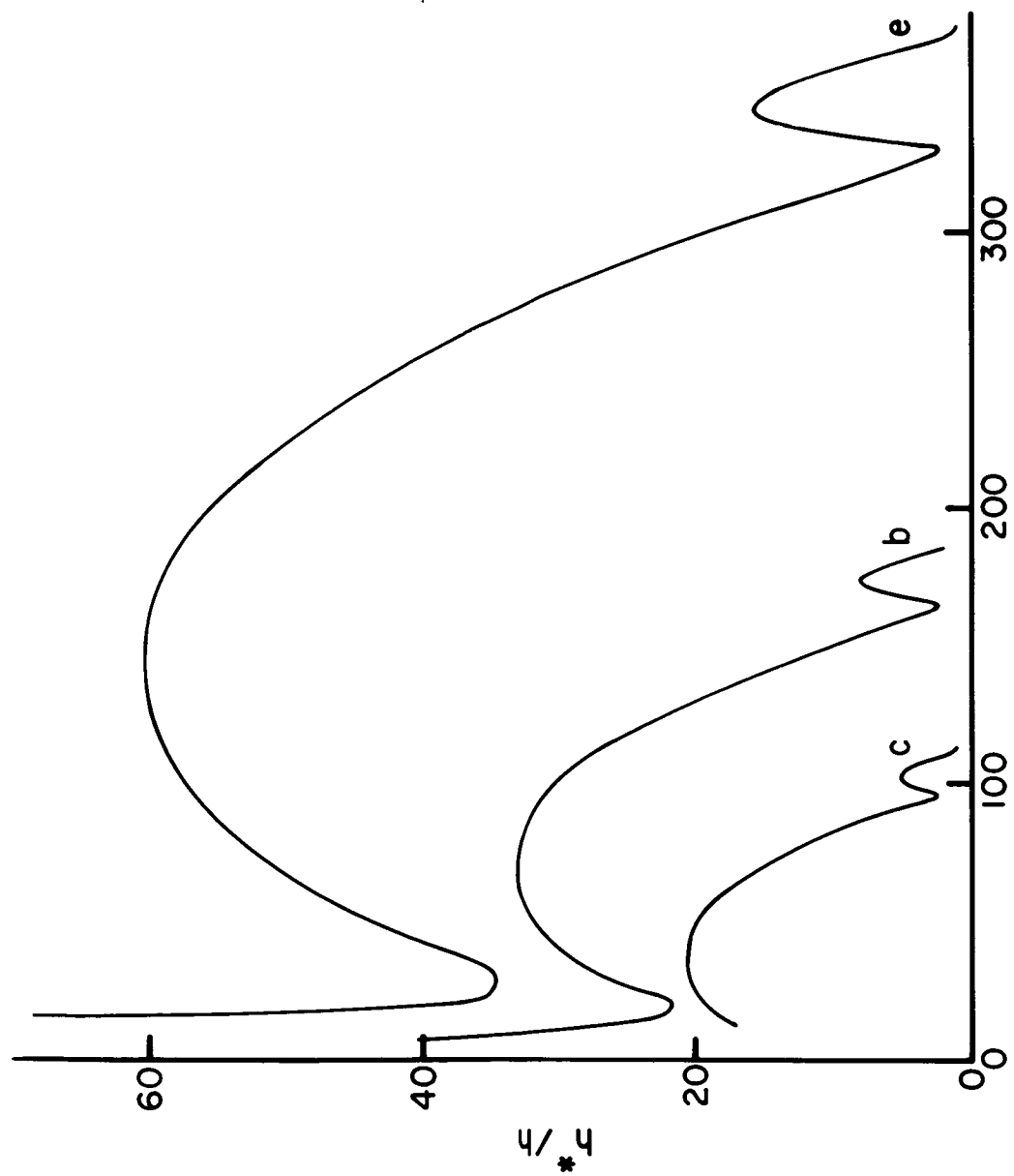


FIG. 2.3

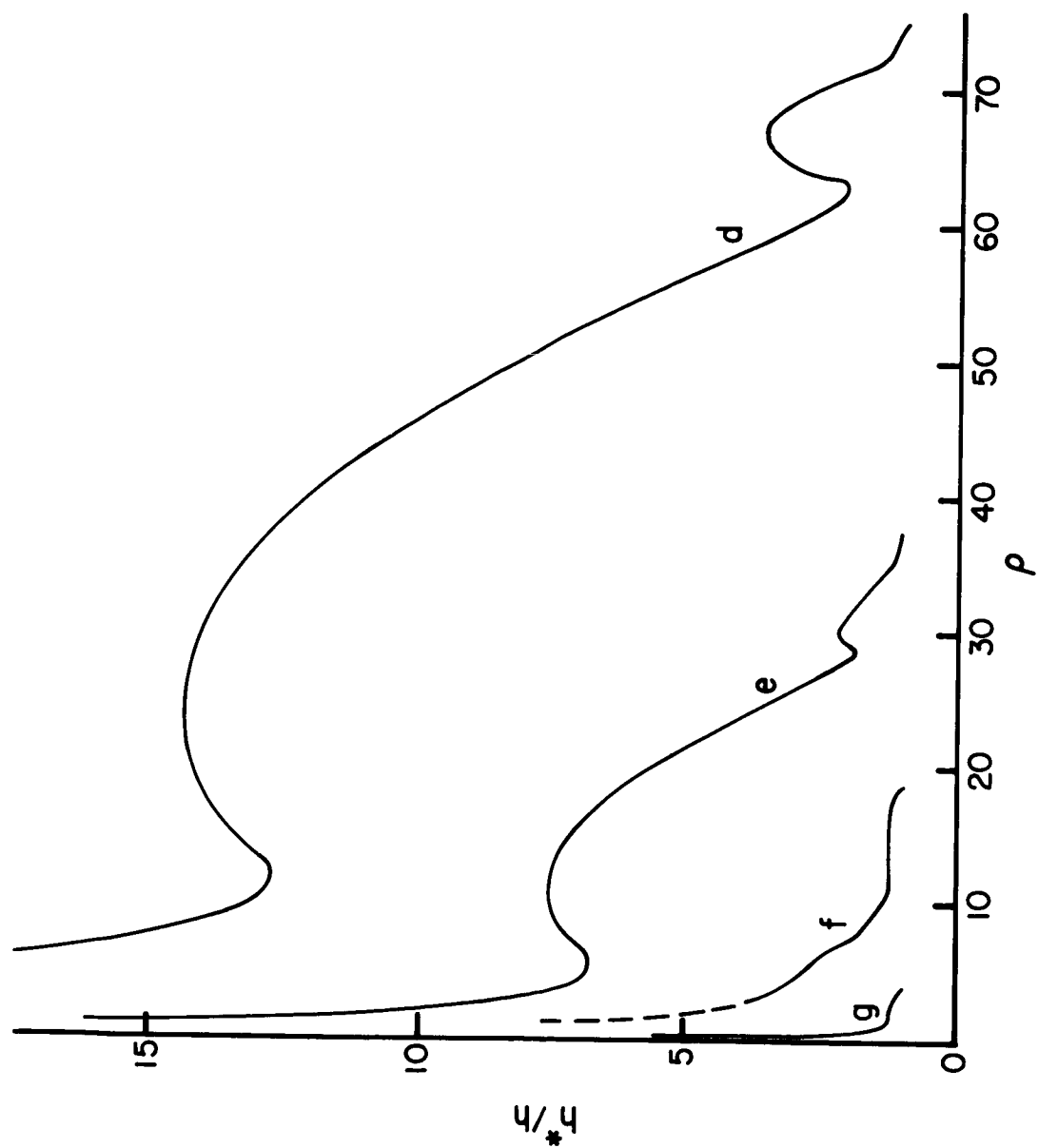


FIG. 2.4

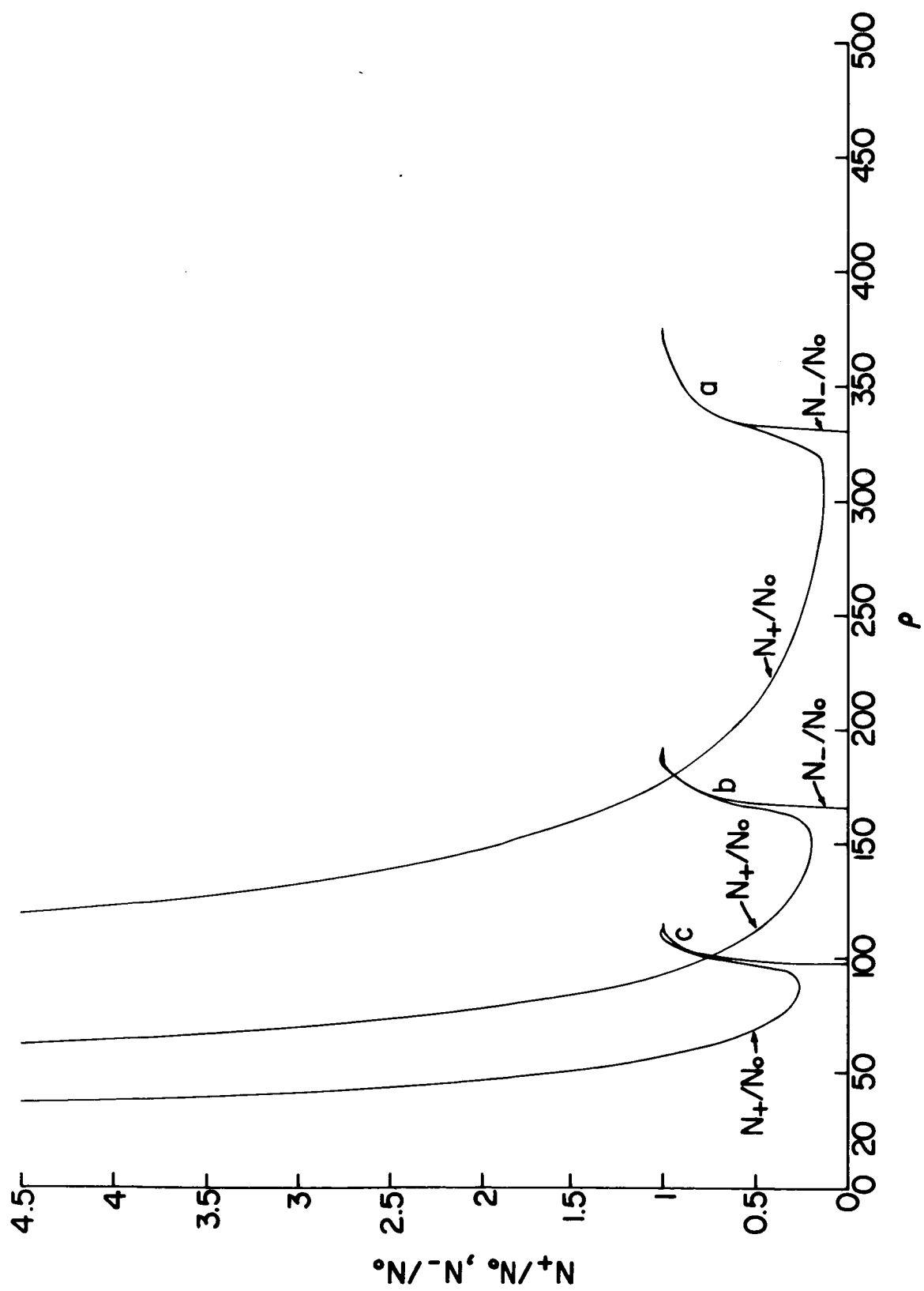


FIG. 2.5

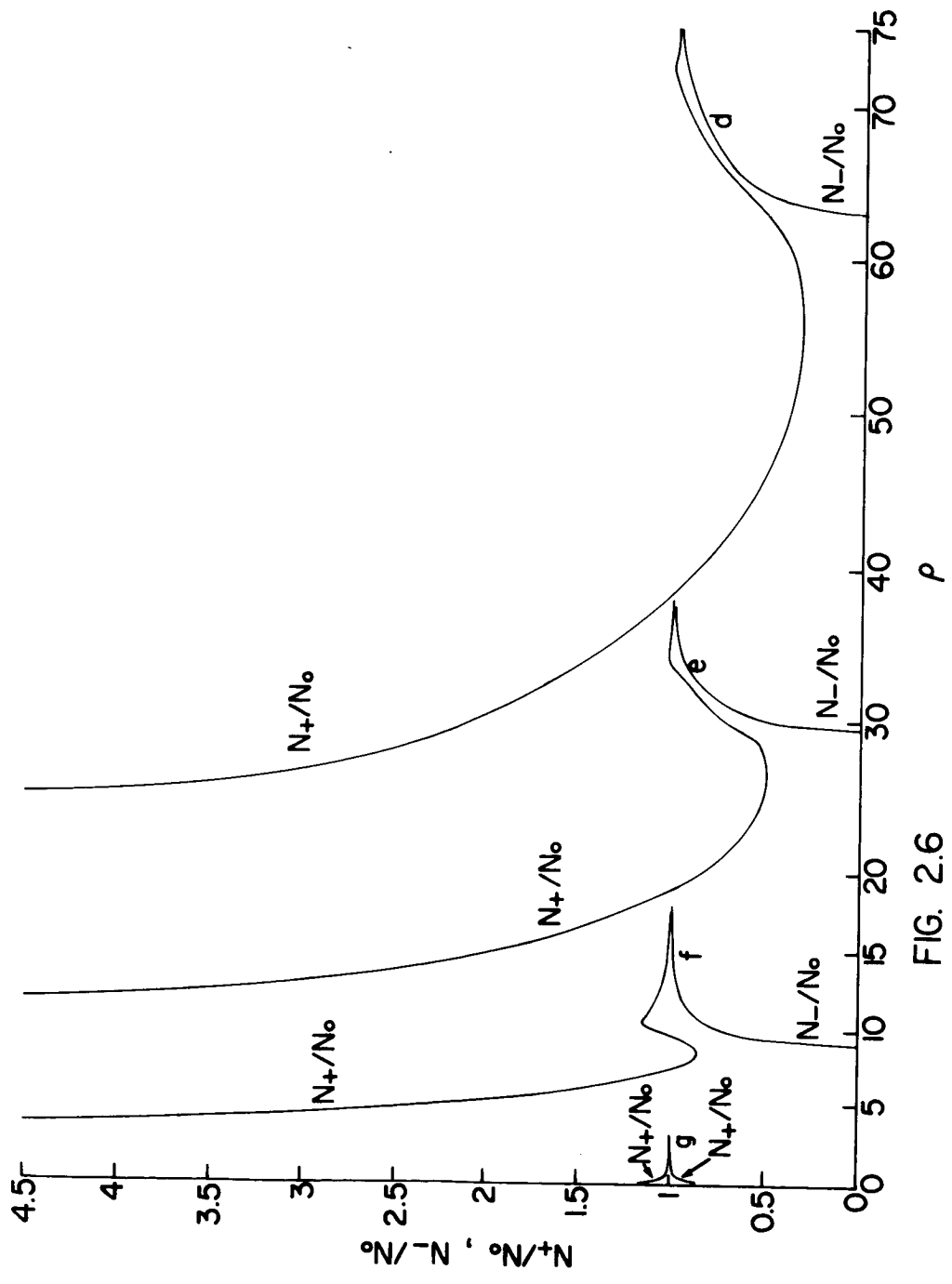


FIG. 2.6

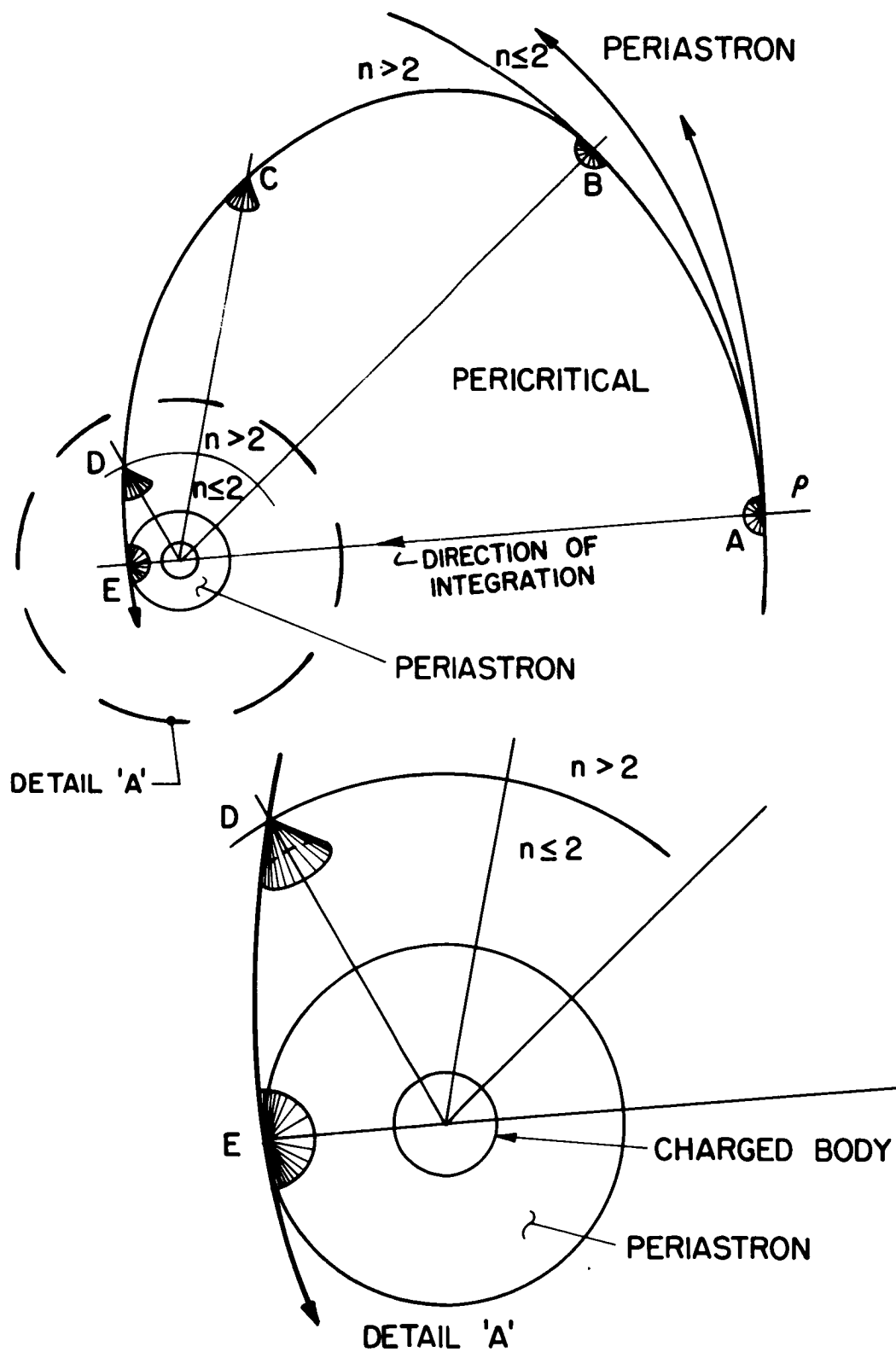


FIG. 2.7

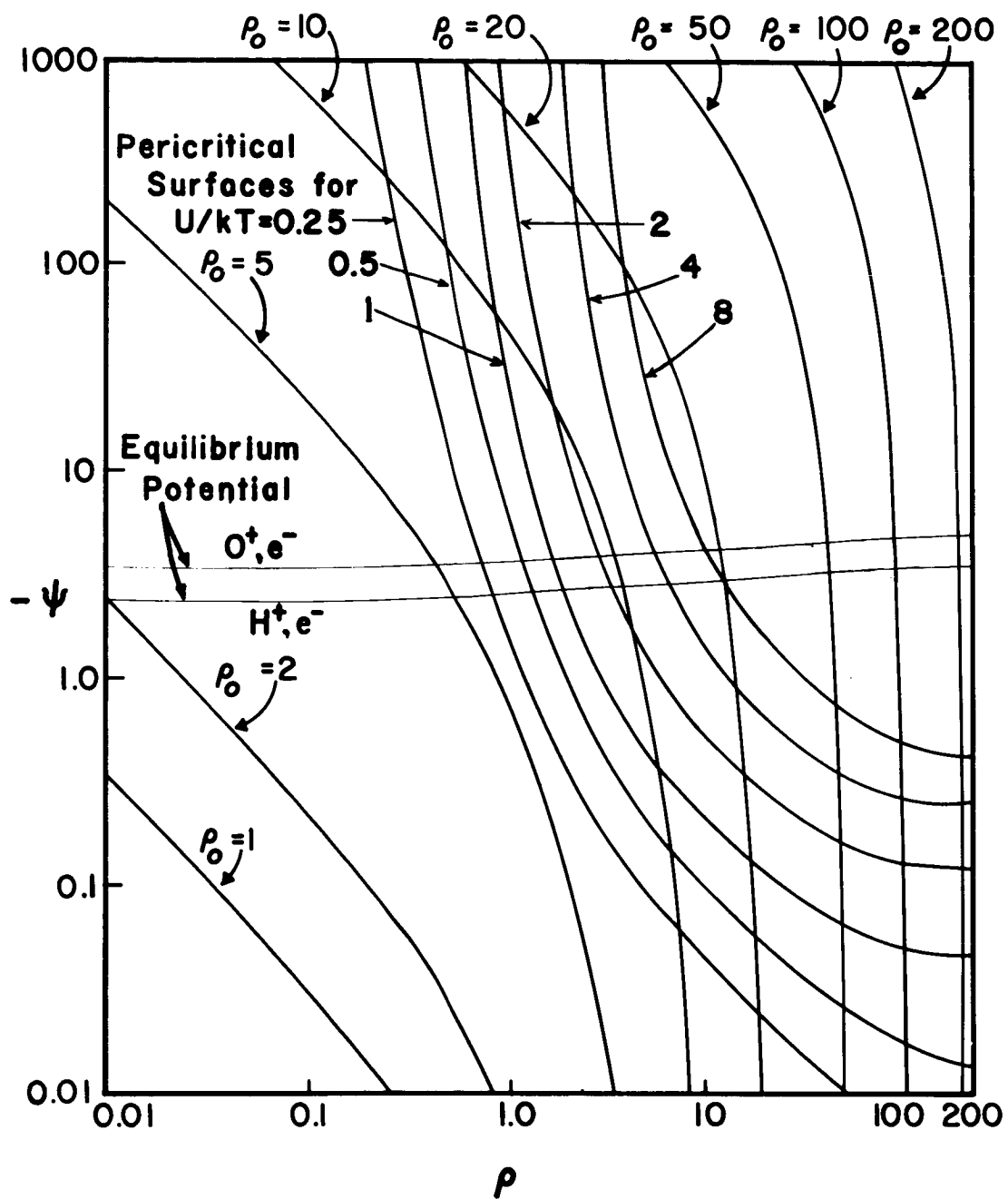


FIG. 2.8

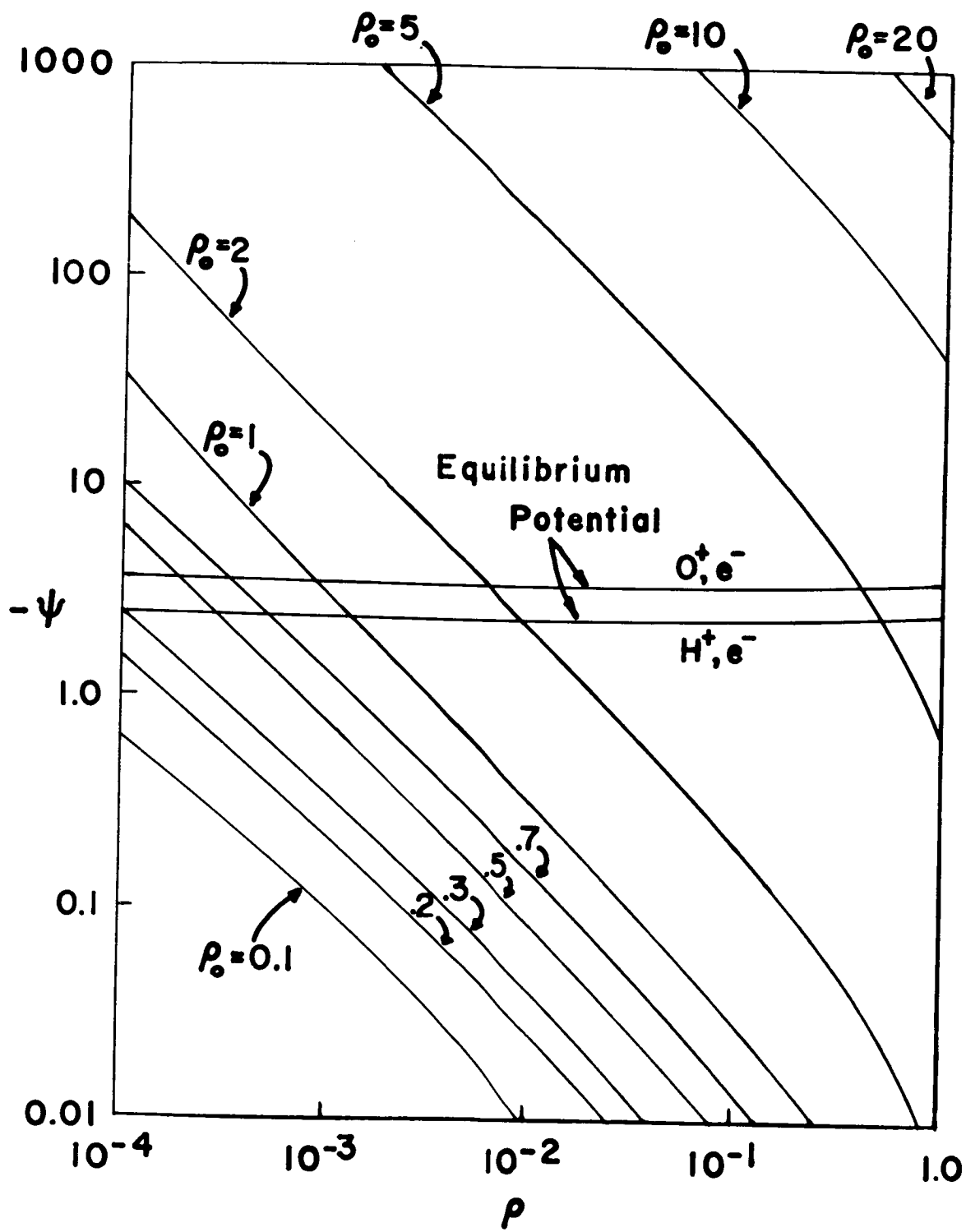


FIG. 2.9

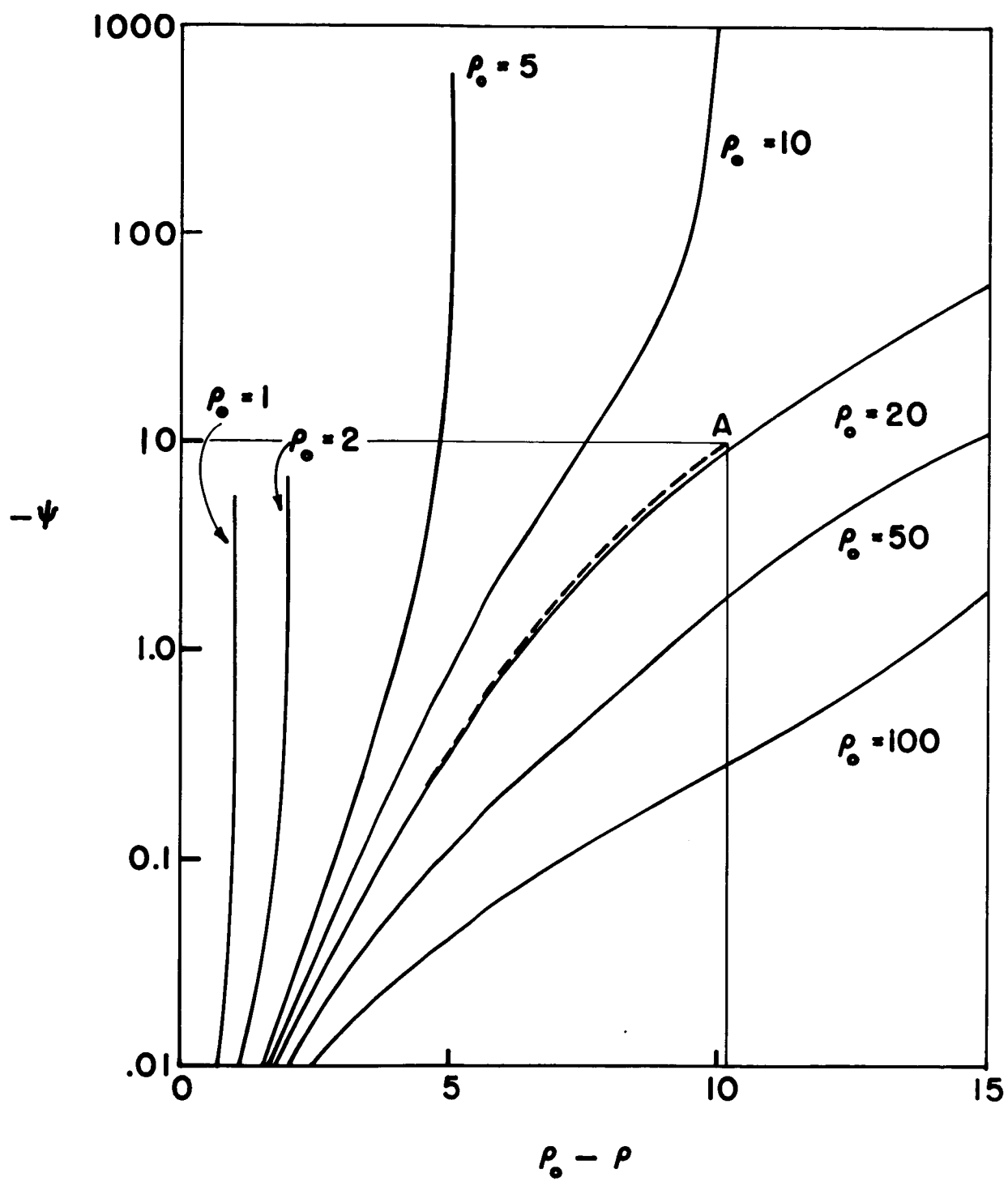


FIG. 2.10

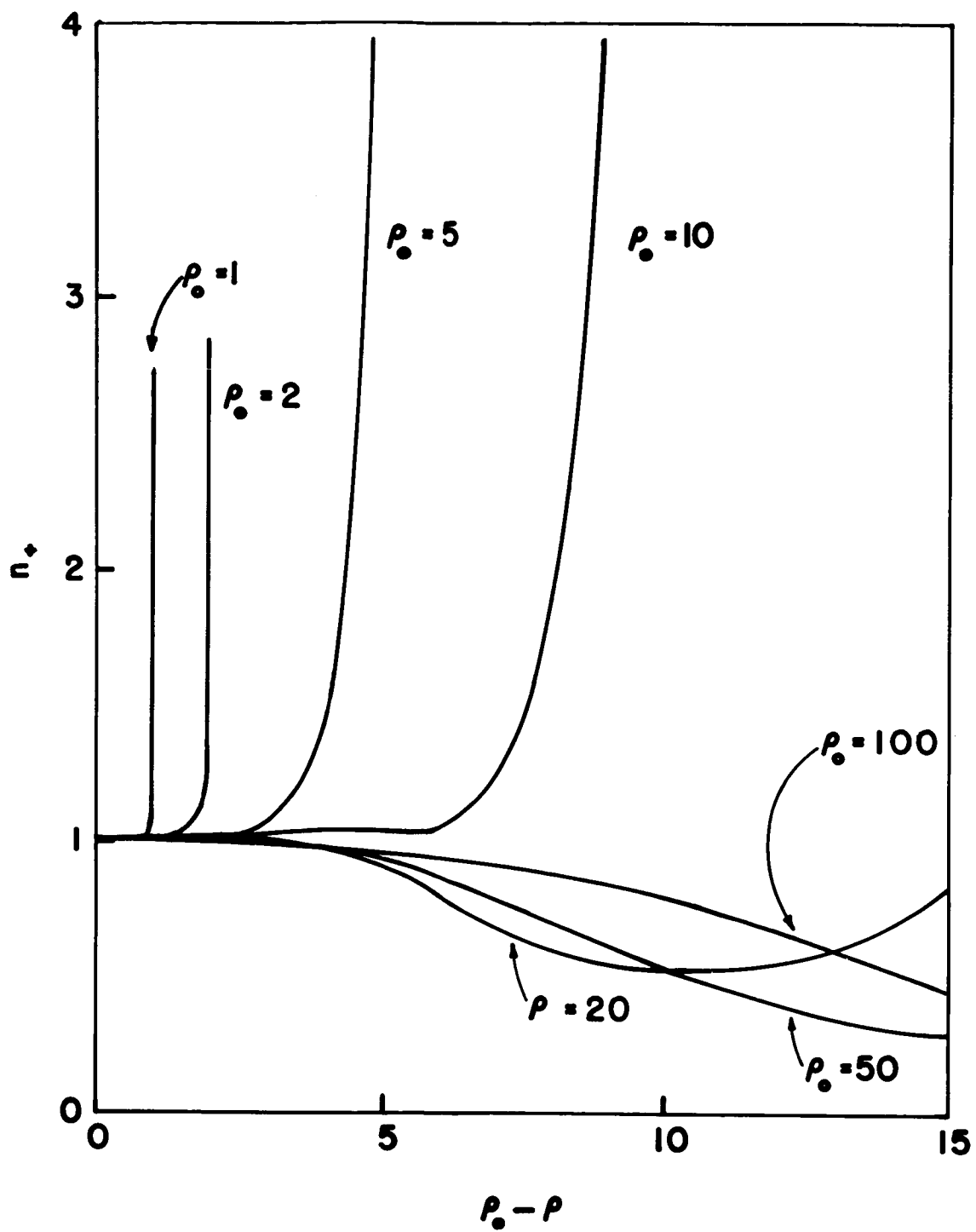


FIG. 2.11

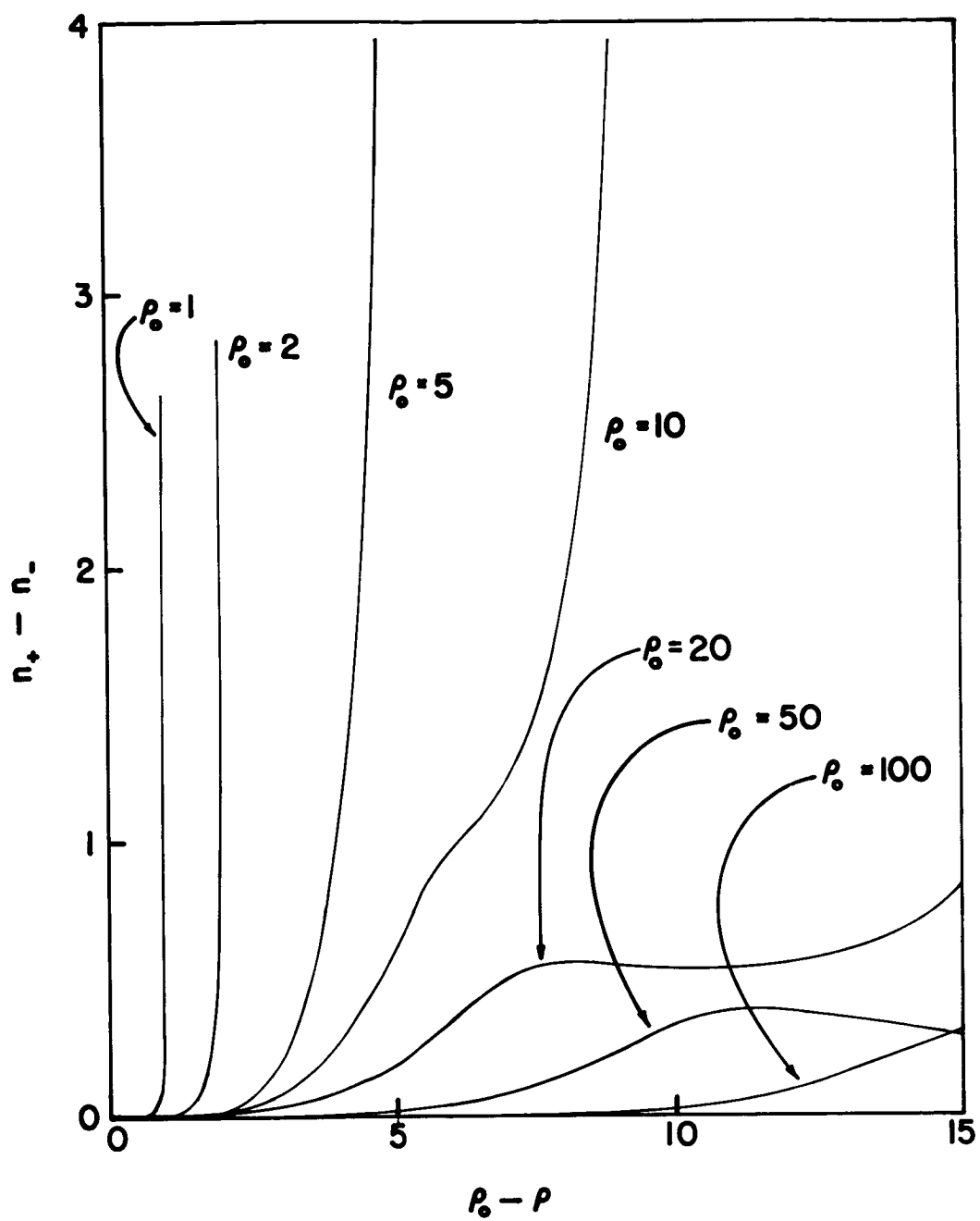


FIG. 2.12

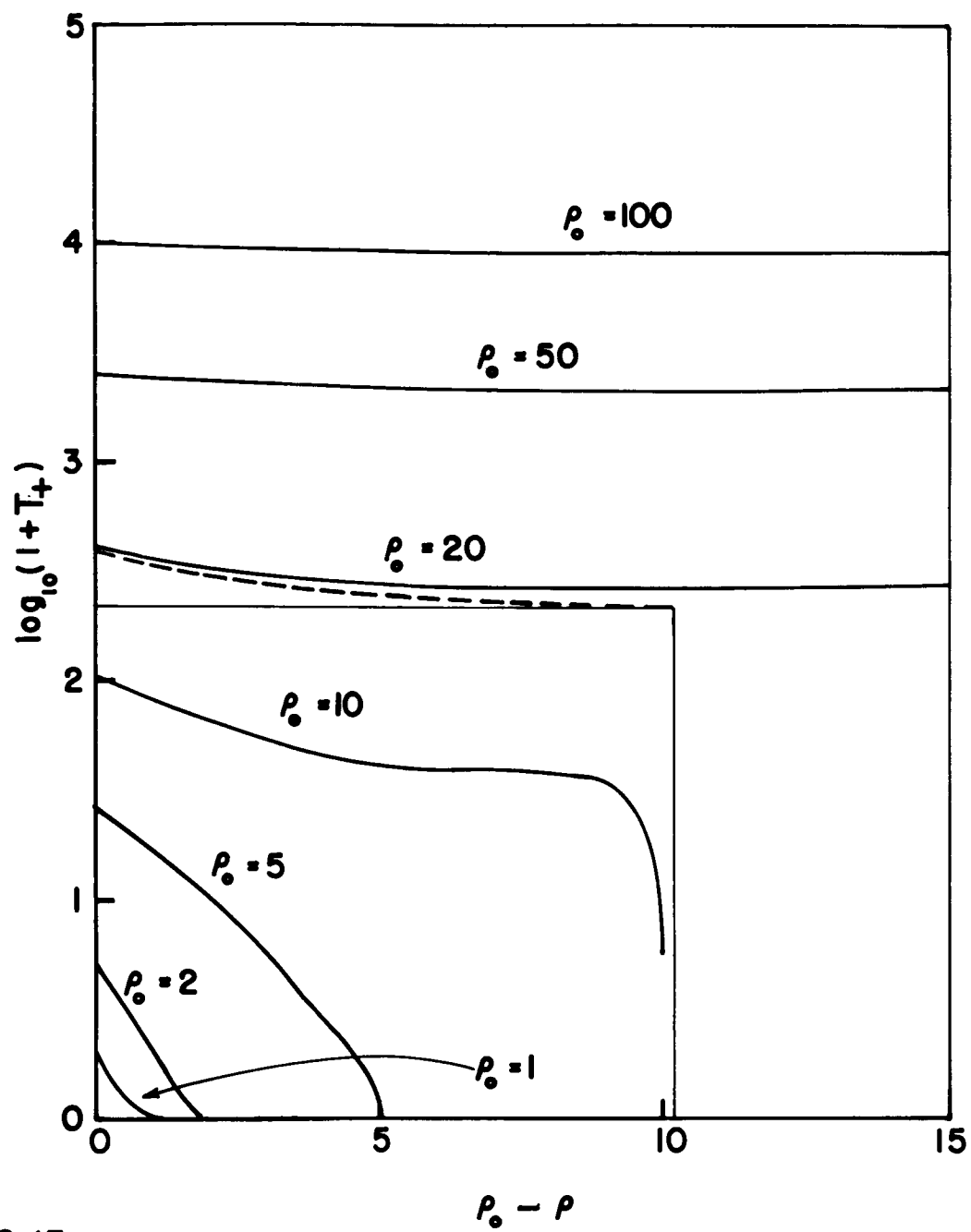


FIG. 2.13

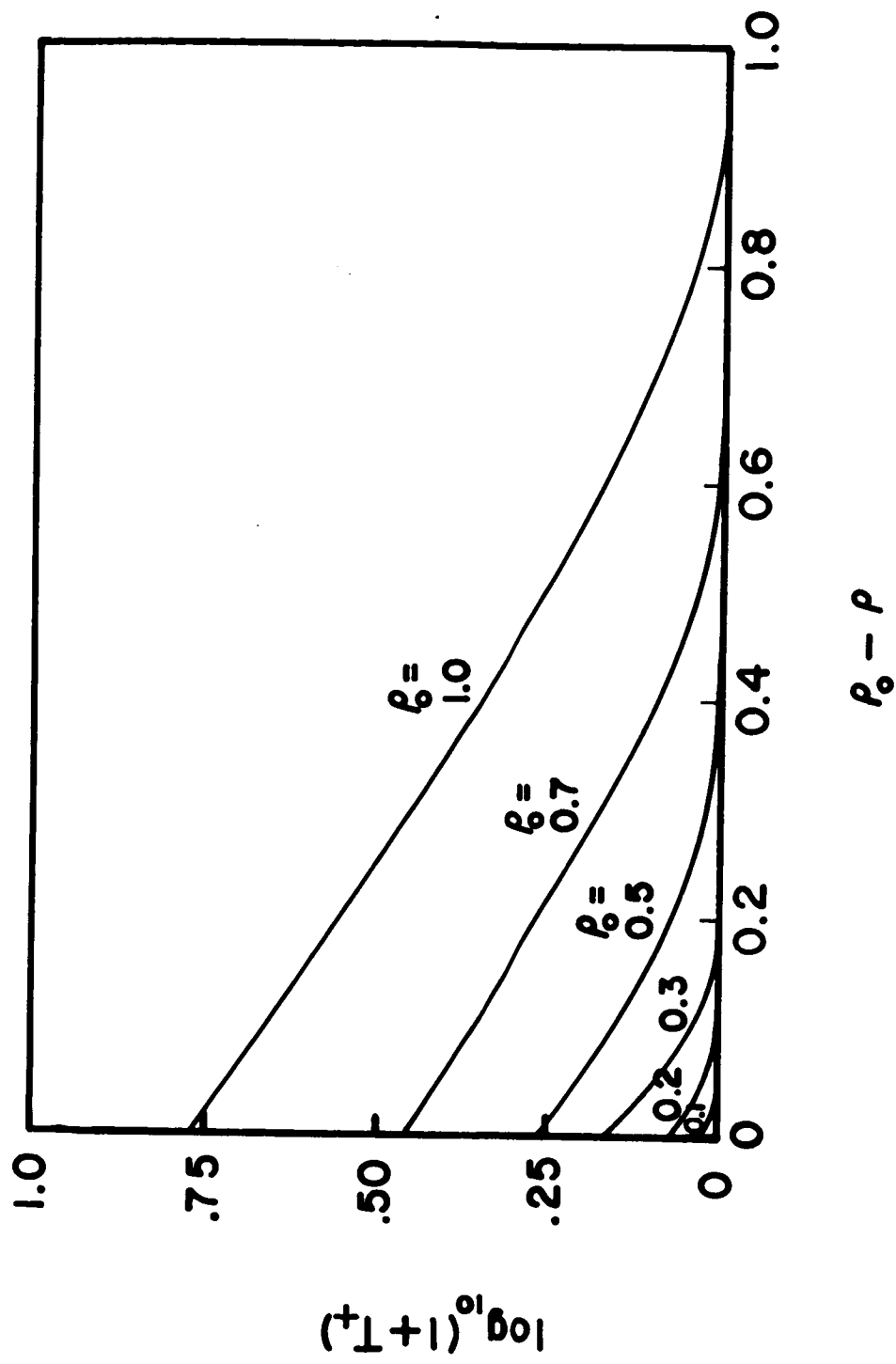


FIG. 2.14

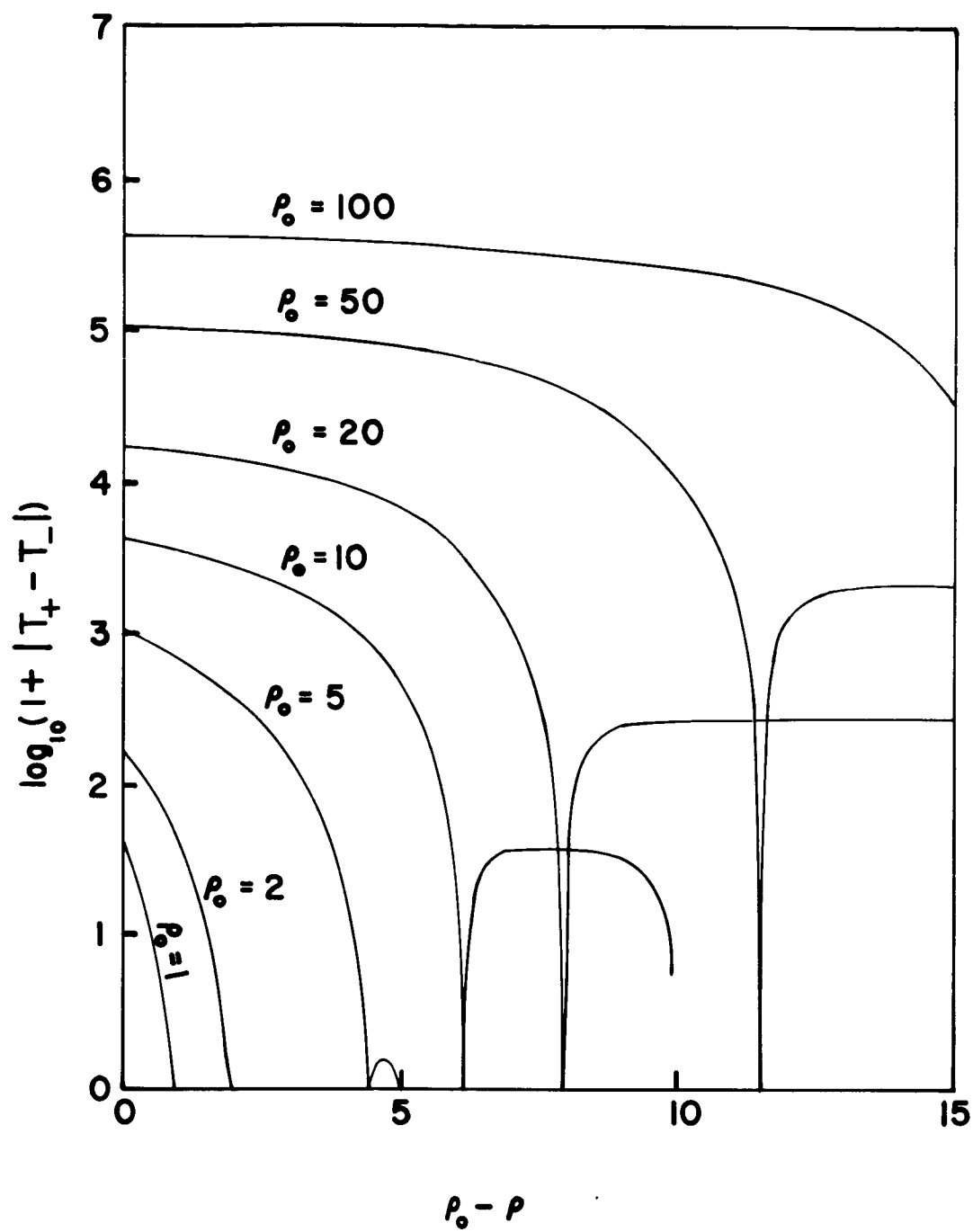


FIG. 2.15

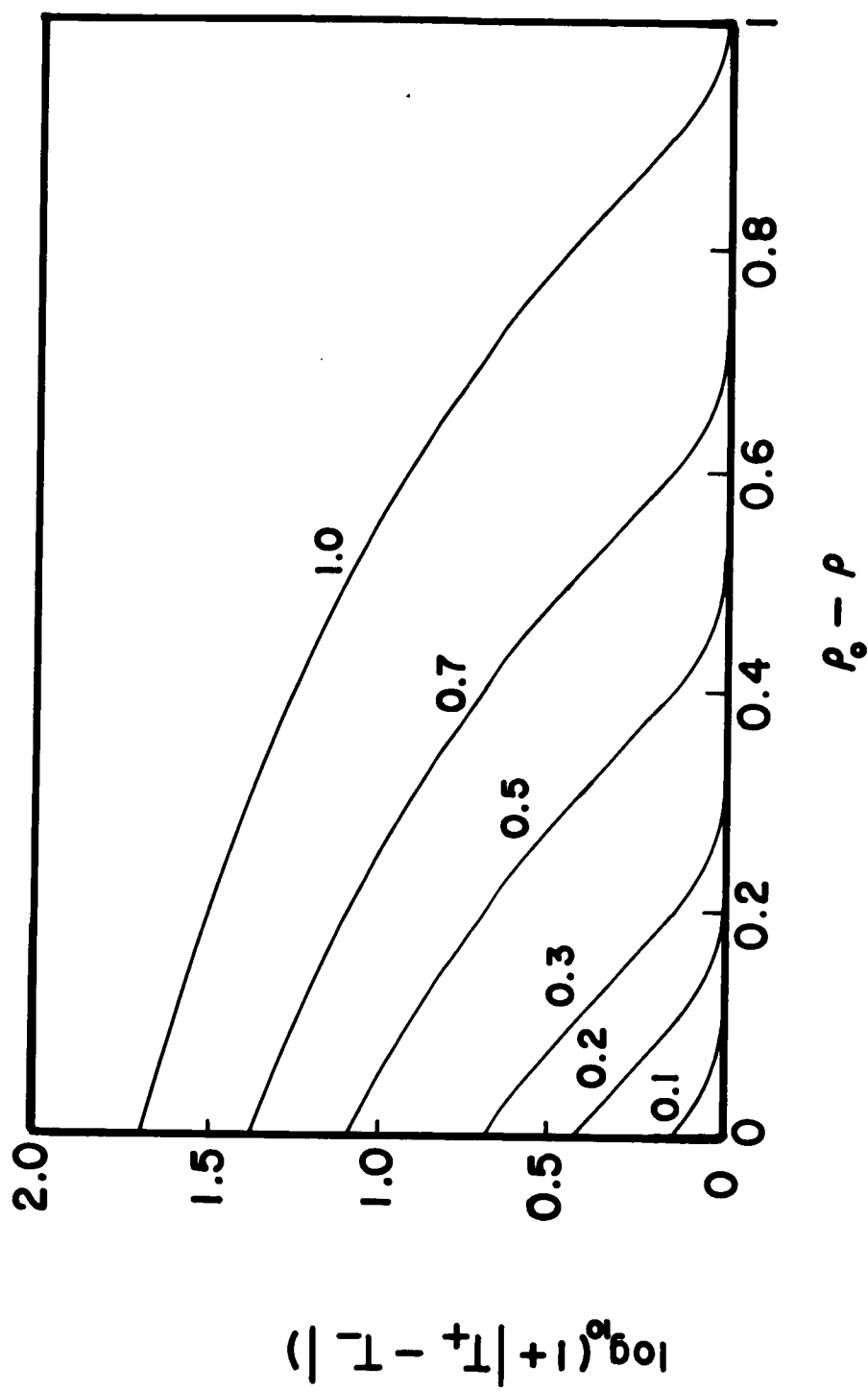


FIG. 2.16

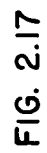


FIG. 2.17

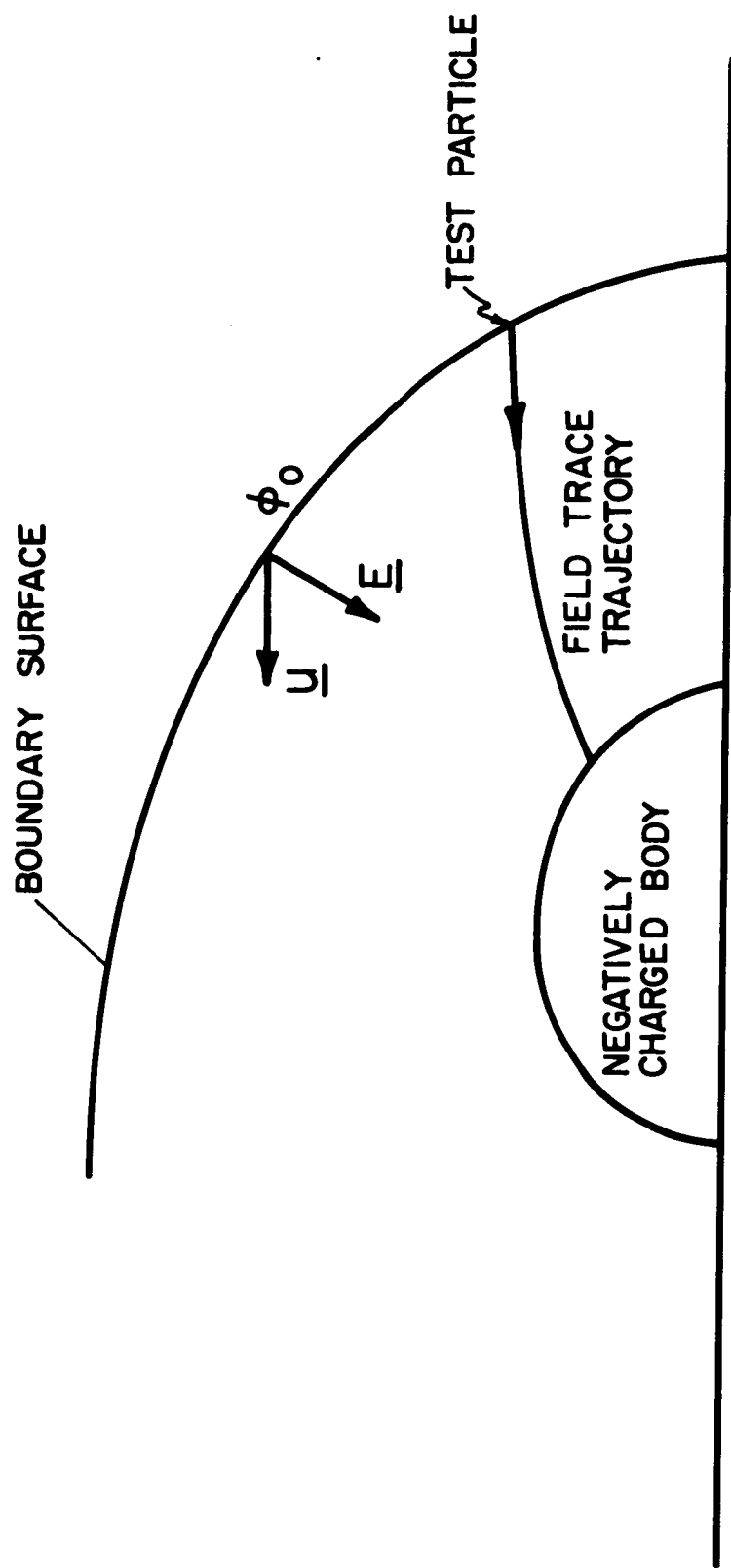


FIG. 4.1

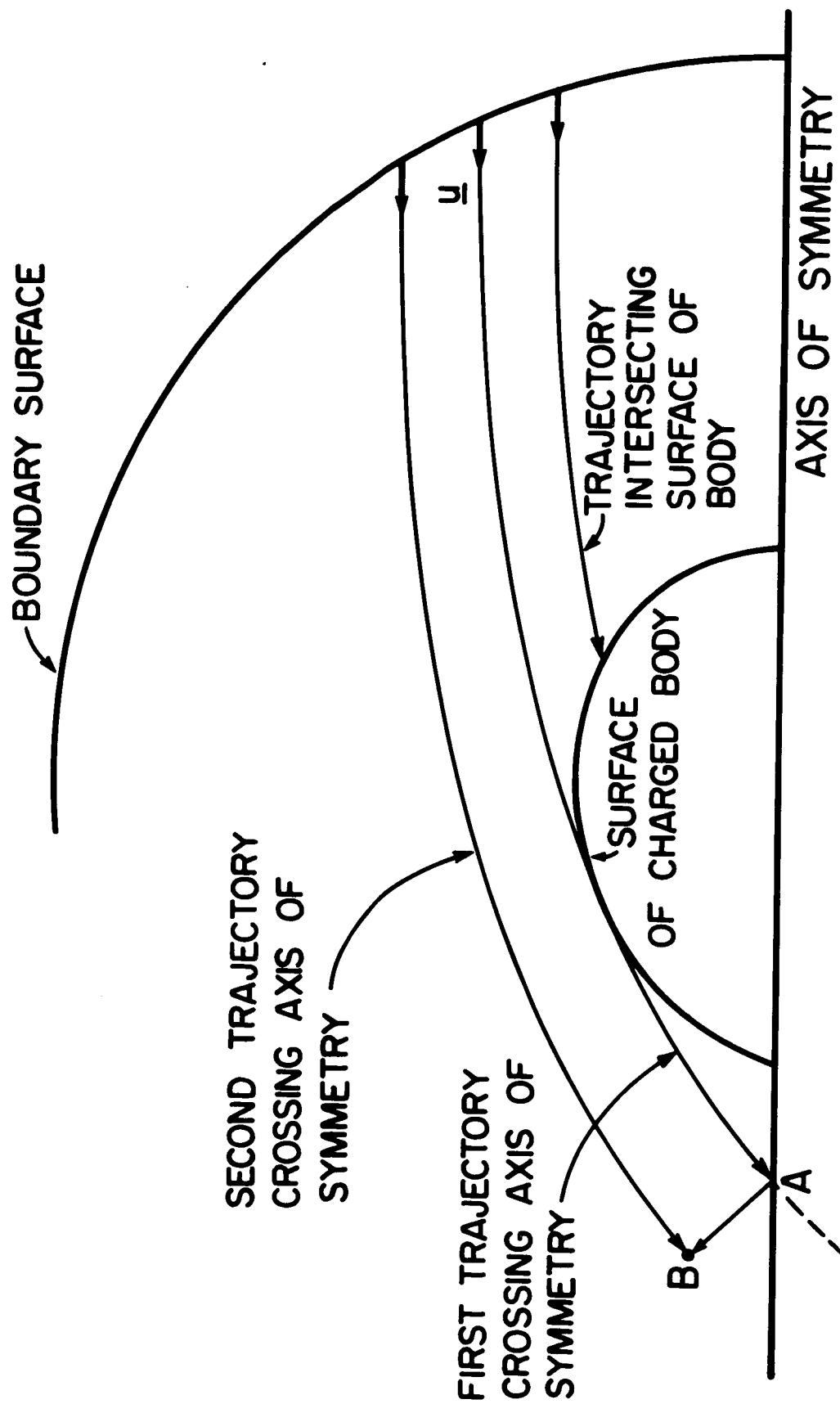


FIG. 4.2

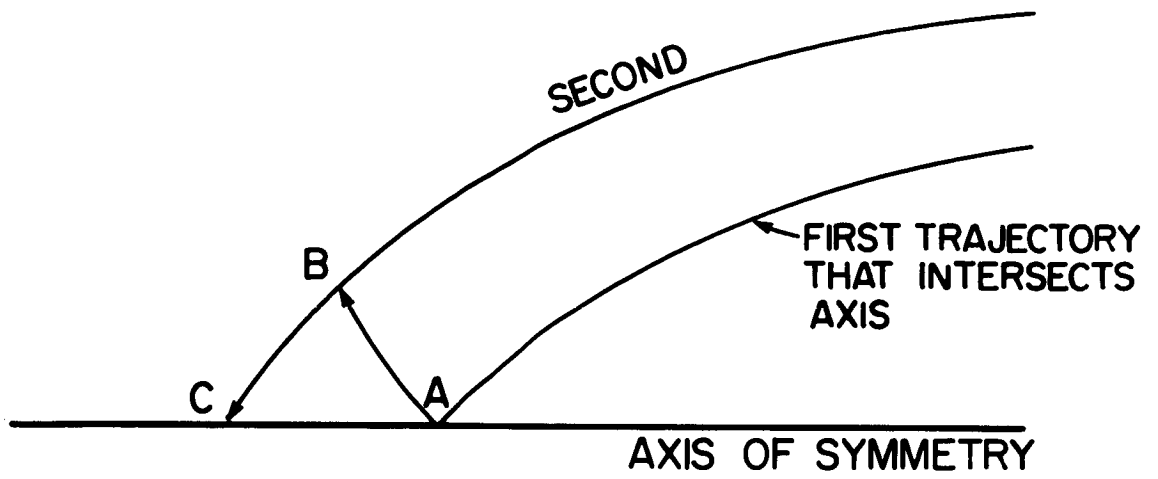


FIG. 4.3 a

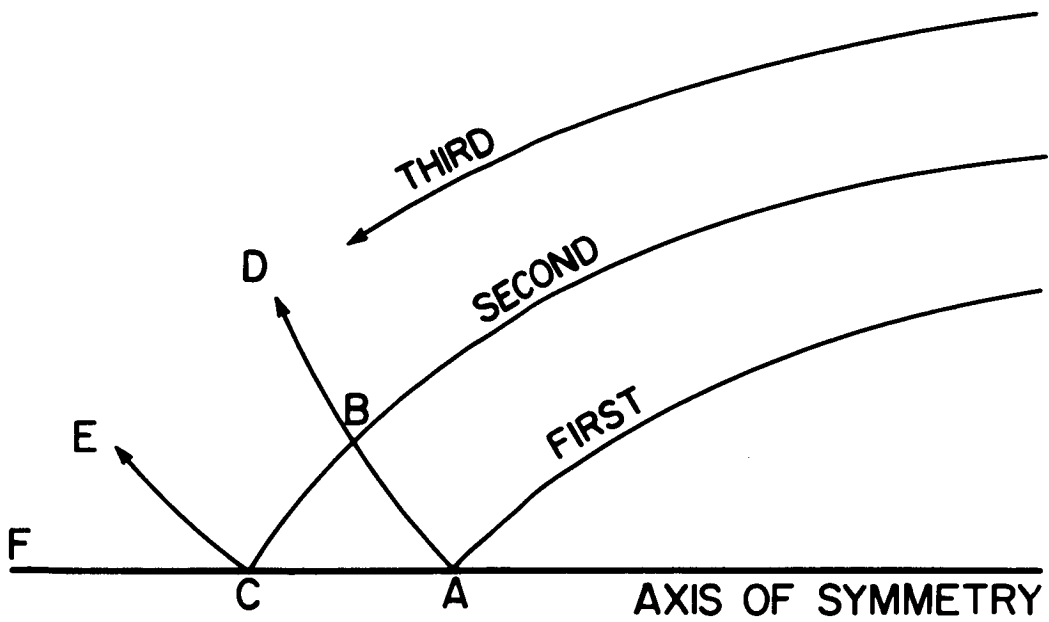


FIG. 4.3 b

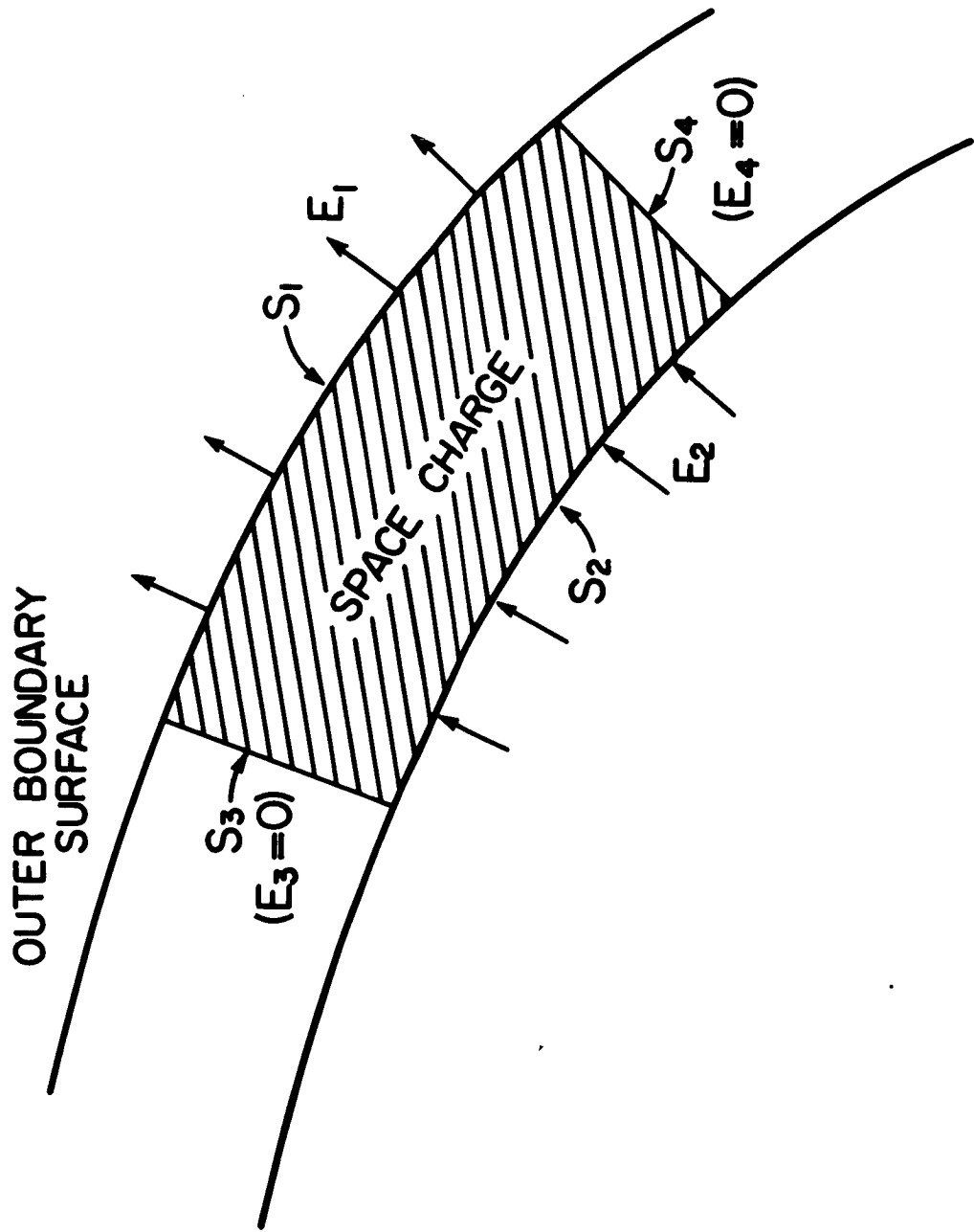


FIG. 4.4

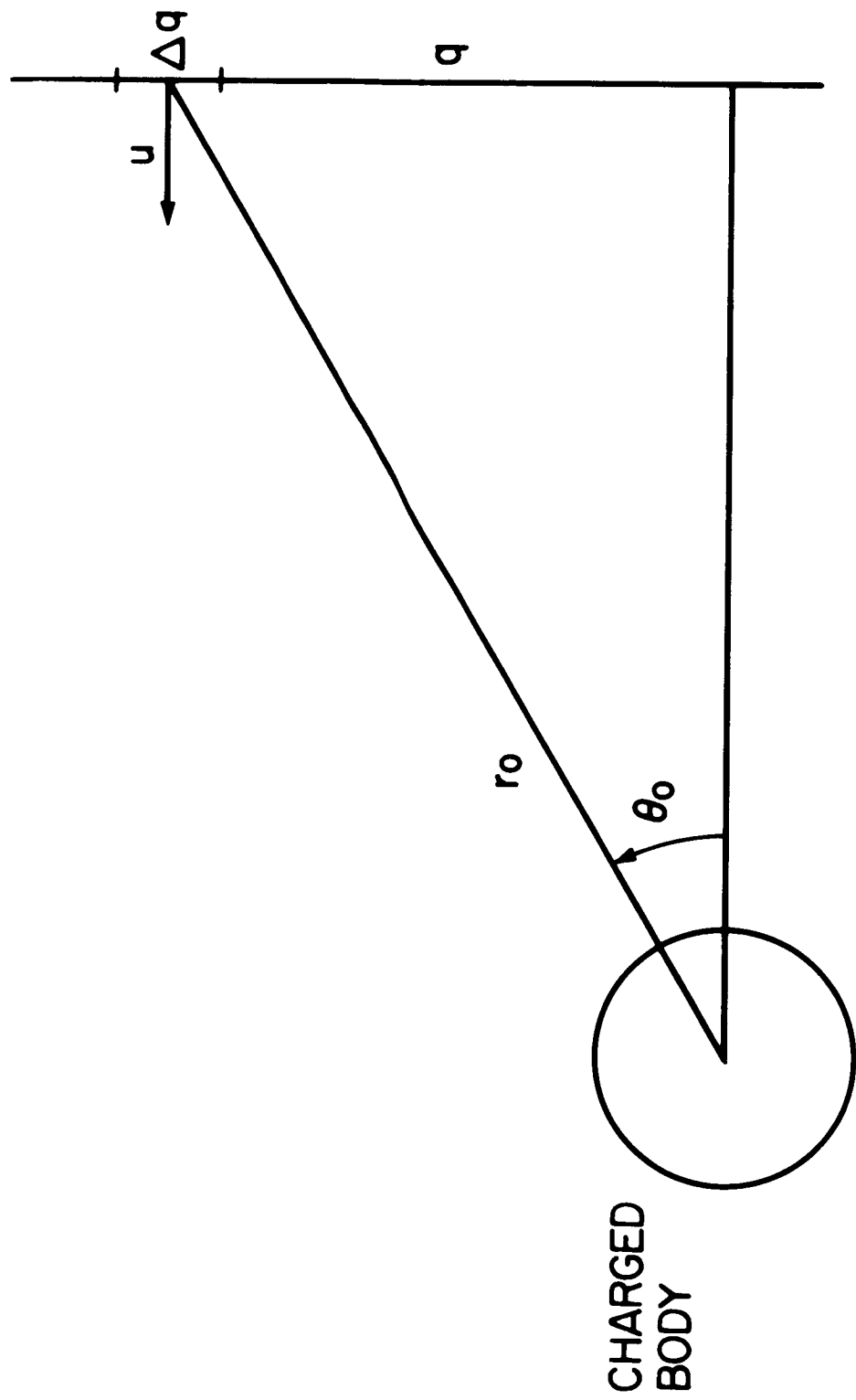


FIG. 5.1

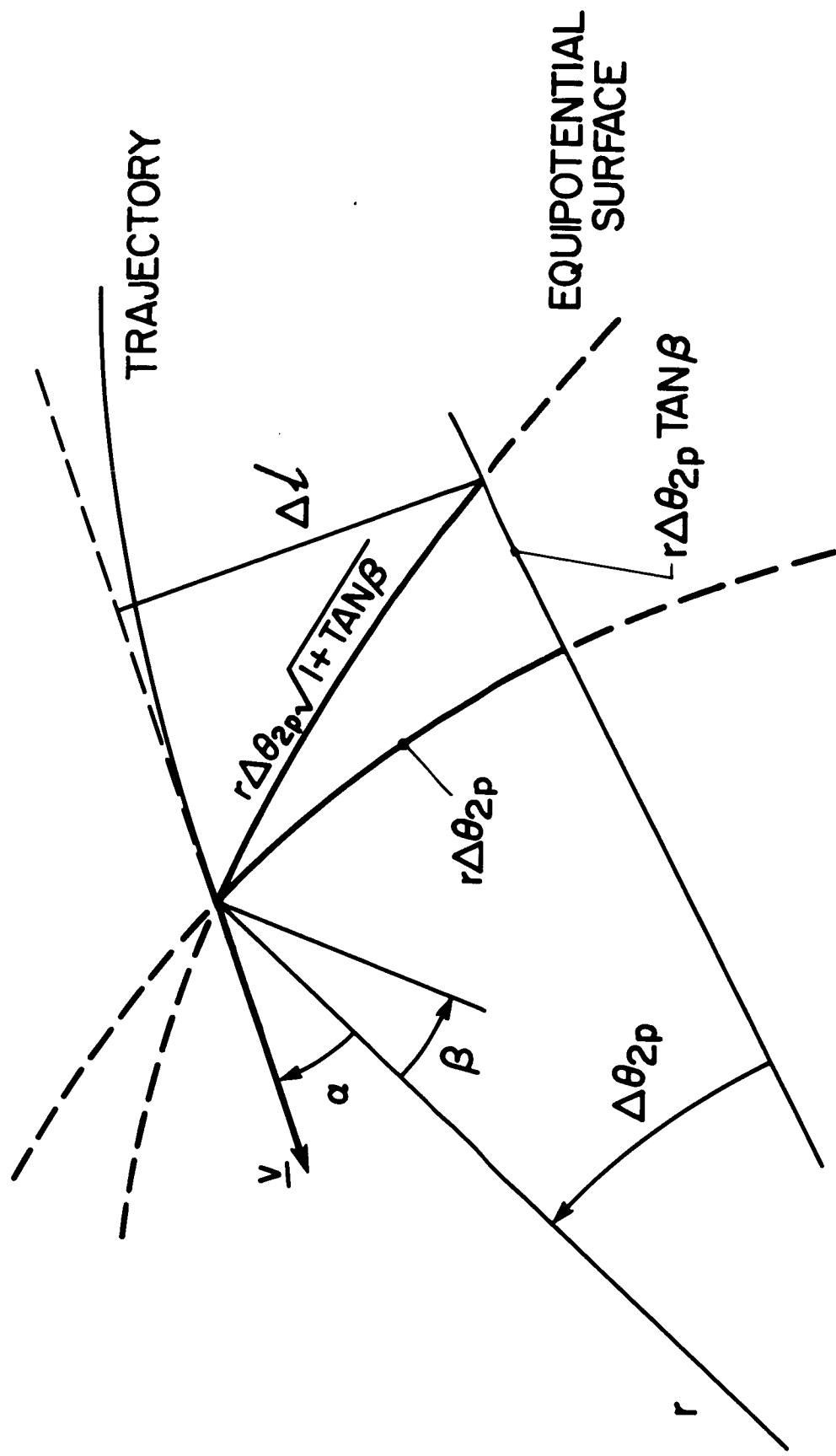


FIG. 5.2

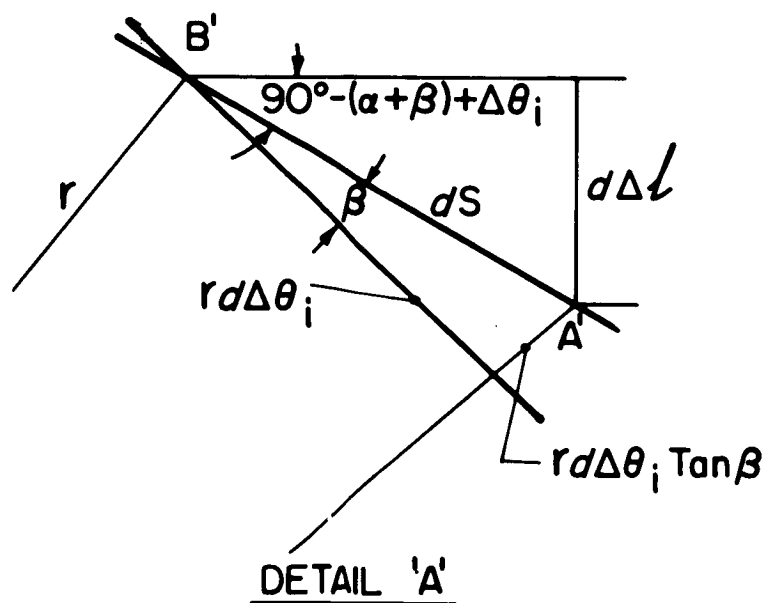
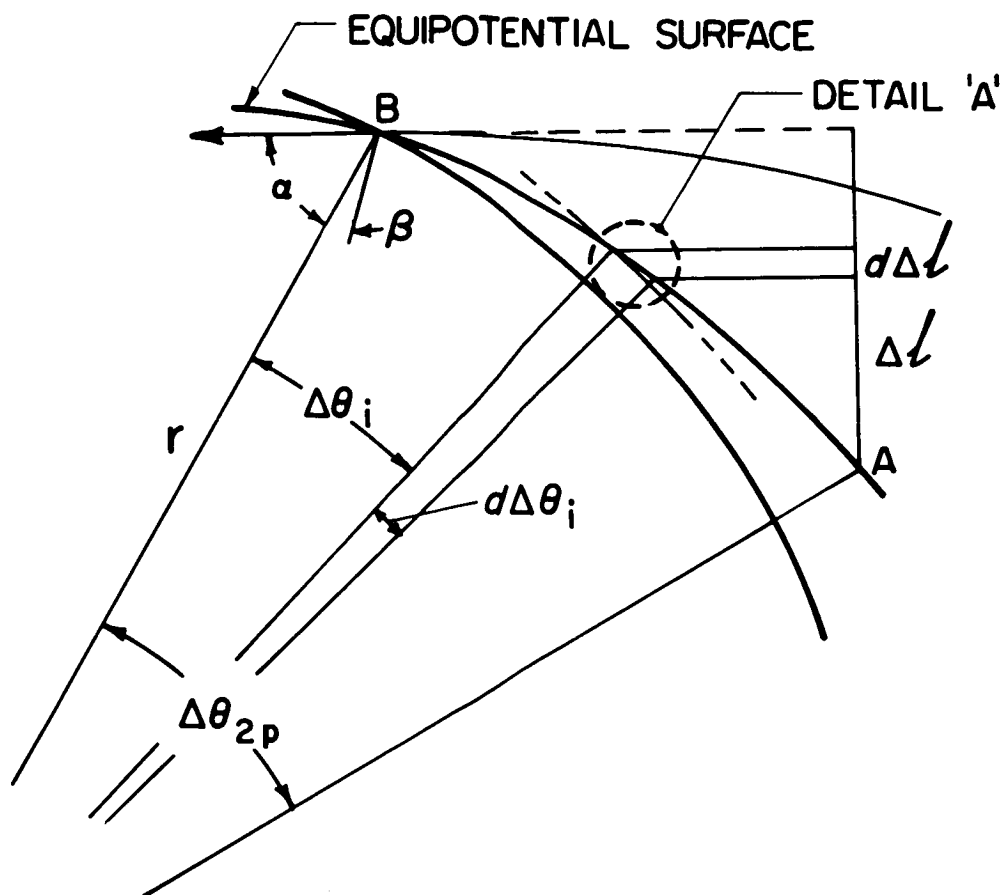
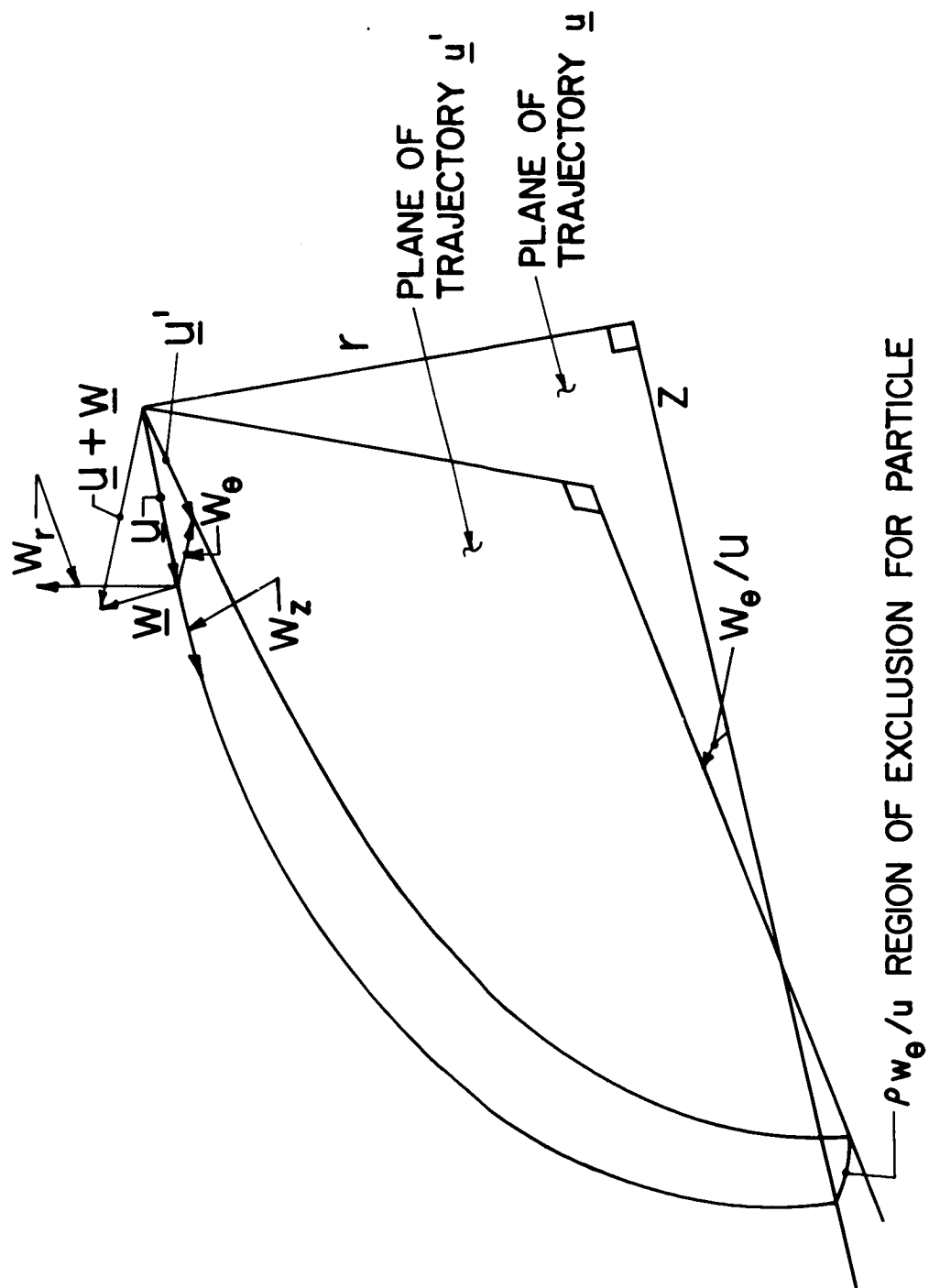


FIG. 5.3



REGION OF EXCLUSION FOR PARTICLE
WITH θ VELOCITY COMPONENT w_θ
OR GREATER

FIG. 5.4

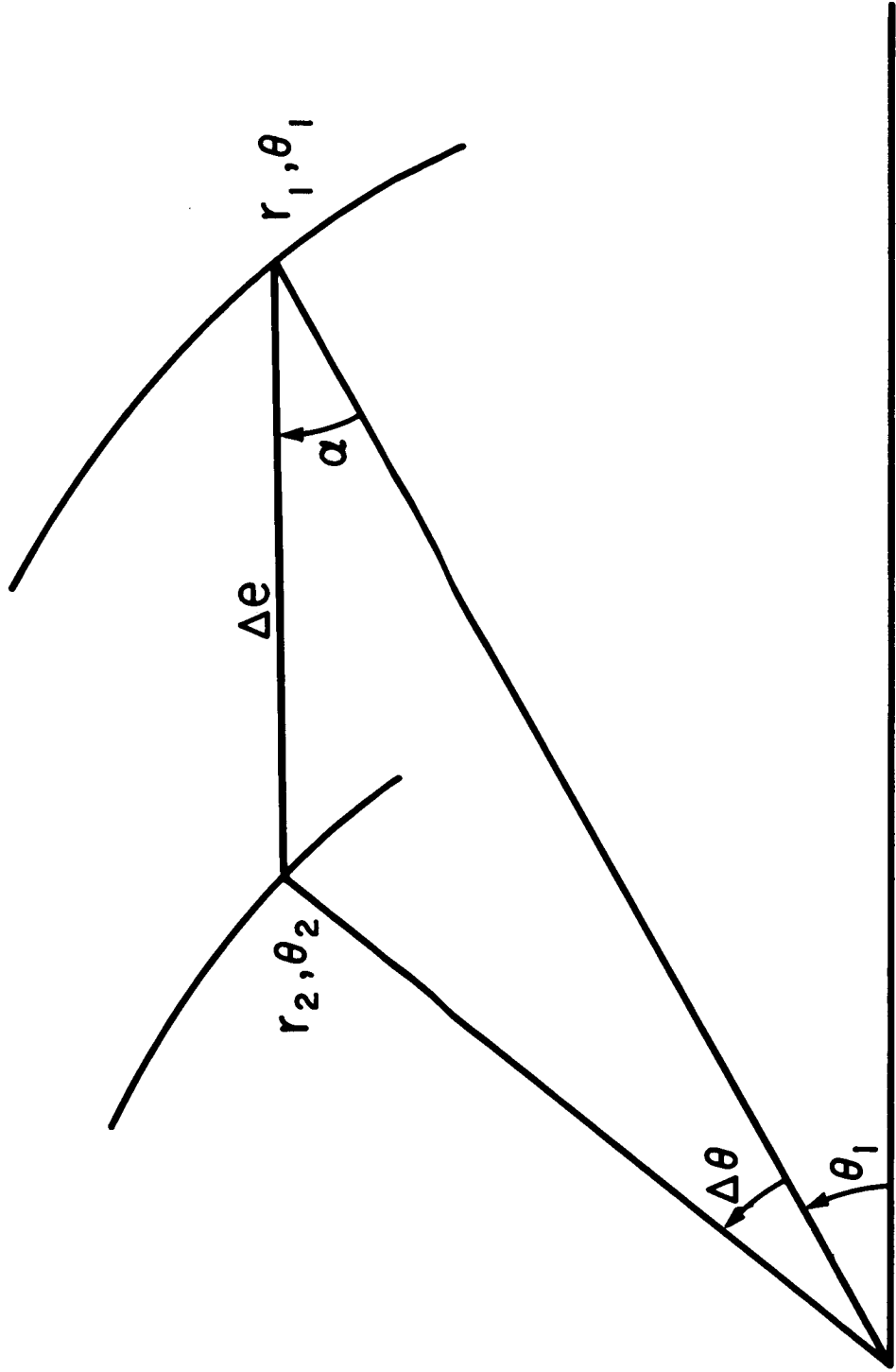


FIG. 6.1

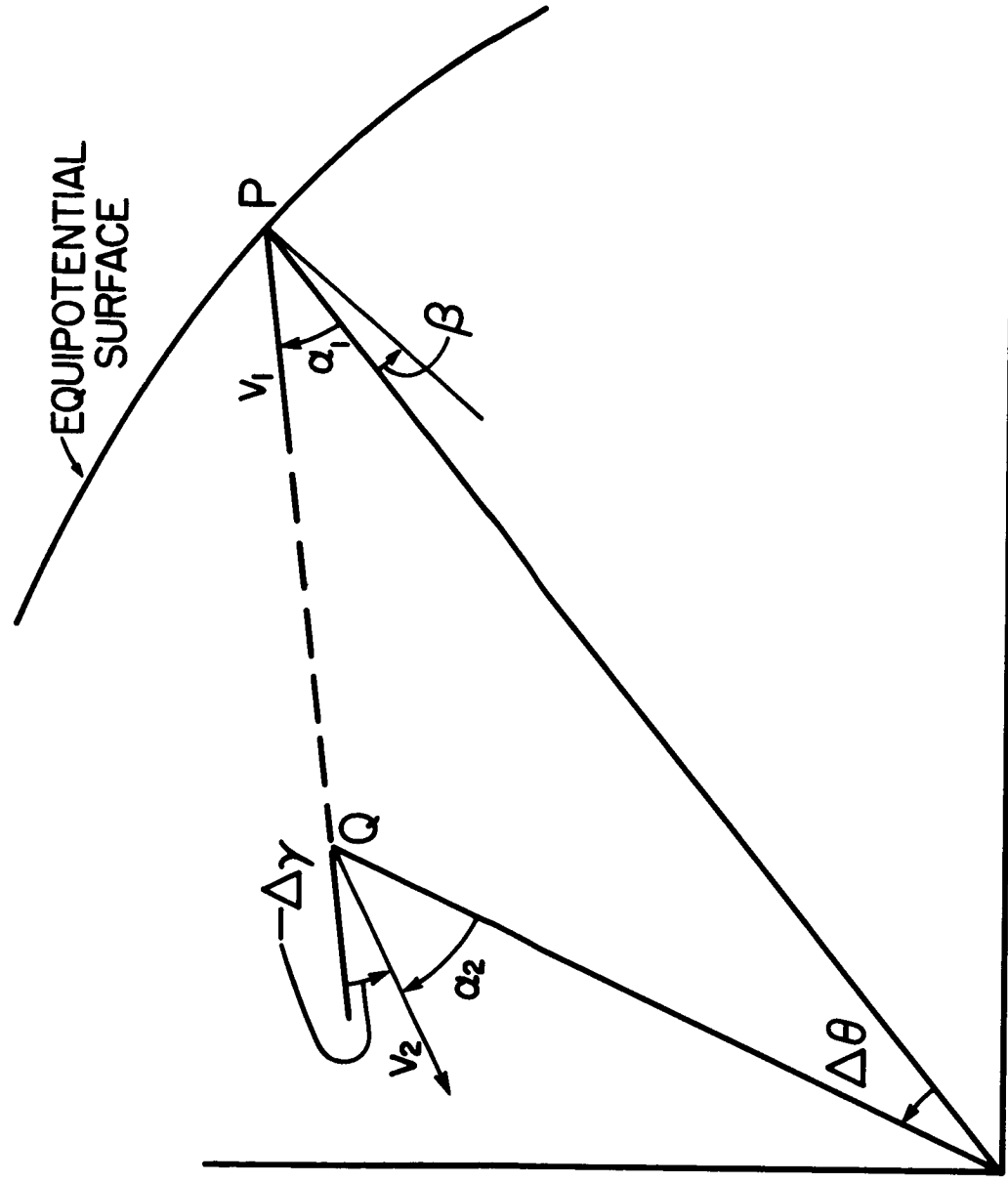


FIG. 6.2

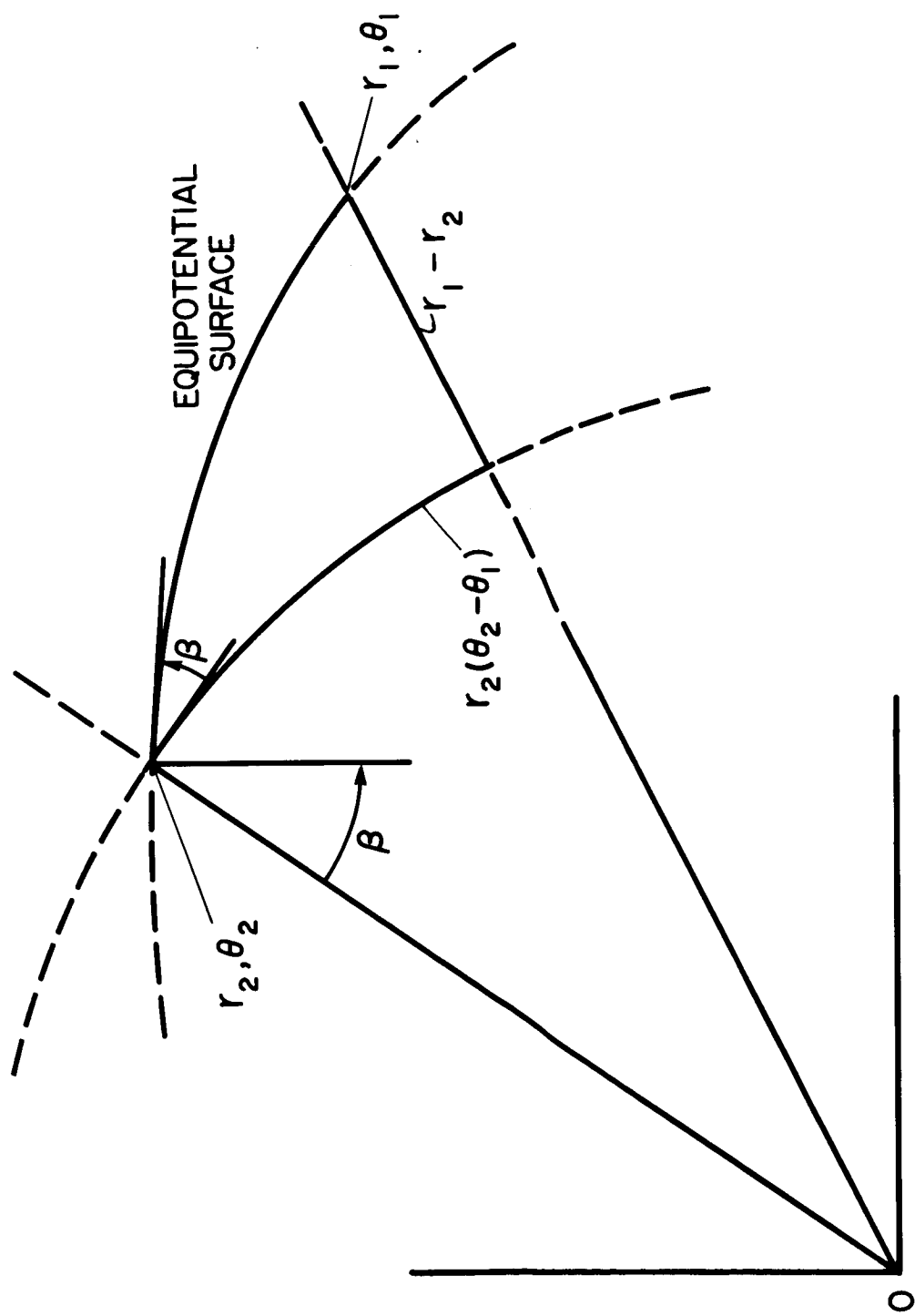


FIG. 6.3

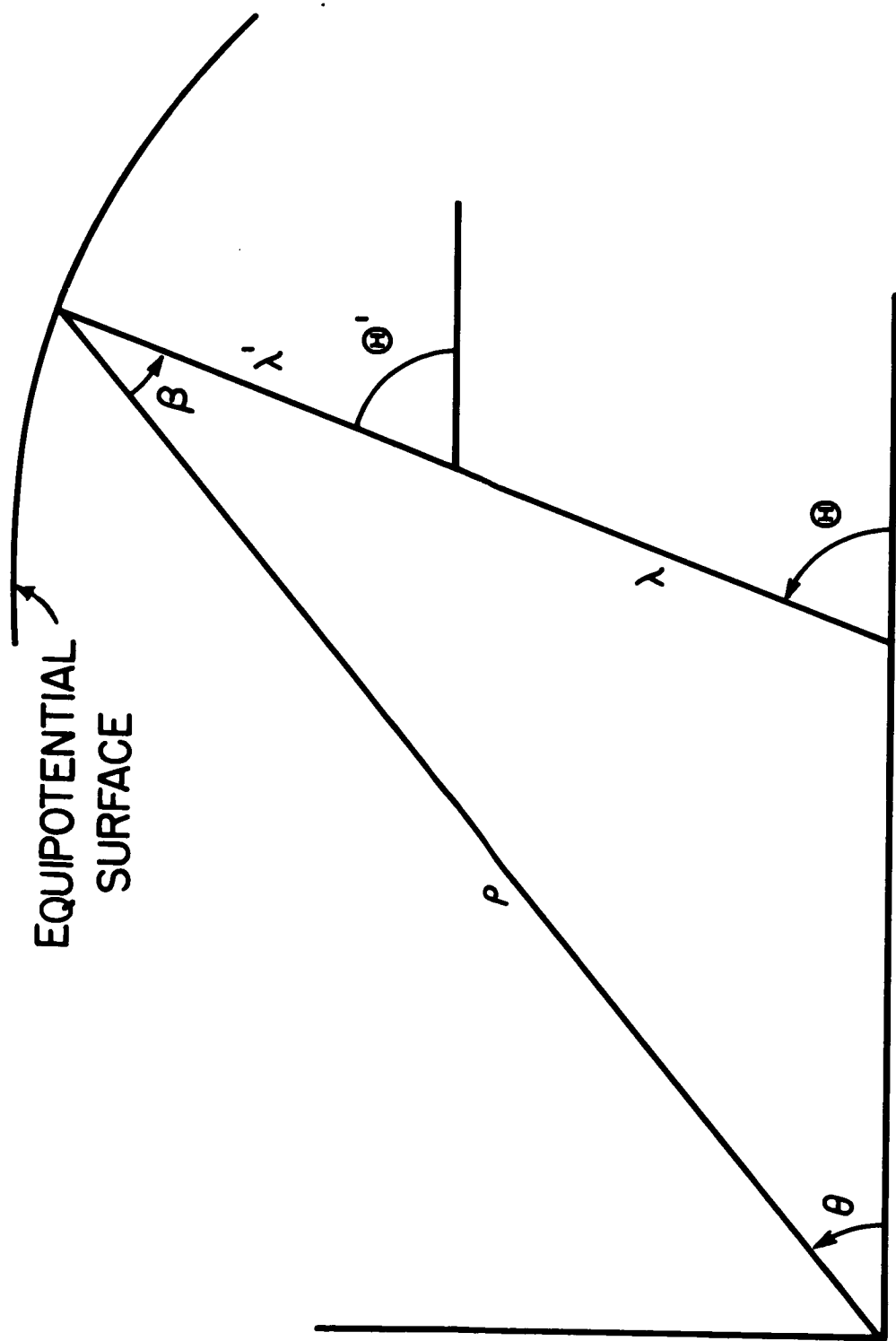


FIG. 6.4

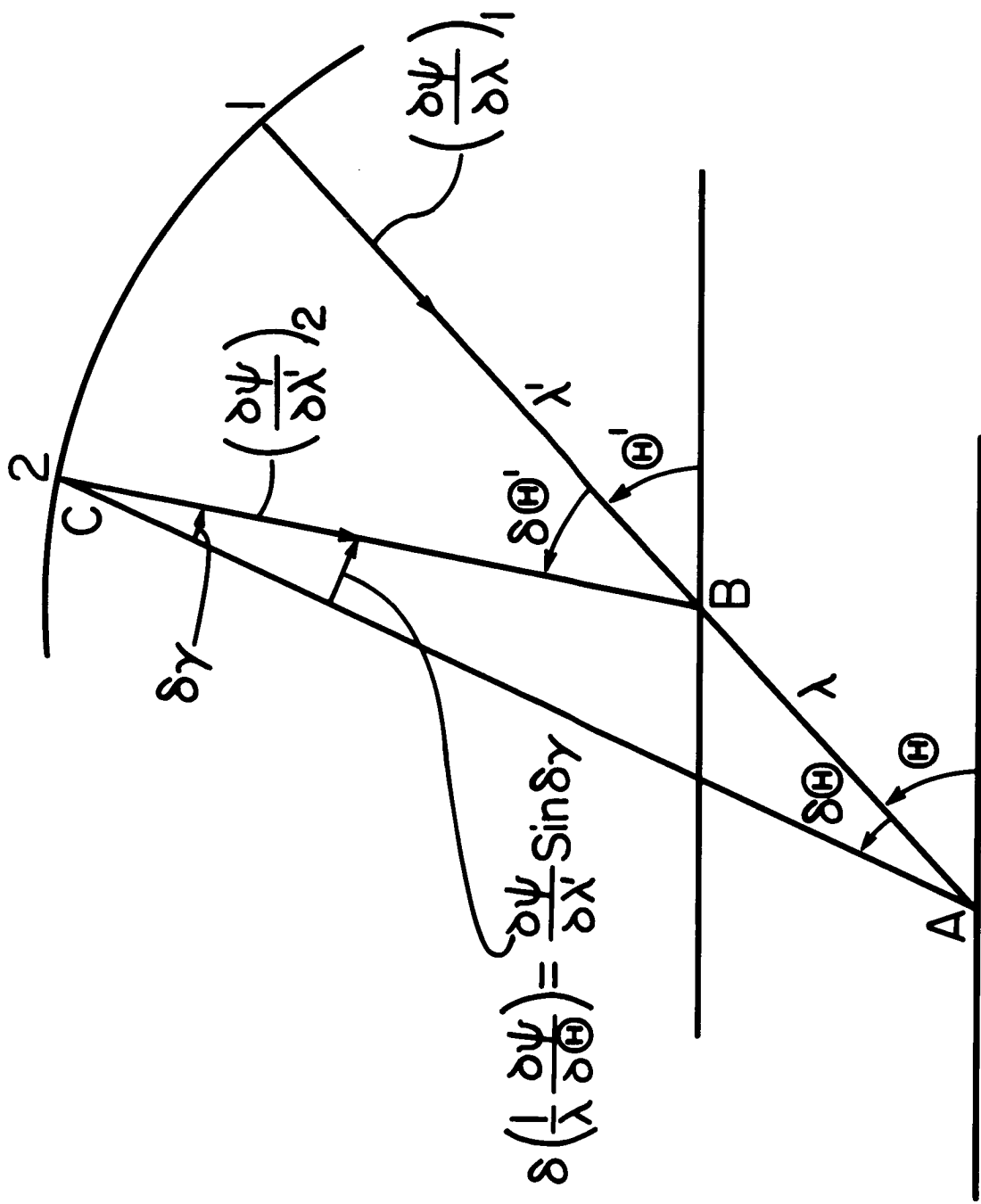


FIG. 6.5

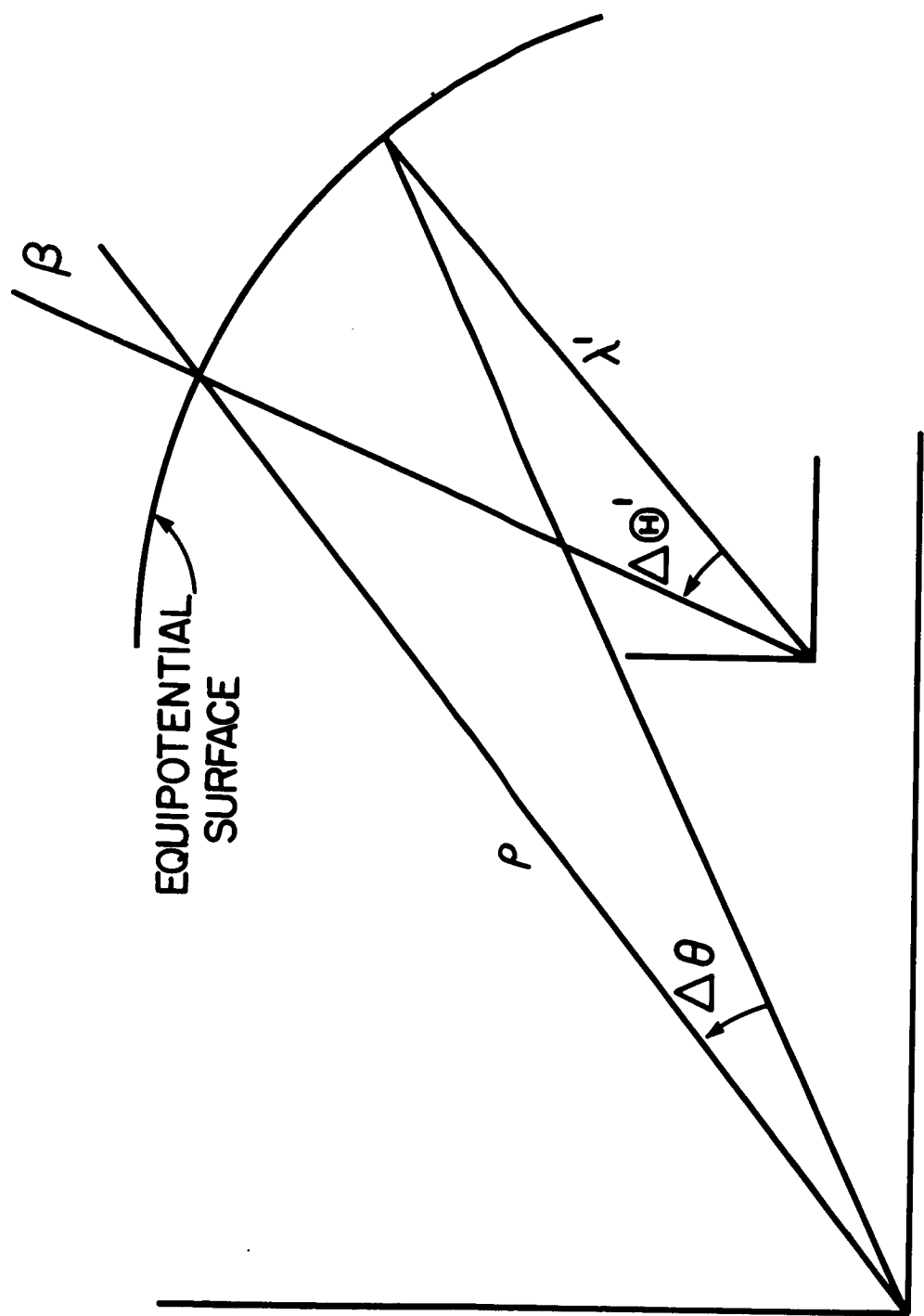


FIG. 6.6

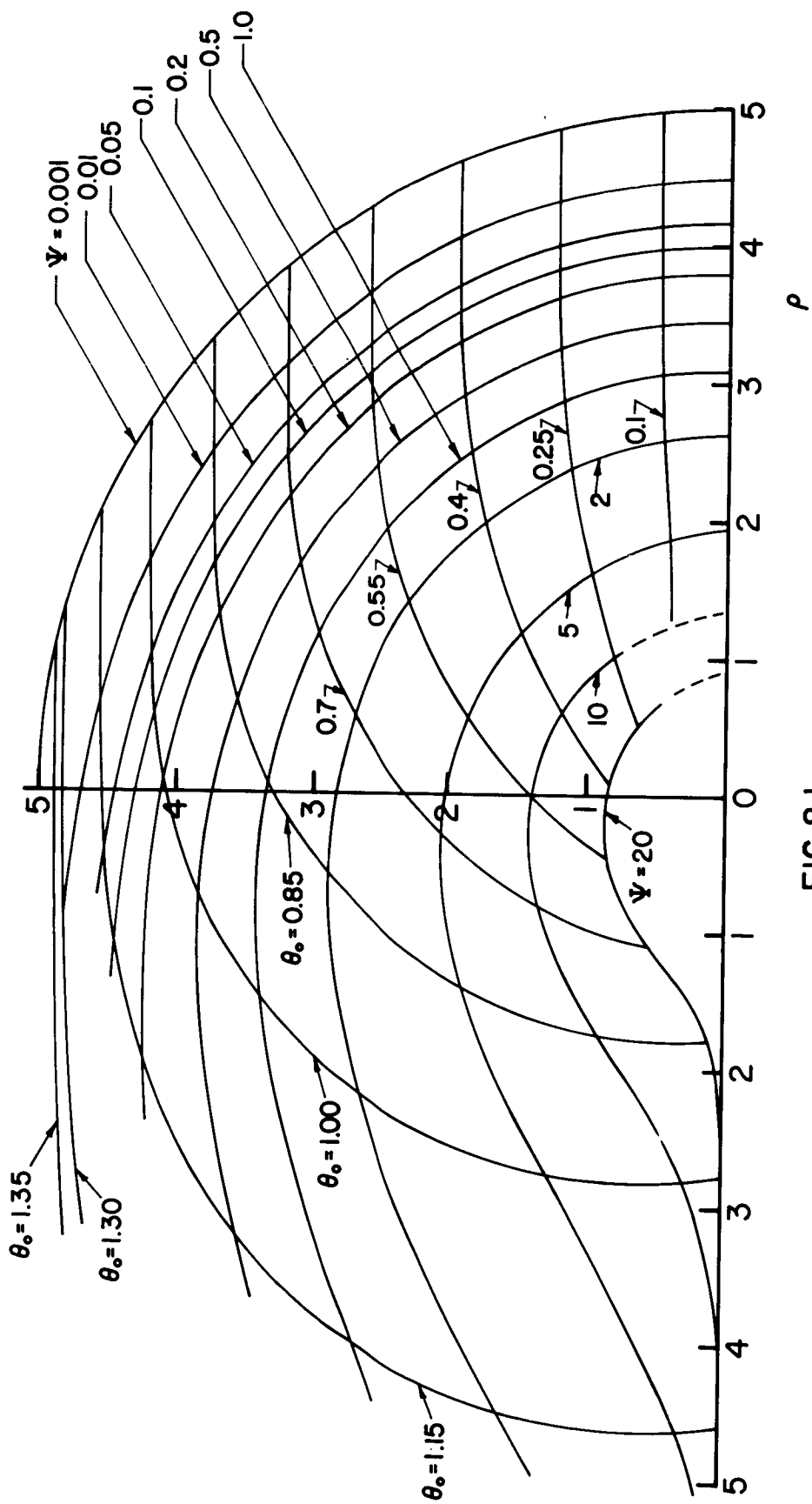


FIG.8.1

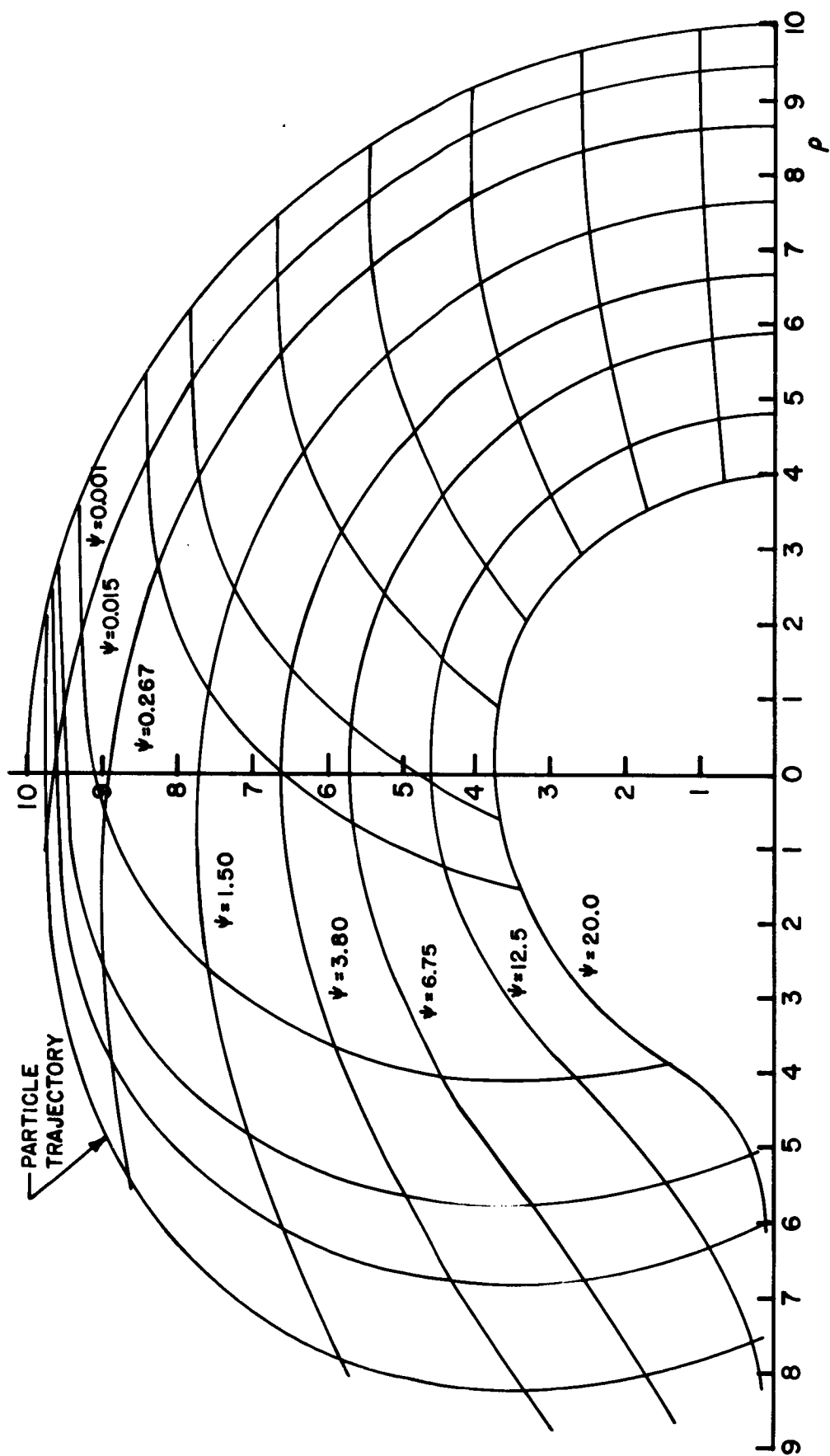


FIG. 8.2

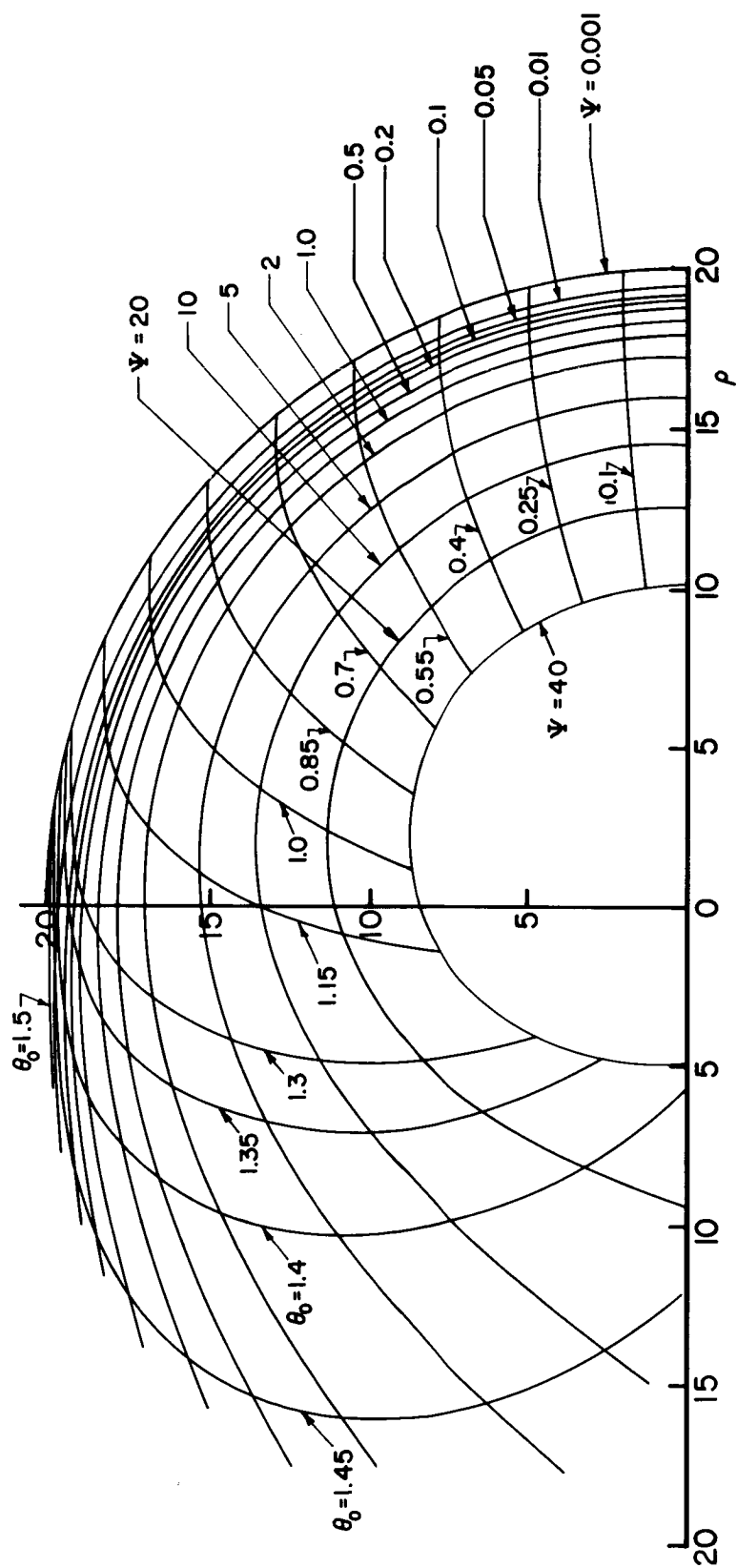


FIG. 8.3

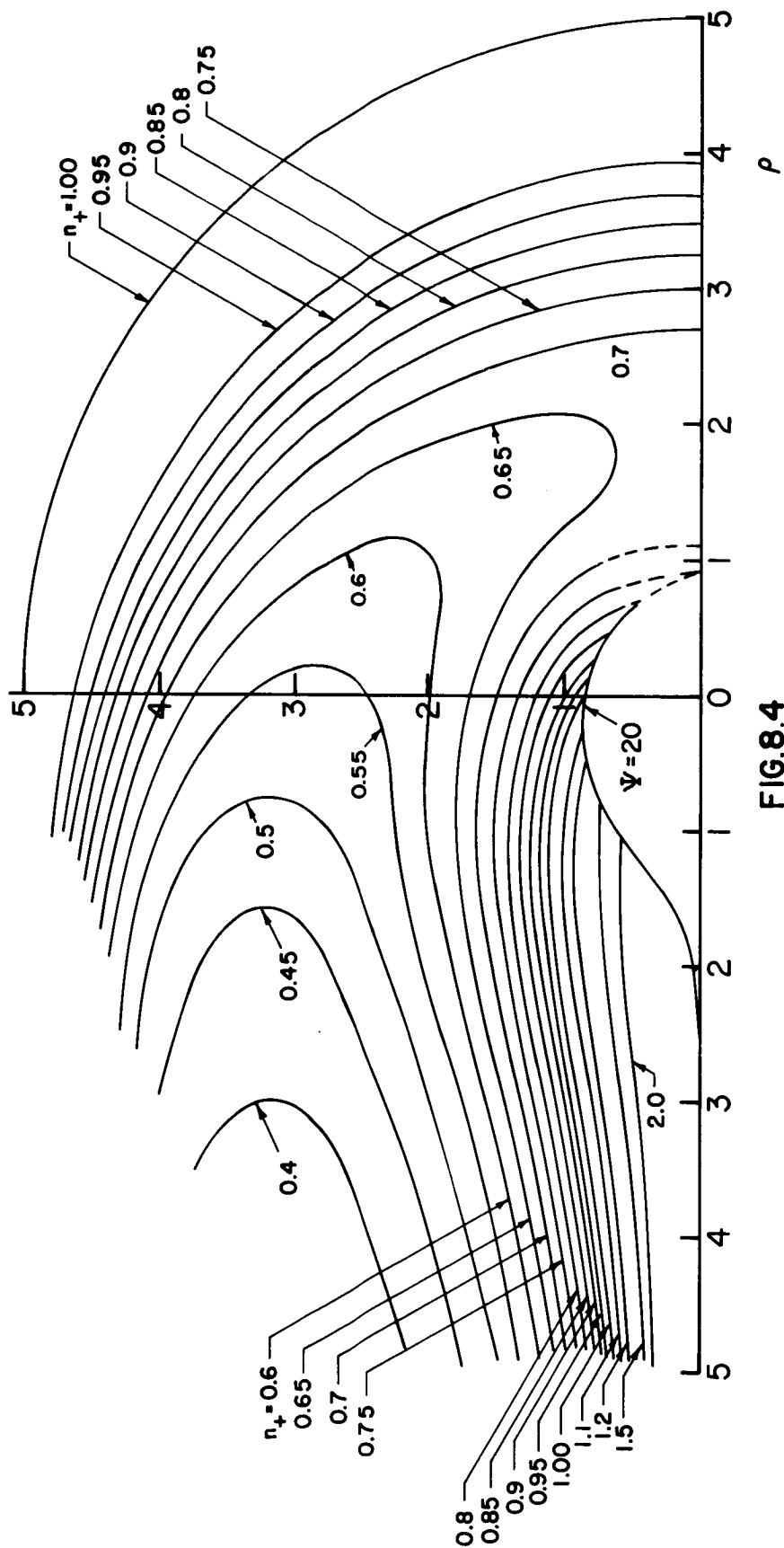


FIG.8.4

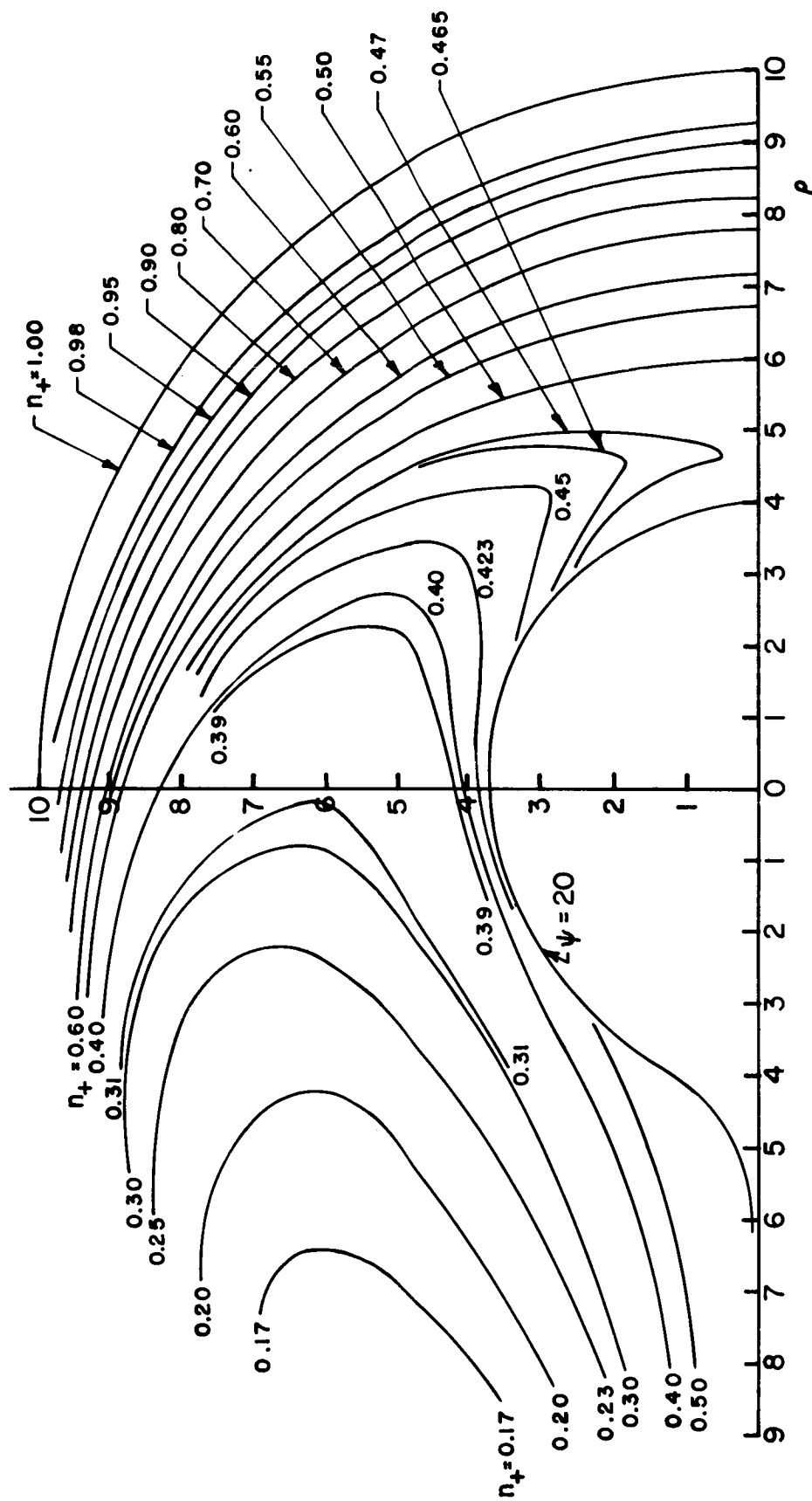


FIG. 8.5

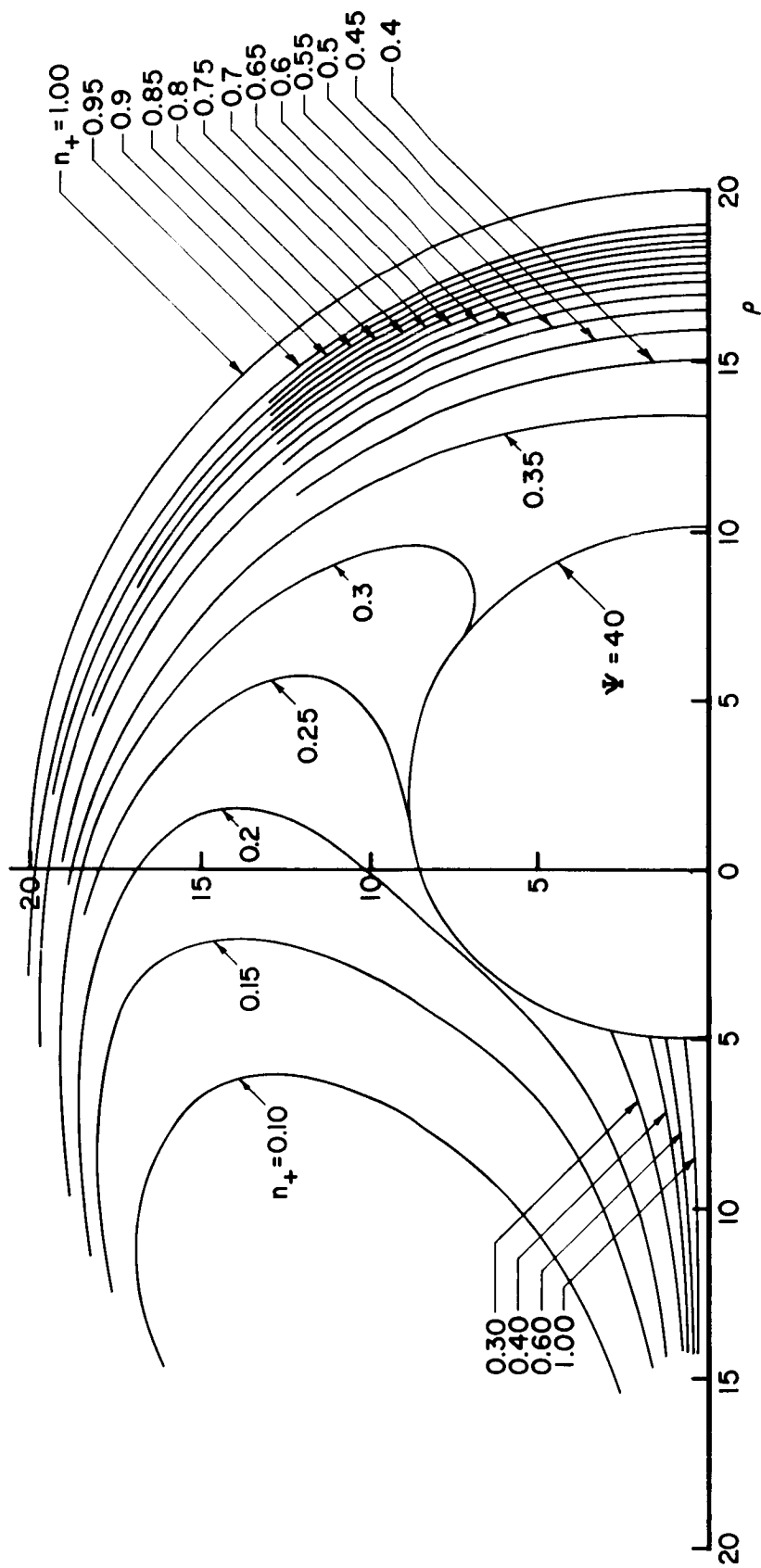


FIG. 8.6

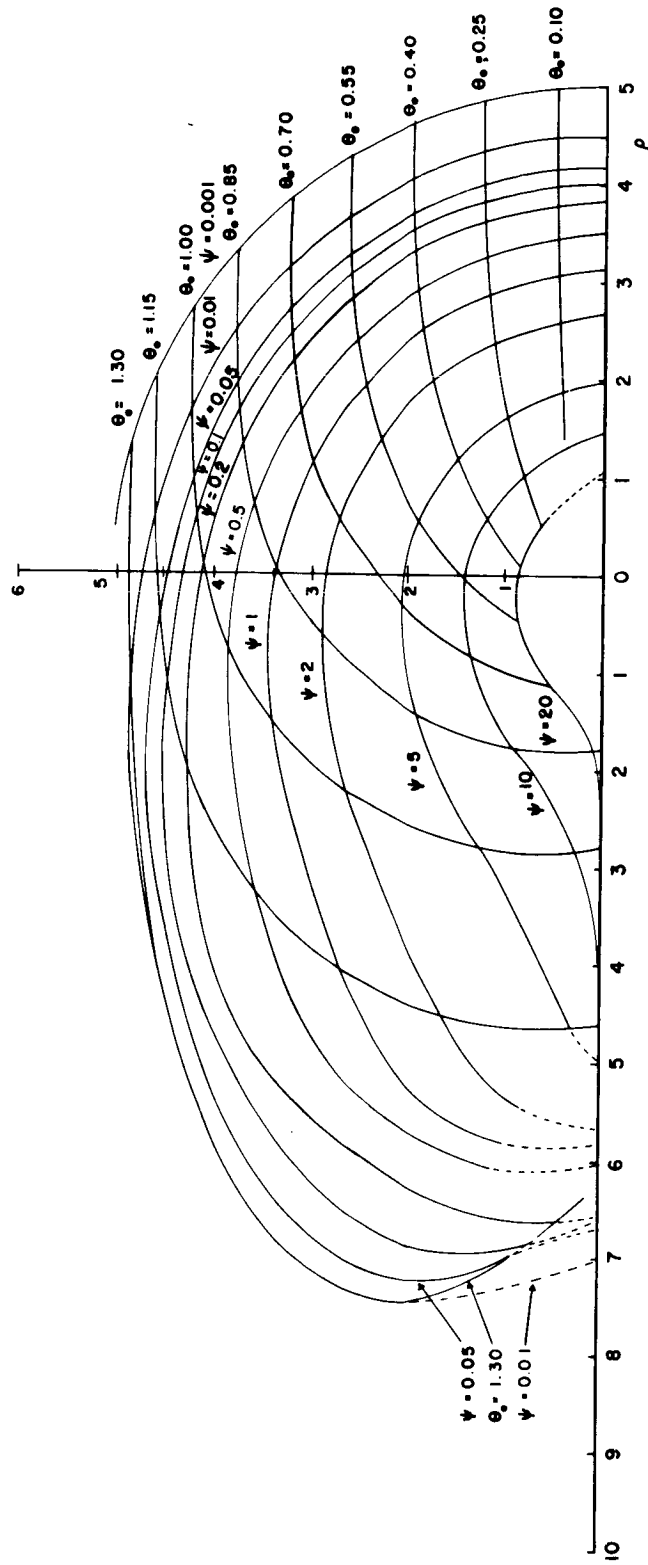
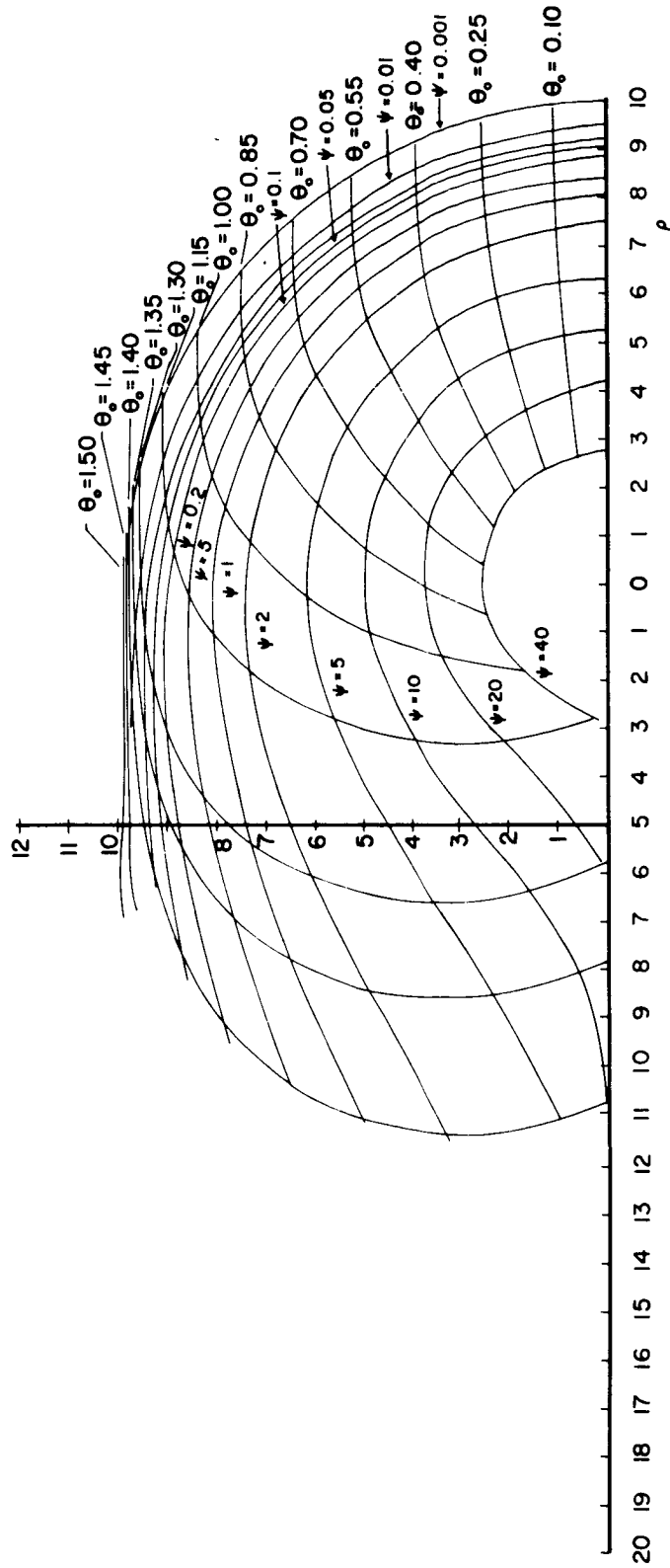


FIG. 8.7

$\rho = 5$ VTV - 0.218443



$\rho = 10$ DNI VTV = .218443

FIG. 8.8

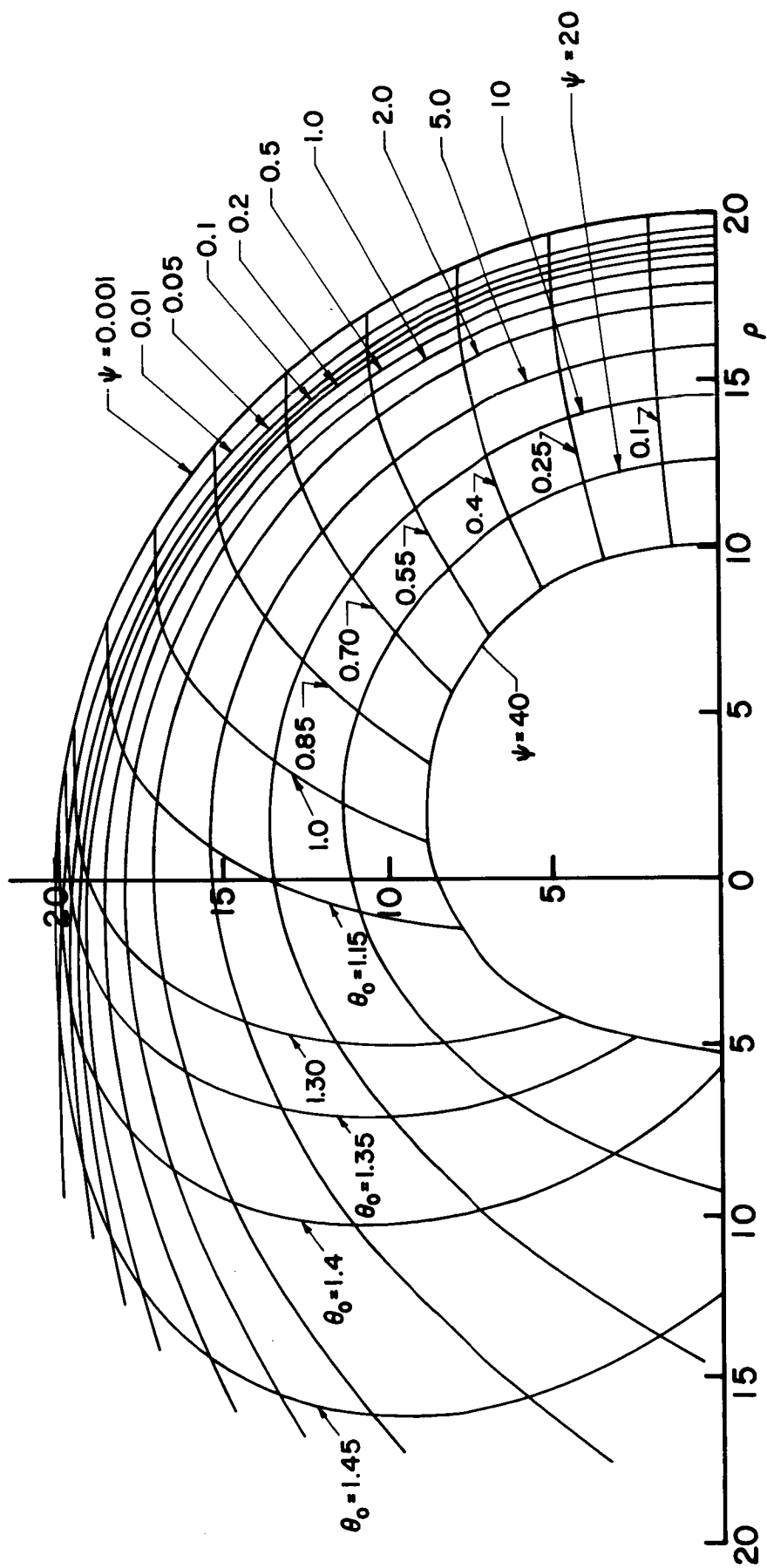


FIG. 8.9

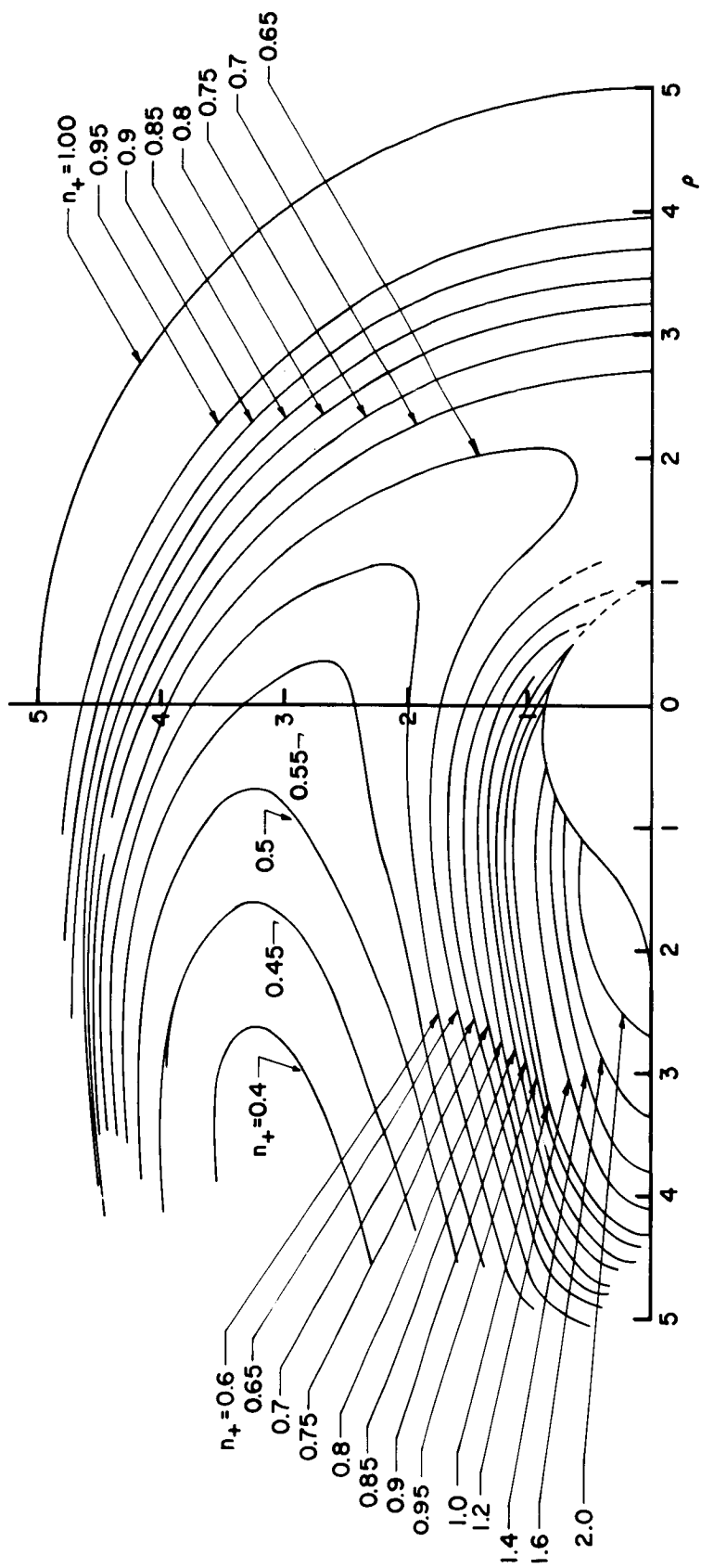


FIG. 8.10

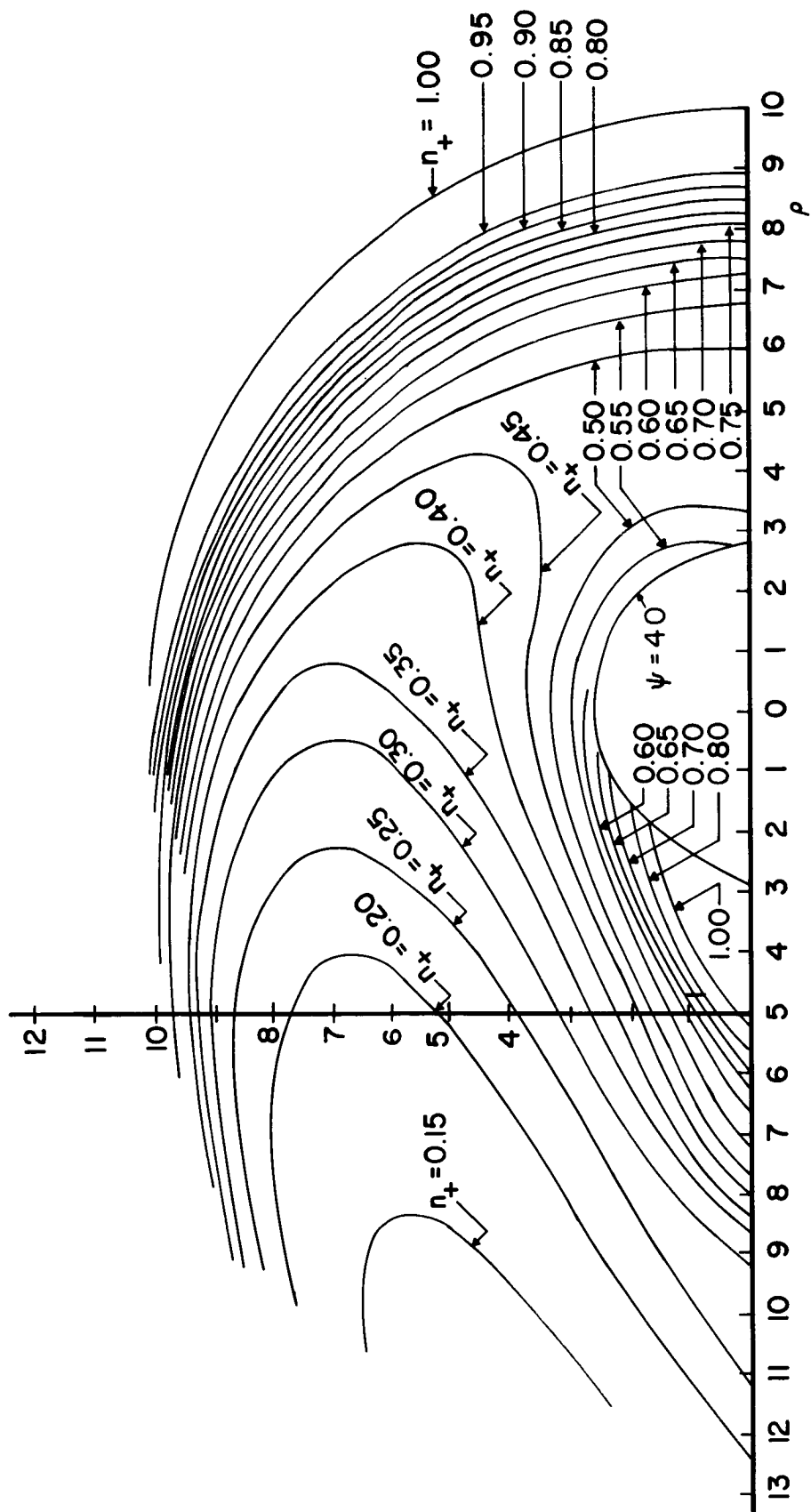


FIG. 8.11

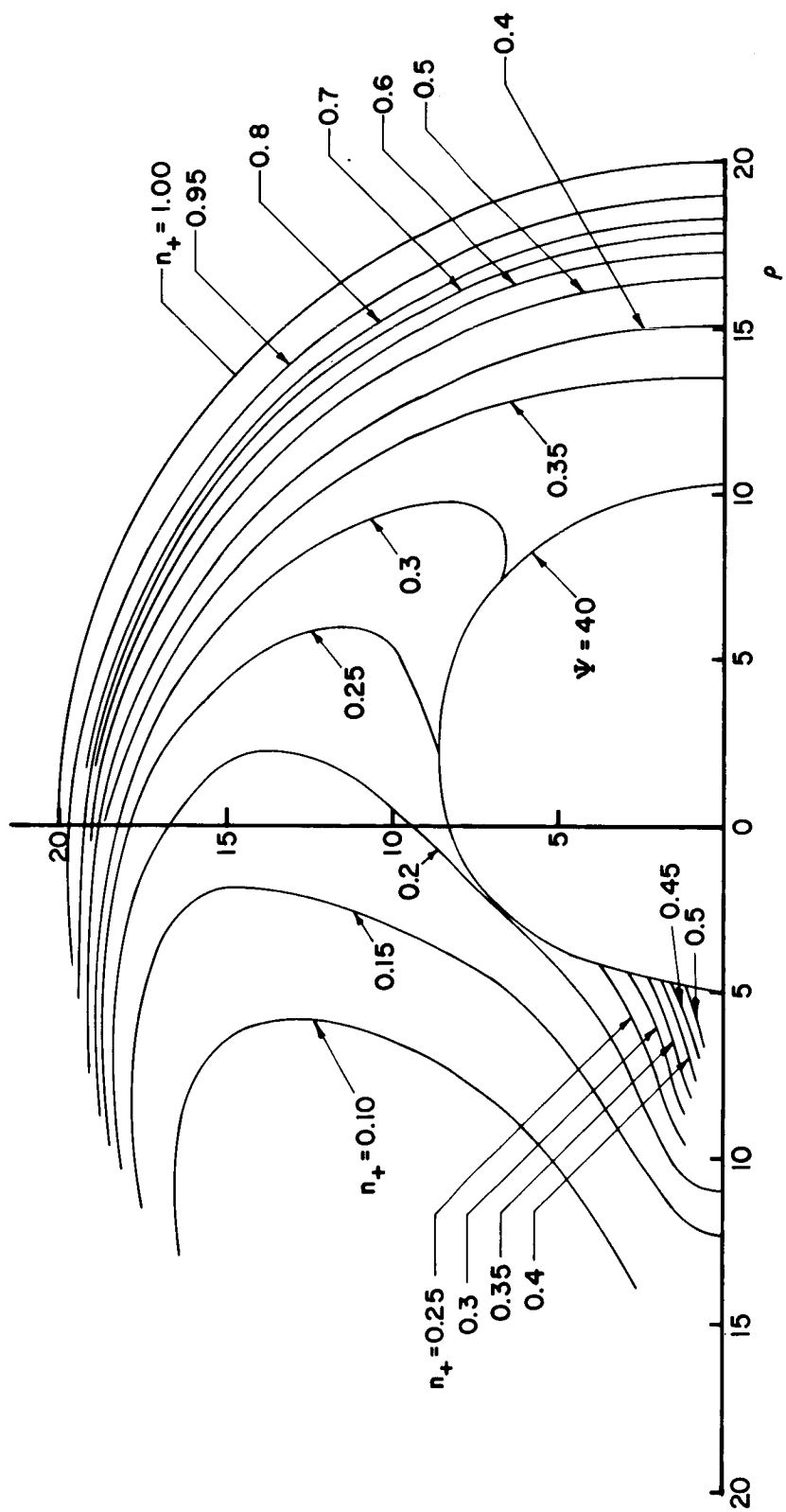
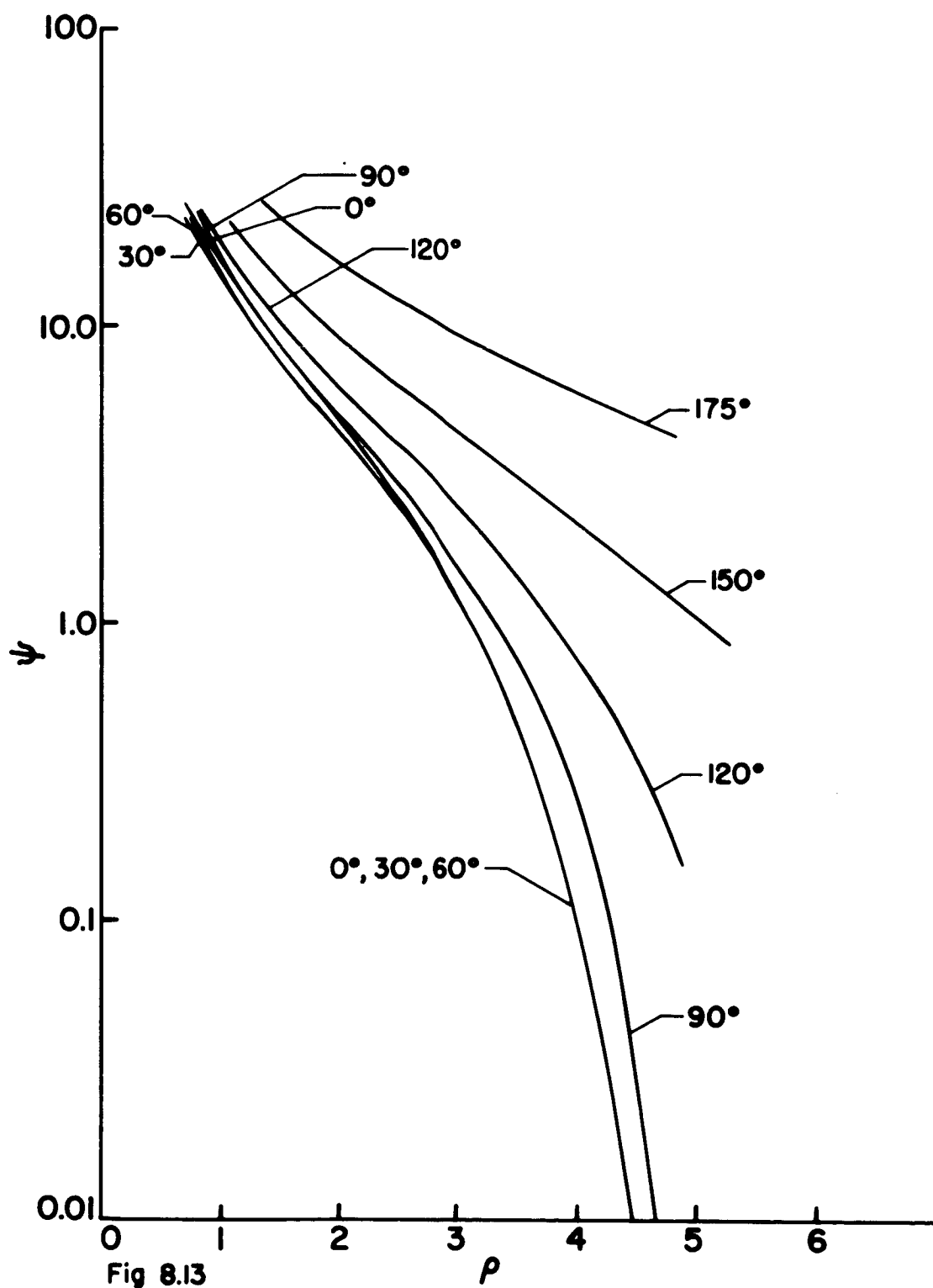
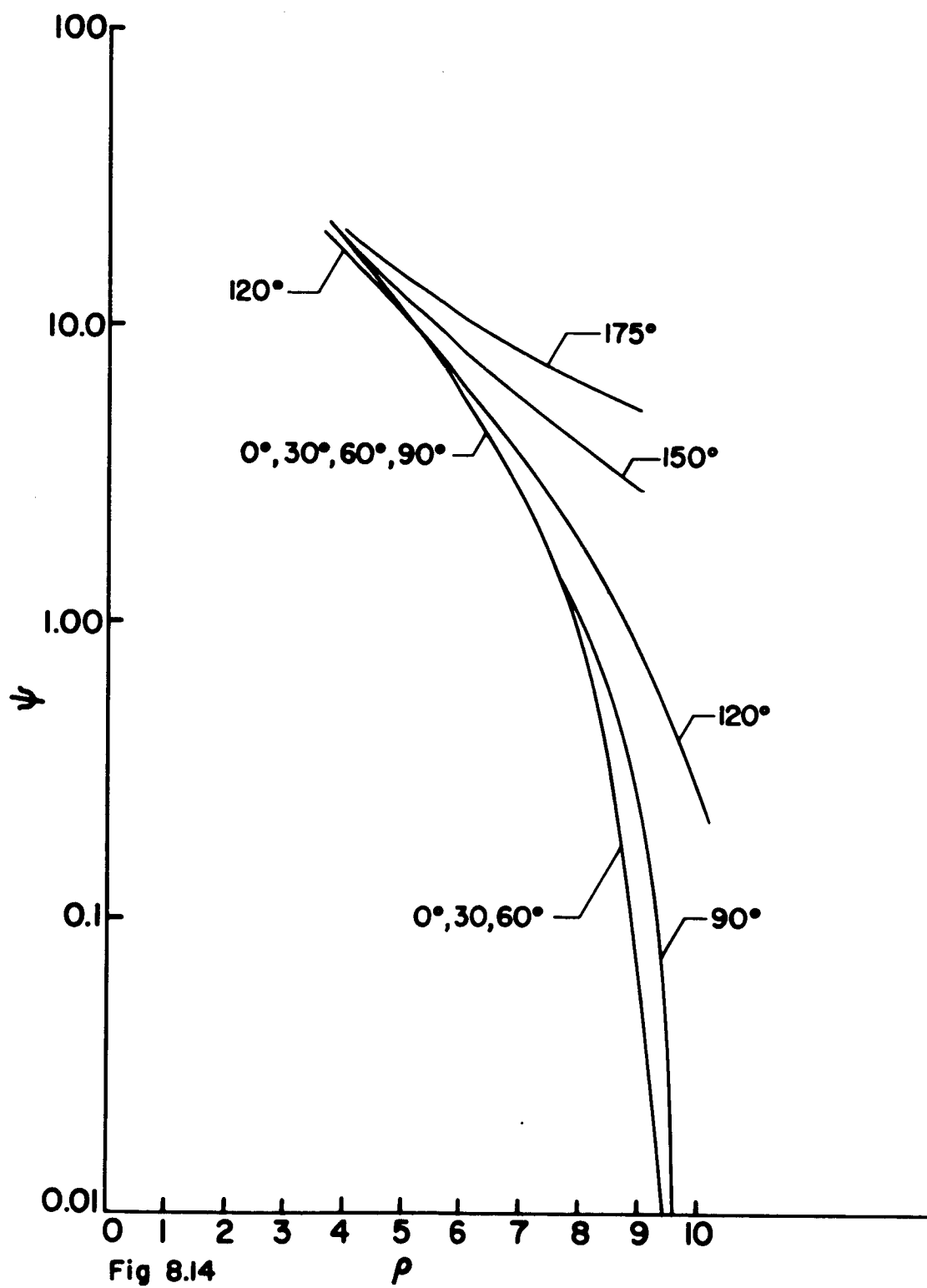
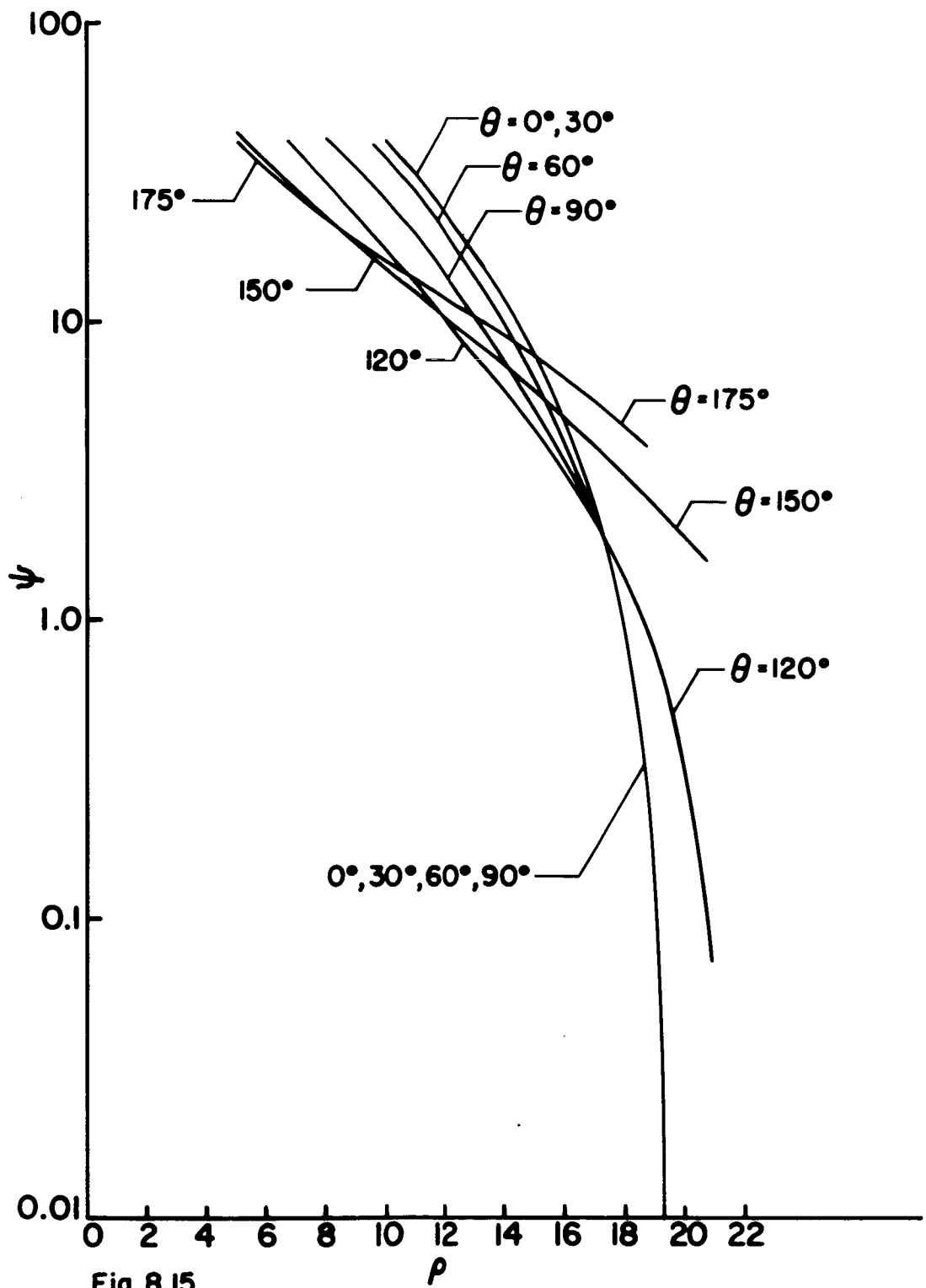


FIG. 8.12







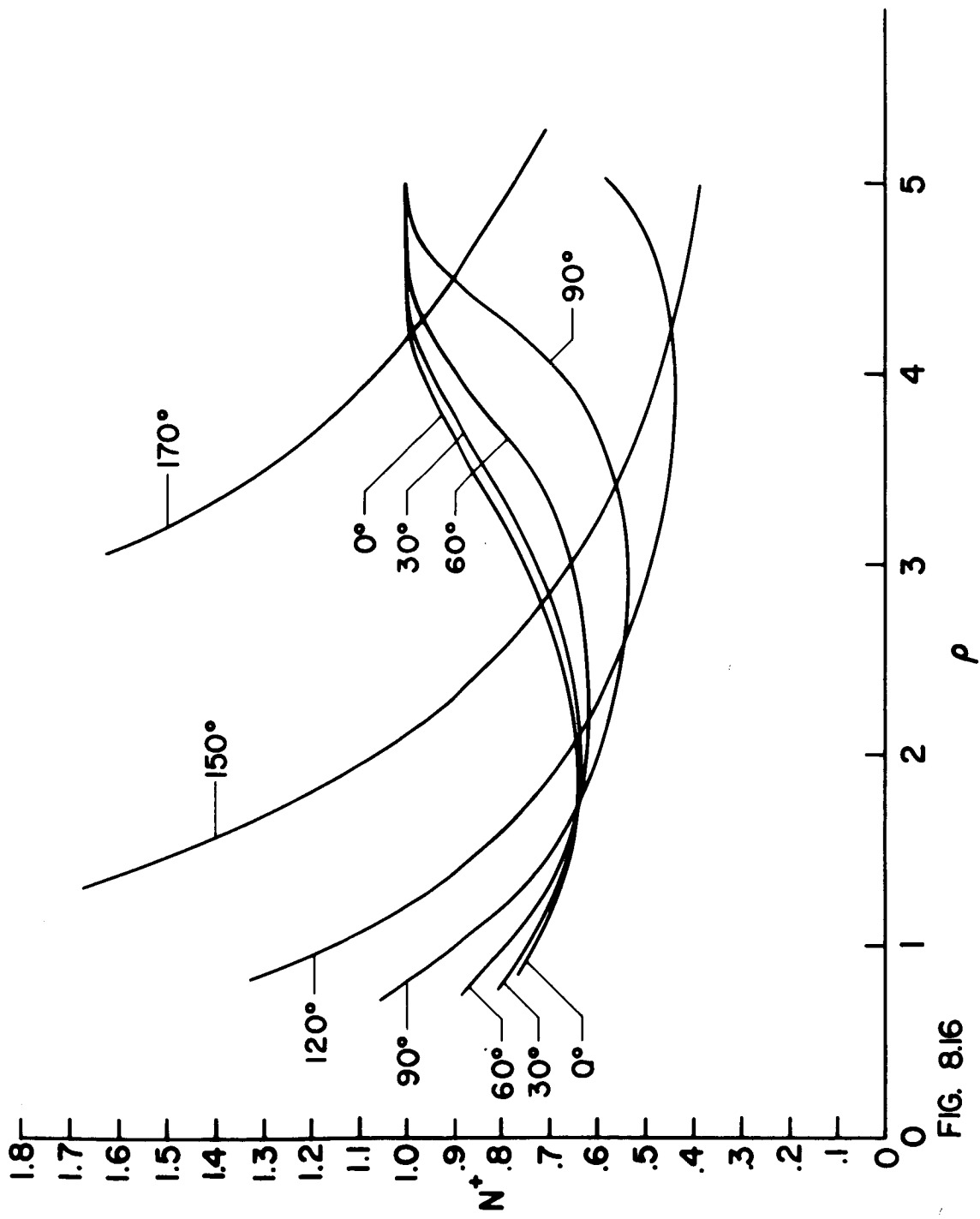


FIG. 8.16

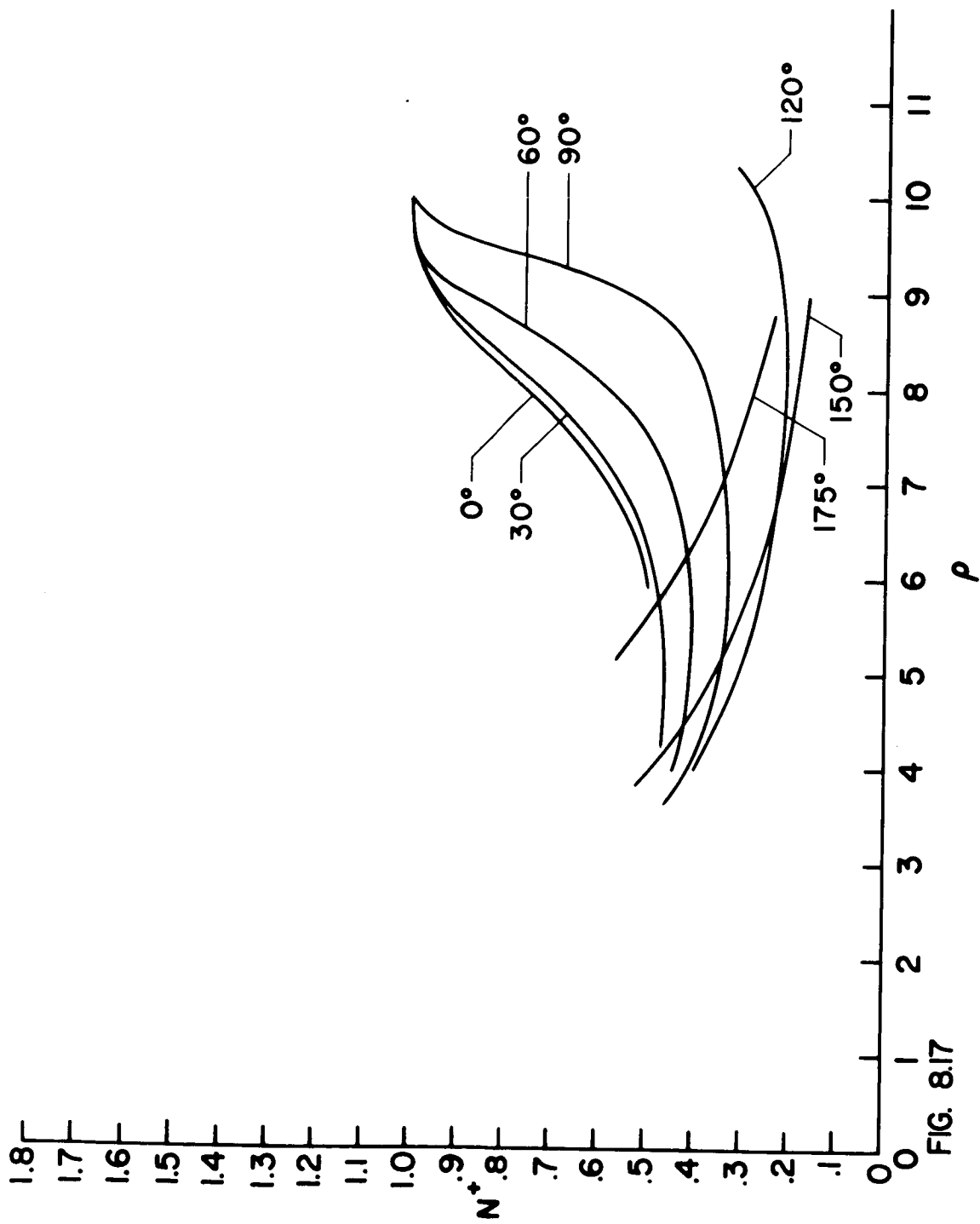


FIG. 8.17

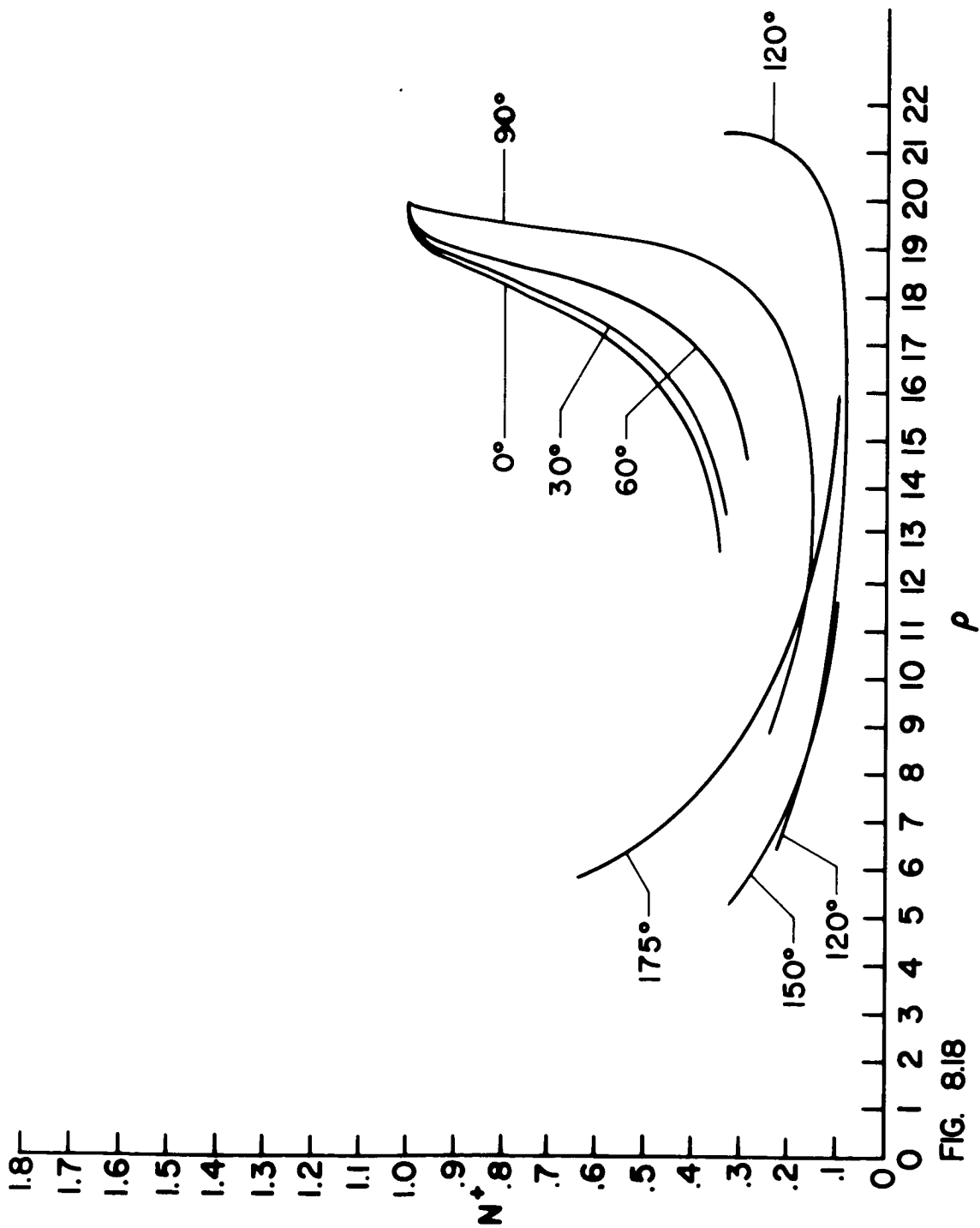
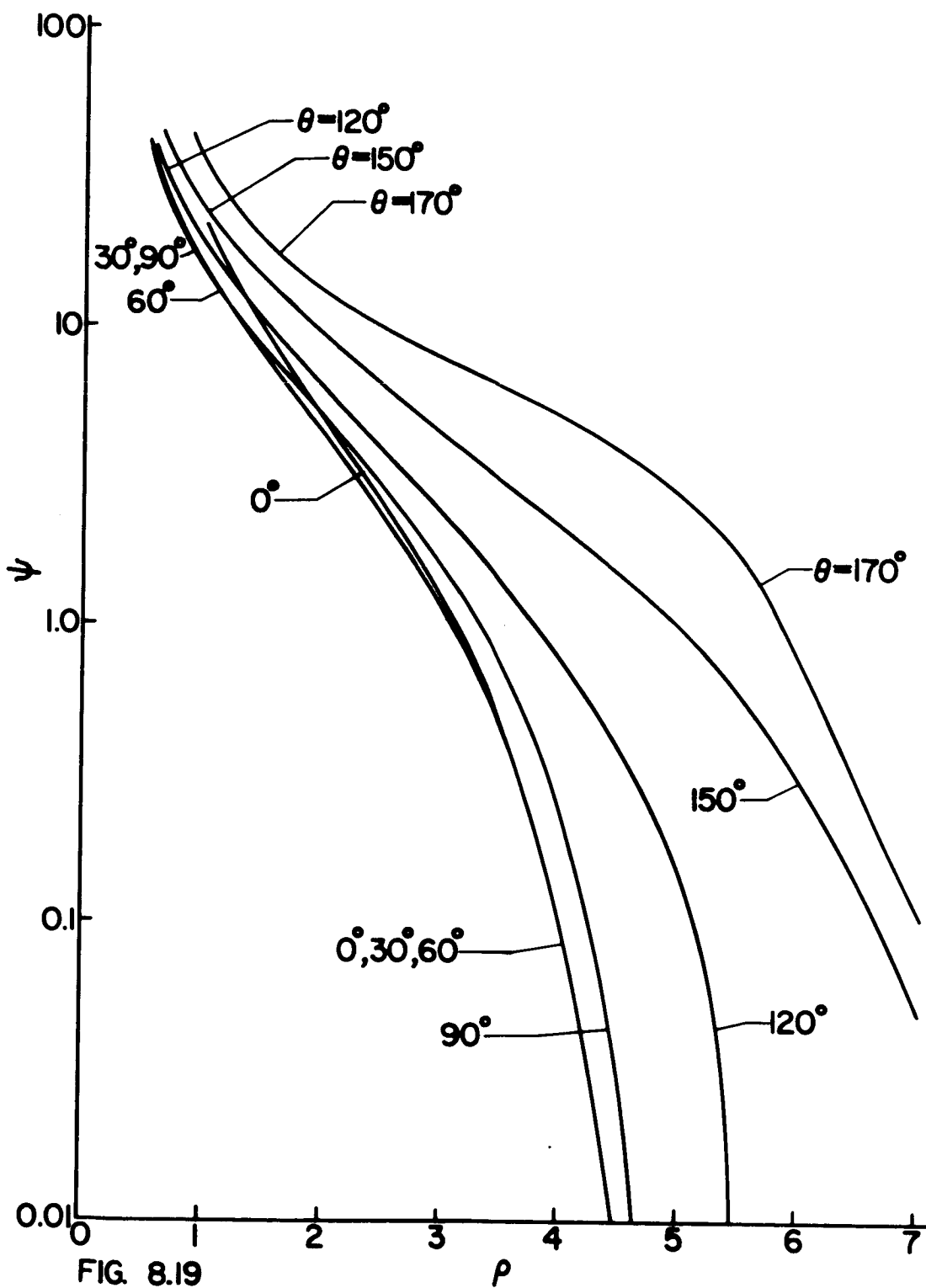
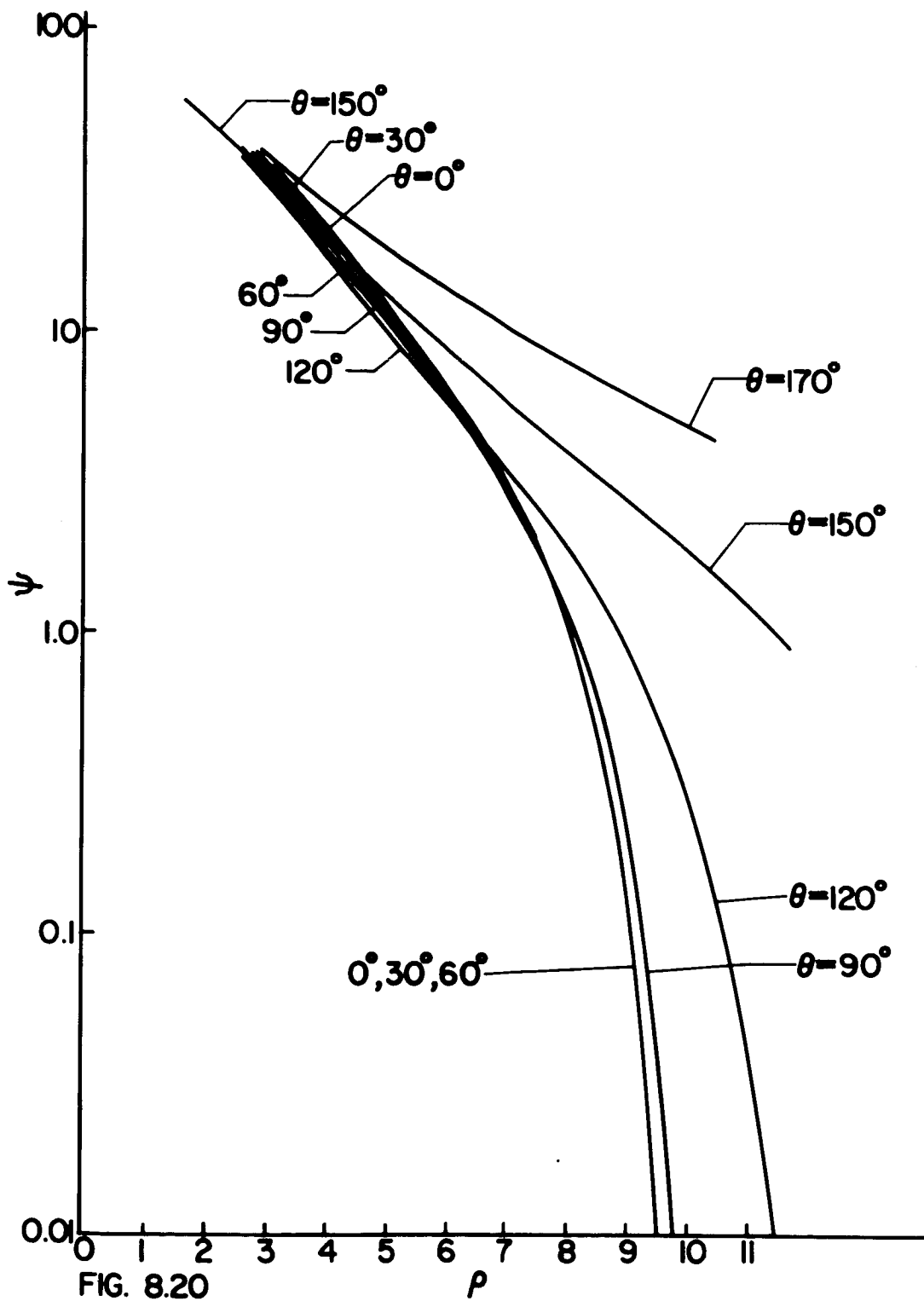


FIG. 8.18





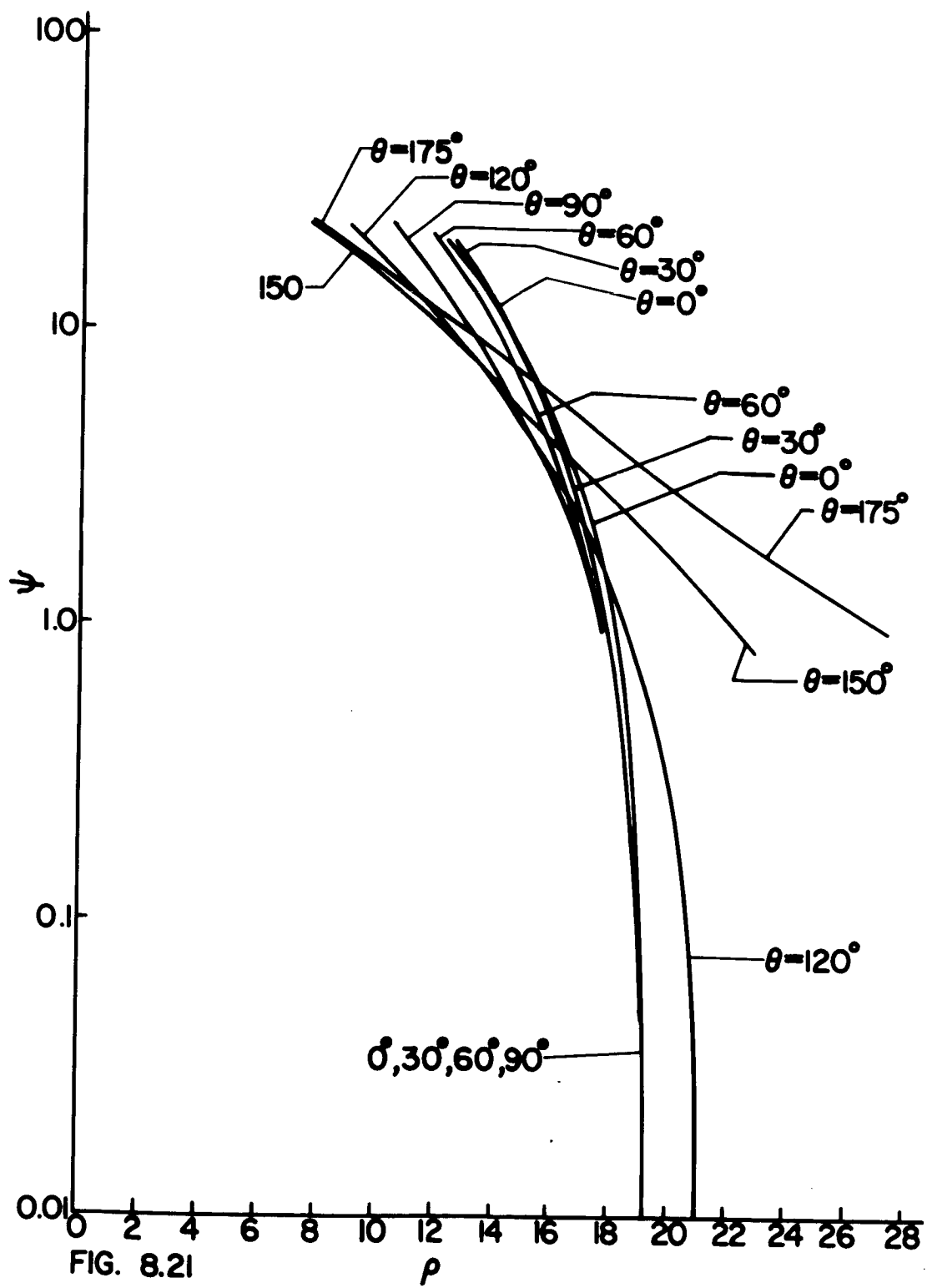


FIG. 8.21

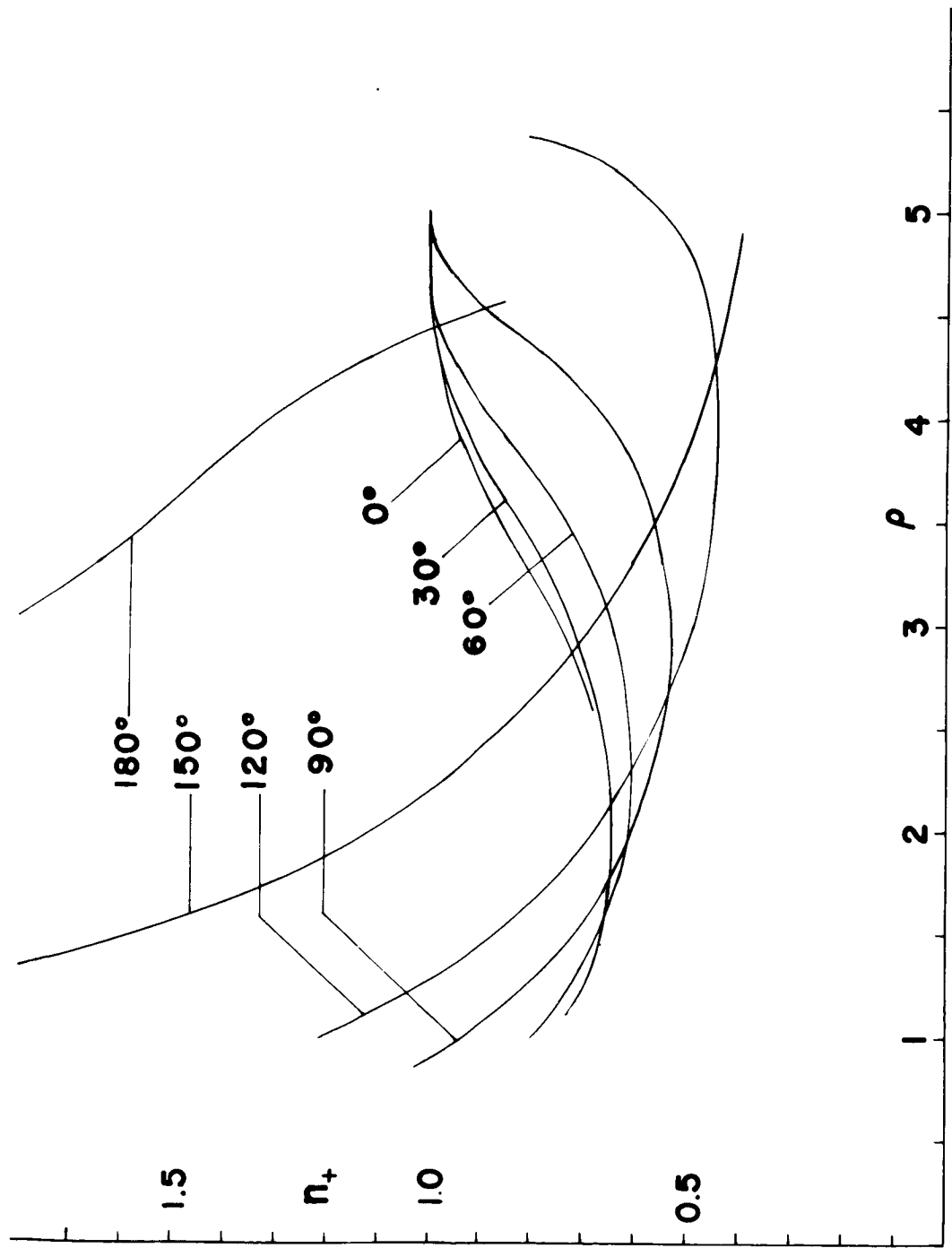


FIG. 8.22

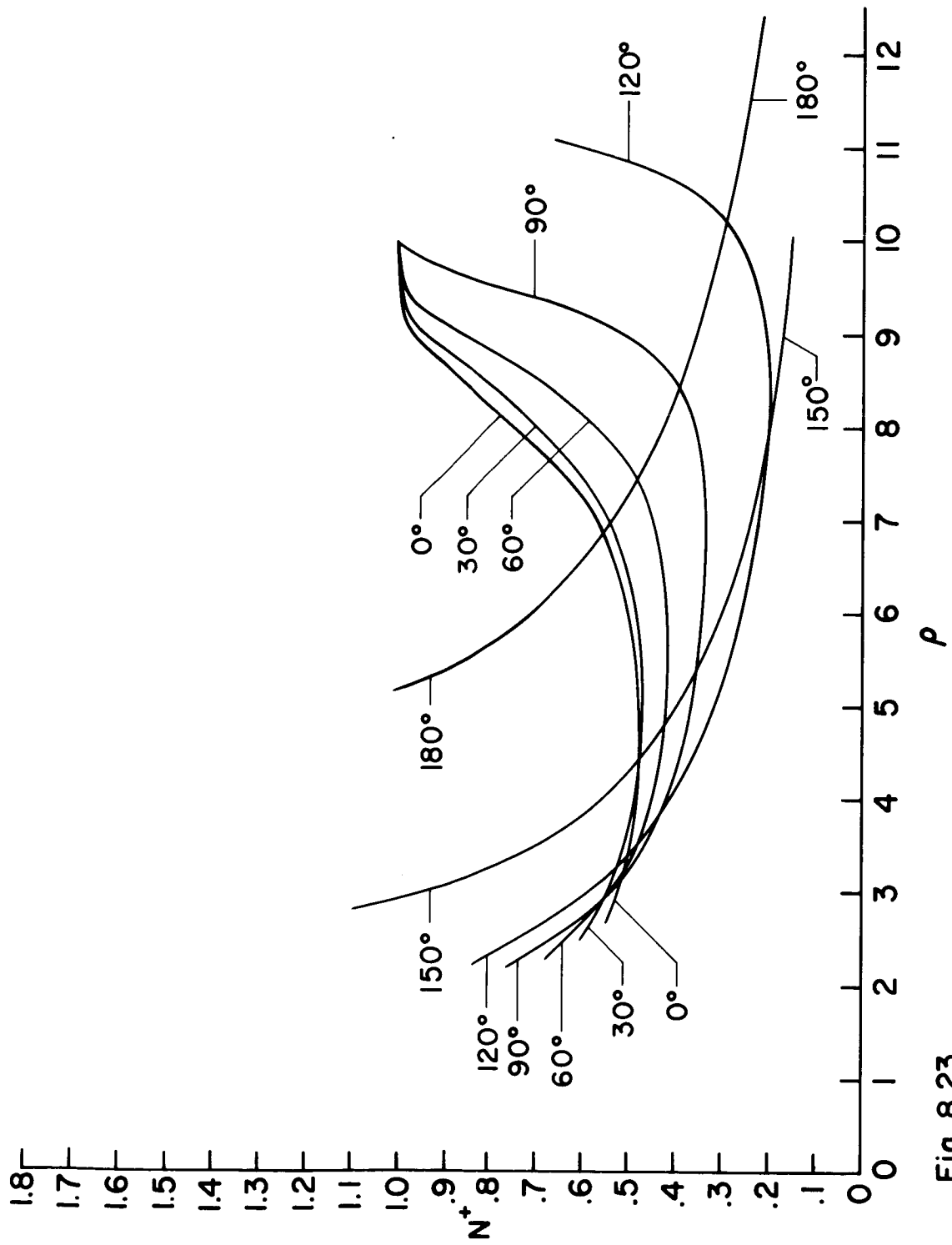


Fig. 8.23

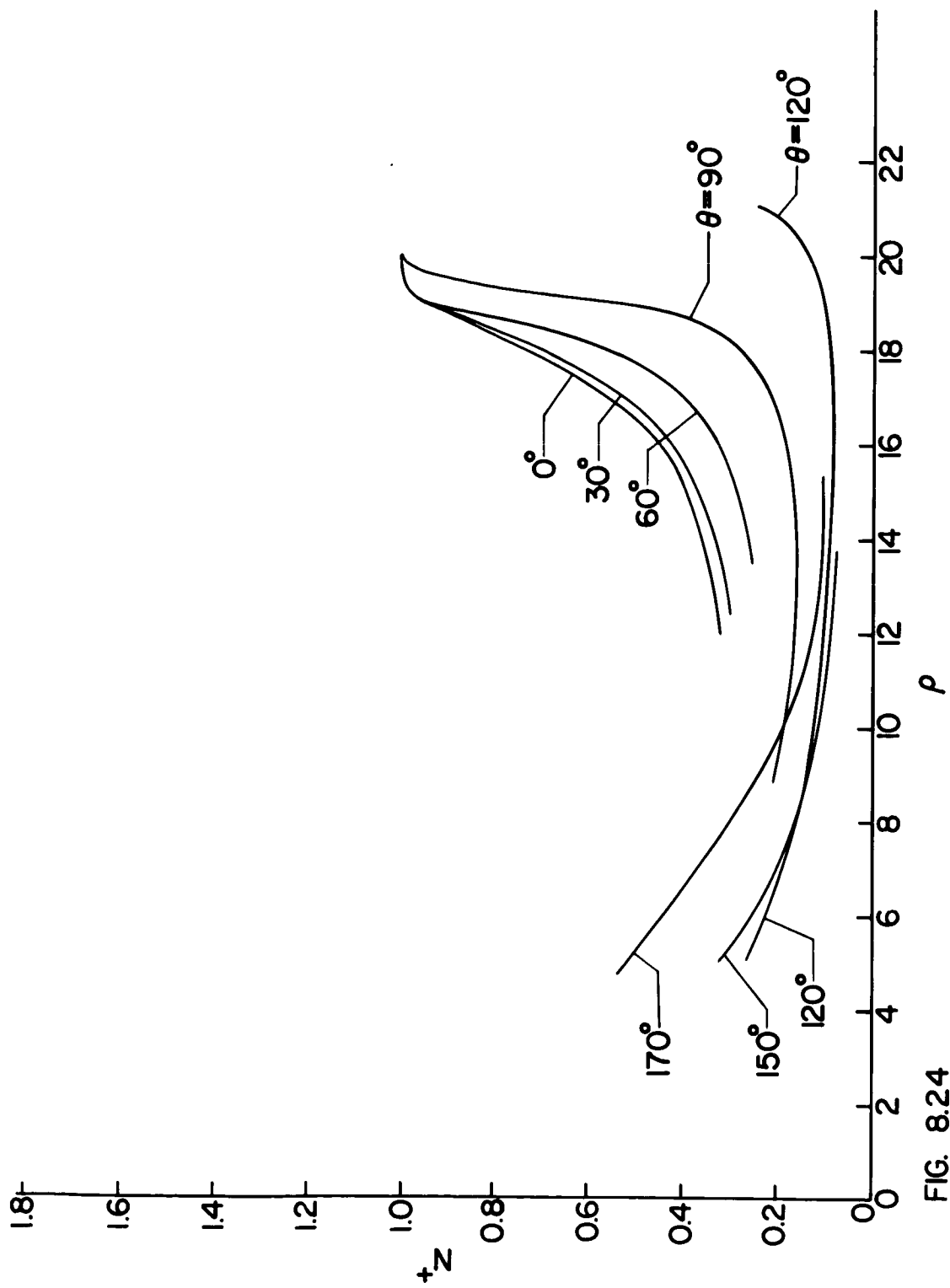


FIG. 8.24

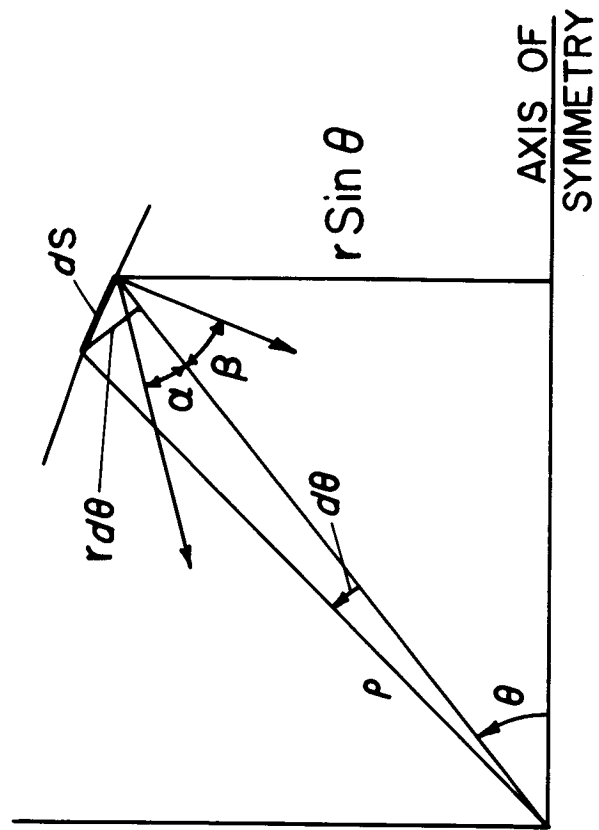
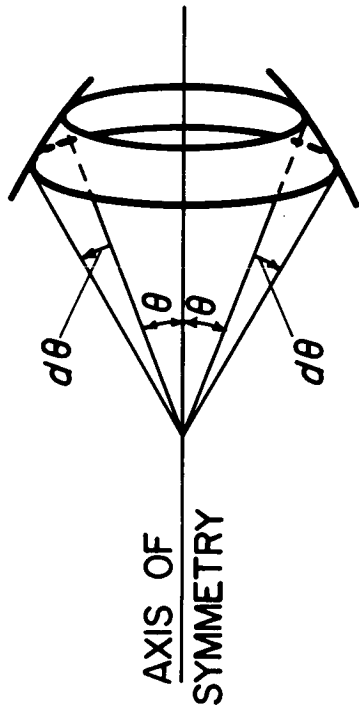


FIG. 9.1



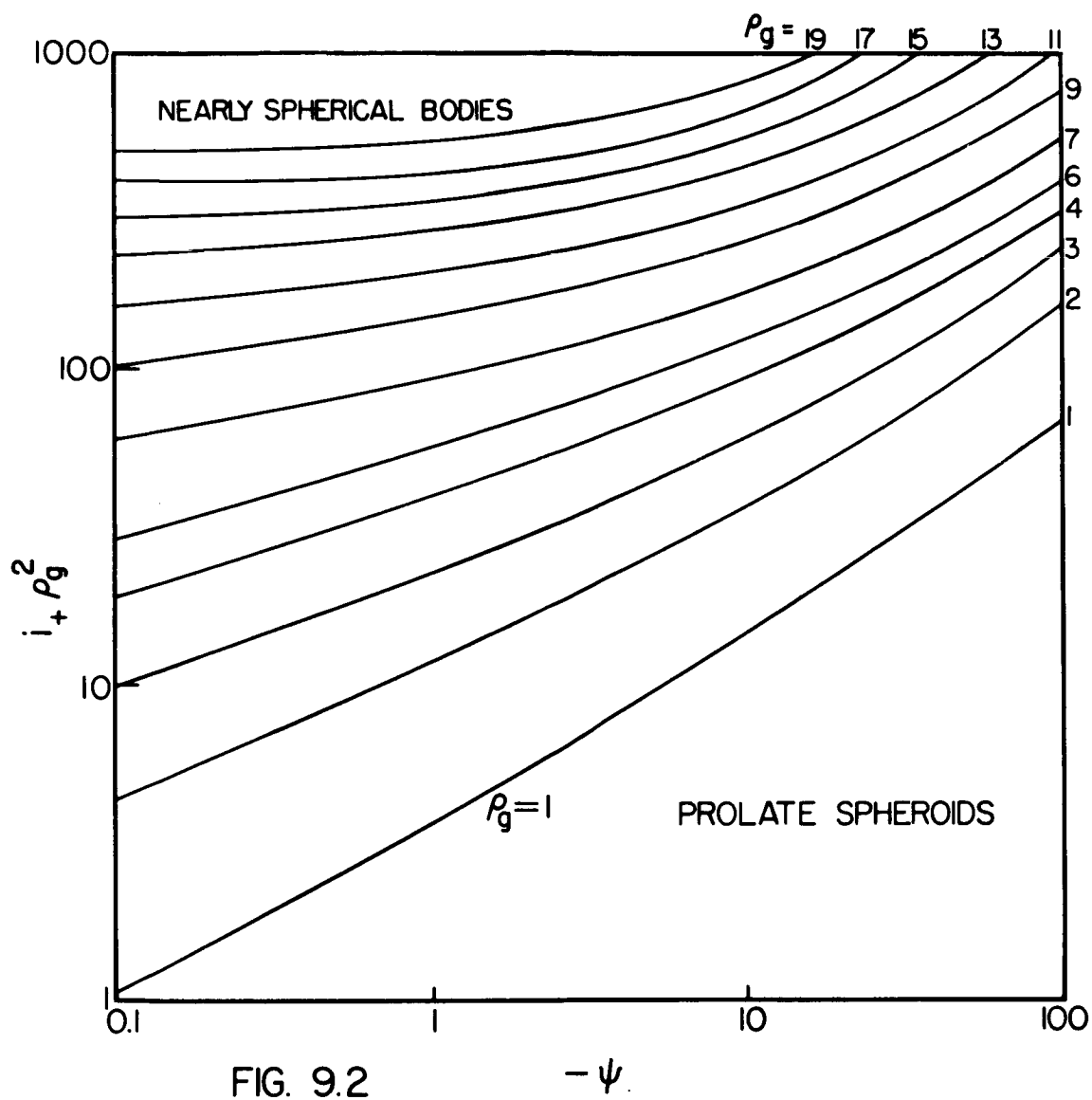


FIG. 9.2

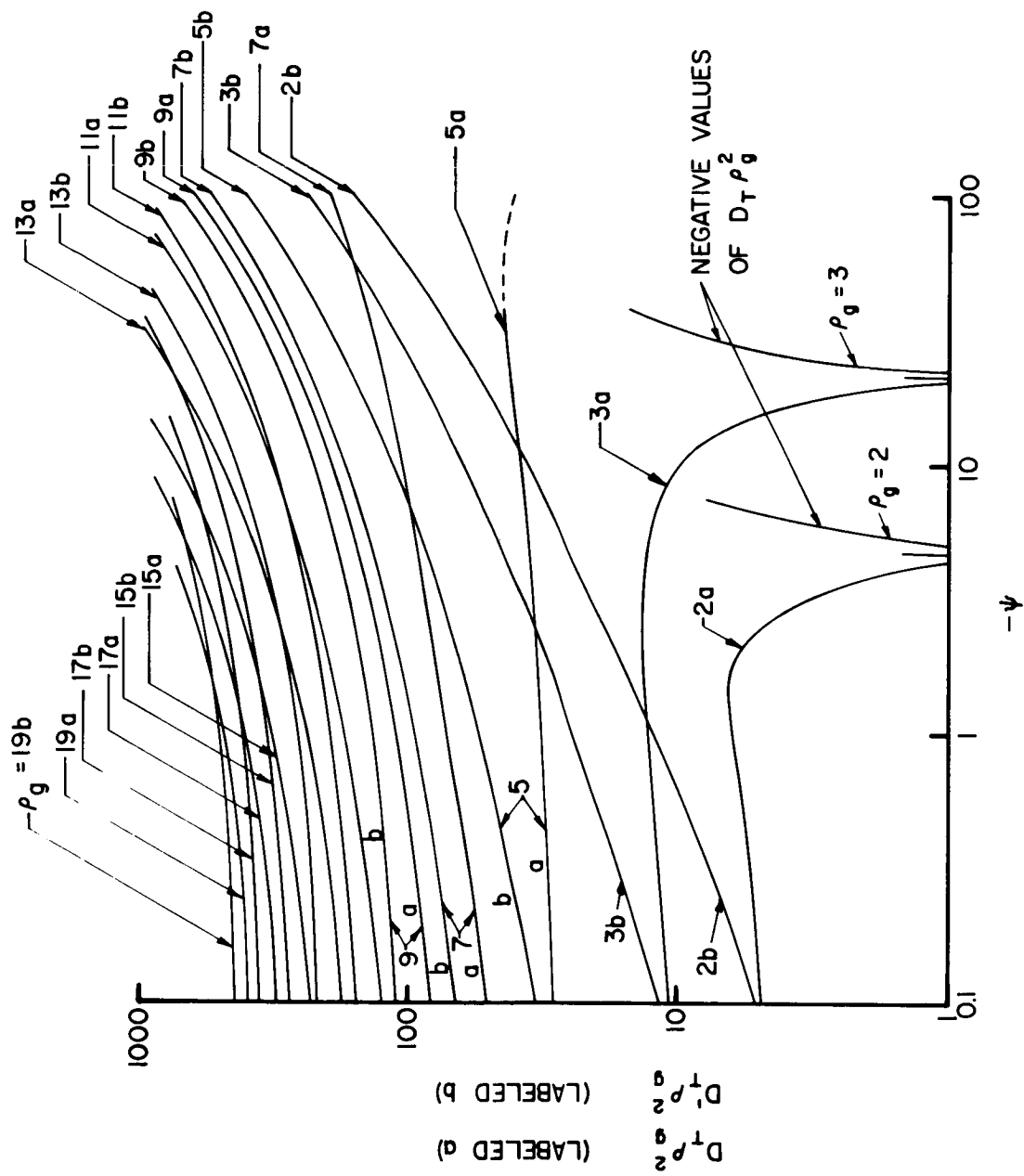


FIG. 9.3